

# Conceptual Design Report for High $p_T$ Upgrade

PHENIX high  $p_T$  upgrade team

July 27, 2003

# Contents

<b>1</b>	<b>Introduction</b>	<b>1</b>
1.1	Overview . . . . .	1
1.2	PID with TOF/Aerogel/RICH . . . . .	2
1.2.1	Aerogel . . . . .	2
1.2.2	Additional TOF . . . . .	2
1.2.3	PID with AEROGEL, RICH and EMCal-time-of-flight . . . . .	4
1.2.4	PID with AEROGEL, RICH and TOF . . . . .	5
<b>2</b>	<b>Mechanical design</b>	<b>7</b>
2.1	Cell design . . . . .	7
2.1.1	Silica Aerogel . . . . .	9
2.1.2	Photomultiplier Tube R6233-01HA (Hamamatsu) . . . . .	9
2.1.3	PMT Base . . . . .	11
2.1.4	Mu-metal Shield for PMT . . . . .	17
2.1.5	Reflector . . . . .	22
2.1.6	Box . . . . .	25
2.1.7	Connectors on Box . . . . .	30
2.1.8	LED Calibration System . . . . .	32
2.1.9	Gas Flow . . . . .	35
2.1.10	Performance . . . . .	37
2.2	Assembly . . . . .	45
2.3	Integration . . . . .	46
<b>3</b>	<b>Readout Electronics</b>	<b>49</b>
3.1	Preamplifier . . . . .	50
3.1.1	Electrical Design . . . . .	50
3.1.2	Mechanical Design and Location . . . . .	52
3.1.3	Cables . . . . .	53
3.1.4	Cross Talk . . . . .	55
3.2	Front End Electronics . . . . .	56
3.3	Level-1 Trigger . . . . .	57
<b>4</b>	<b>Simulation</b>	<b>62</b>
4.1	Expected PID capability . . . . .	62
4.2	PISA . . . . .	67
4.2.1	Overall Radiation Length . . . . .	68
4.2.2	Effect on EM-Cal . . . . .	70
4.3	Level-2 Trigger . . . . .	71

<b>5</b>	<b>Appendix</b>	<b>73</b>
5.1	Appendix A: Heating Test . . . . .	73
5.2	Appendix B: Connector List . . . . .	76
5.3	Appendix C: Parts List . . . . .	83

# 1 Introduction

## 1.1 Overview

One of the important features of PHENIX experiment is capability of particle identification (PID). High resolution time-of flight counter (TOF), ring-imaging Cherenkov counter (RICH) and Pb-Sc. electromagnetic calorimeter (EMCal) with timing measurement capability provides PID as shown in upper two rows of Fig.1. The TOF is limited to moderately low  $p_T$ , while at high  $p_T$  RICH provides pion identification. Clearly, the present TOF & RICH configurations leave a significant hole in the particle identification capabilities of PHENIX.

New features found in the first RHIC data sets has focused people's attention to the importance of particle identification in the region above 2 GeV/c. The addition of an aerogel Cherenkov counter with an index of refraction of 1.01 would provide pion, kaon, and proton identification seamlessly up to  $p_T$  of almost 10 GeV/c as illustrated in Fig.1.

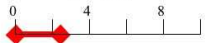

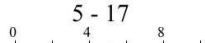
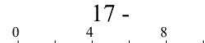
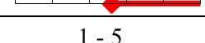
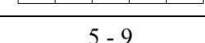
		Pion-Kaon separation	Kaon-Proton separation
TOF	$\sigma \sim 100$ ps	0 - 2.5 	- 5 
RICH	$n=1.00044$ $\gamma_{th} \sim 34$	5 - 17 	17 - 
Aerogel	$n=1.01$ $\gamma_{th} \sim 8.5$	1 - 5 	5 - 9 

Figure 1: Hadron PID of PHENIX and Aerogel Cherenkov Counter. See section 1.2 for the details.

An Aerogel Cherenkov counter with limited acceptance will be installed in the PHENIX West Arm. Geometrical size of the counter will be  $\sim 390(z) \times 120(\phi) \times \sim 30(r)$  cm<sup>3</sup> and is segmented into 160 ( $16(z) \times 10(\phi)$ ) cells. According to current design, each cell has  $22(z) \times 11(\phi) \times 12(r)$  cm<sup>3</sup> of aerogel with refractive index of  $\sim 1.01$ , followed by an integration cube viewed by two 3" PMT's (left of Fig.2). Test beam experiments done at KEK in May 2002 shows that positional uniformity with this configuration is the best of all configurations studied. To eliminate dead space, cells will be stacked reversing the orientation of the cell in alternating rows as shown in right of Fig.2. With this configuration, all the sensitive aerogel volumes are kept in one plane and there is minimal dead space in between, which contributes to the uniform detector response. The disadvantage of this configuration is particles enter in the reverse direction into half of the cells. However, beam tests at KEK have shown that when a particle enters from the integration cube to the aerogel, number of p.e. is only smaller by  $10 \sim 20\%$ , which is not significant. We can obtain  $\sim 15$  p.e. by adjusting the thickness of the aerogel.

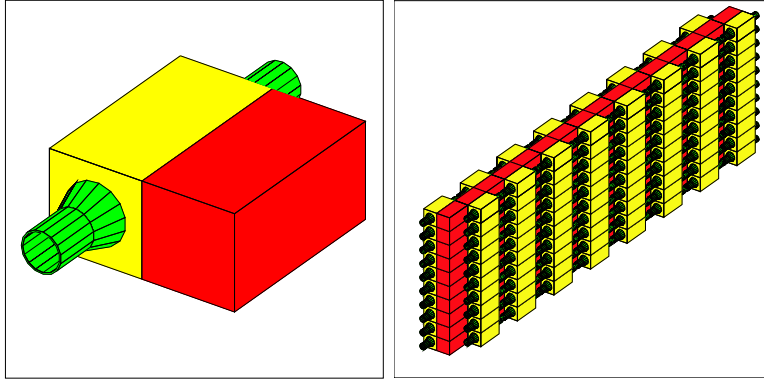


Figure 2: Left; Current design with integration cube. Right; Stack of cells.

## 1.2 PID with TOF/Aerogel/RICH

In addition to the current configuration of the detector, the AEROGEL provides the PID capabilities by two kinds of combinations with the other PID detectors. One is with AEROGEL, RICH and EMCAL-time-of-flight. And the other is AEROGEL, RICH, and additional TOF (as well as EMCAL-time-of-flight).

### 1.2.1 Aerogel

To see the threshold momenta for the different indices of AEROGEL, the expected number of emitted photon are calculated through empirical equation 1, and plotted in 3.

$$N_{p.e.} \simeq 55 \times L [cm] \times \{1 - (1/n\beta)^2\} \quad (1)$$

In the equation, L denotes radiator length, and for aerogel it is assumed to be 12cm, and for RICH ( $n=1.00041$  for  $CO_2$ ) it is 150 cm. The constant term, 55, is based on the beam test results at KEK. For the RICH, the constant is chosen so that the maximum number of photoelectrons is  $\sim 10$ .

Especially for the identification of kaon at the high momentum region (from 3.5 to 5.5 GeV/c), the matching is needed between the lowest threshold momentum (5.5 GeV/c) for pion rejection by RICH counter, and the lowest threshold (3.5 GeV/c for the  $n=1.0114$  with threshold at 10 % of maximum number of photoelectrons) of light emission in AEROGEL by kaon as well as by pion.

### 1.2.2 Additional TOF

There is an idea to implement additional TOF in the west-arm in order to extend hadron PID capability of the arm. The difference of flight time in 5 meter is shown in Fig. 4.

The identification of pion and kaon is done up to 2.5 GeV/c, and proton is identified up to 4.2 GeV/c with 3 sigma separation for 100 ps resolution, which the additional TOF is aiming for. In case of 400 ps resolution, which EMCAL-time-of-flight would give without

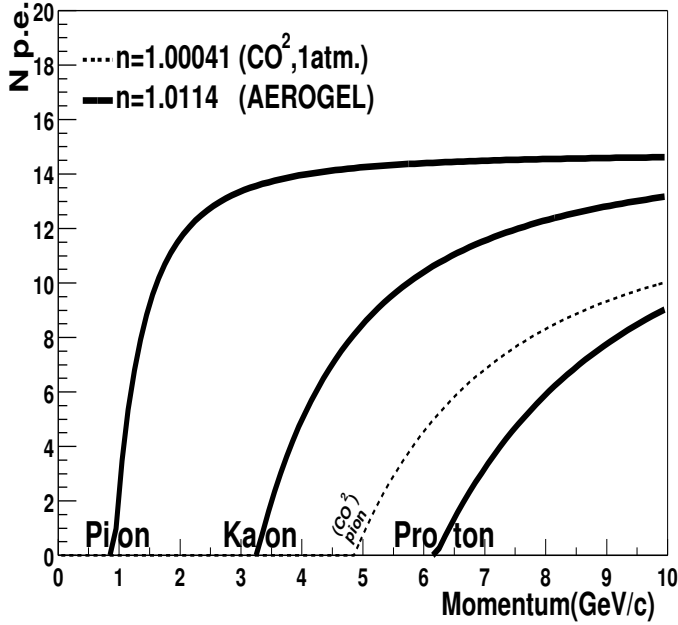


Figure 3: Evaluated number of photo-electron for [solid line]  $n=1.0114$ , and [dashed line] RICH ( $CO_2$ ,  $n=1.00041$ , 1 atm.) as a function of momentum.  $N_{p.e.}$  is for the 12 cm thick of aerogel.

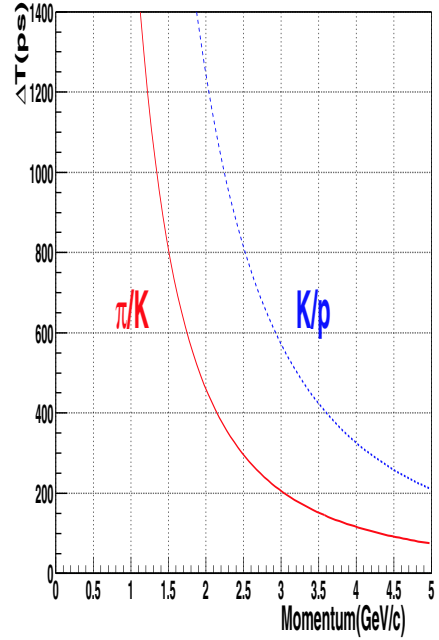


Figure 4: Difference of time-of-flight [ps] at 5 m vs. momentum, between pion and kaon [solid line], and between kaon and proton [dashed line].

the additional implementation of TOF, pion and kaon is identified up to 1.2 GeV/c, and proton is identified up to 2 GeV/c for the 3 sigma separation.

#### Disadvantage of configuration without additional TOF

The disadvantages of the configuration without the additional TOF are following 3 points. These disadvantages are mainly for the kaon where both TOF and AEROGEL are required for PID.

- (1) Increase of systematic error in single spectra of kaon in the region  $p_T$  region between 2 GeV/c and 3.5 GeV/c, due to the systematic error between east and west arm.
- (2) Loss of the track-by-track physics for kaon in the  $p_T$  region between 2 GeV/c and 3.5 GeV/c.
- (3) Loss of consistency check for lower systematic error. Overlap of detector coverages in track-by-track bases (between 1 to 2.5 GeV/c for pion and kaon, and between 3.5 to 4.2 GeV/c for proton) are lost.

### 1.2.3 PID with AEROGEL, RICH and EMCal-time-of-flight

The schematic diagram for PID with AEROGEL, RICH and EMCal-time-of-flight is shown in Fig. 5.

Without TOF  
AEROGEL : ( $n=1.0114$ , threshold= 10% of Max. Np.e.)

Momentum [GeV/c]	1. 0.5	2. 1.2	3. 3.5	4.	5. 5.5	6. 6.5	7.	$\sim 10.$ (momentum limit)
$\pi$	EMCal		AEROGEL			RICH		
K	EMCal		AEROGEL			RICH		
	EMCal(proton)		AEROGEL			RICH		
p	EMCal		AEROGEL			RICH		

Figure 5: PID capabilities with AEROGEL, RICH and EMcal-time-of-flight, but without additional TOF. Aerogel is based on  $n = 1.0114$  with threshold at 10 % of maximum number of photoelectrons.

As a whole, charged pion can be identified from 0.5 to 3.5 GeV/c and from 5.5 to some 10 GeV/c (as high as momentum can be measured and statistics allows). Kaon are identified from 0.5 to 2 GeV/c, and then 5.5 to 6.5 GeV/c. And (anti-)proton are identified from 0.5 to 2 GeV/c, and then 3.5 to 6.5 GeV/c. Those momentum range is based on (I) the EMcal-time-of-flight resolution is 400 ps, and (II) the AEROGEL ( $n = 1.0114$ ) threshold is at 10 % of the maximum number of photoelectrons.

One should need additional consideration when only veto logic is used for AEROGEL and RICH counter in proton identification. If these are needed as a trigger, an additional trigger logic to identify as a charged track is required to reject photon.

#### Note

To reduce the gap between 3.5 GeV/c and 5.5 GeV/c (for pion and kaon), it is needed either (i) RICH uses higher index of gas than 1 atm of  $CO_2$  ( $n = 1.00041$ ) in order to make the 5.5 GeV/c down, or (ii) separation with AEROGEL according to the pulse height (for momentum range more than 10 % of maximum number of photoelectron) is possible to make the 3.5 GeV/c up. And the region above 6.5 GeV/c (for kaon and proton), the method (ii) is needed.

Please note that in Fig. 1, the threshold is raised to some 50 % of maximum number of photoelectrons.

### Pion identification

It is done first by EMCal-time-of-flight, from 0.5 GeV/c, up to 1.2 GeV/c. Then AEROGEL covers pion identification from 1 to 3.5 GeV/c (when kaon fires AEROGEL). Above 5.5 GeV/c, RICH takes care pion identification up to the highest momentum, where statistics and momentum measurement allows, and where it is less than 17 GeV/c (where kaon begins to contaminate into pion for RICH).

### Kaon identification

First, from 0.5 to 1.2 GeV/c, kaon identification is done by EMcal-time-of-flight as same way as pion. Second, from the 1.2 to 2 GeV/c, kaon PID is done veto-AEROGEL with EMCal-time-of-flight as non-(anti-)proton. Third, from 5.5 up to 6.5 GeV/c (when proton is contaminated into kaon), kaon PID is done by veto-RICH and AEROGEL.

### Proton identification

First from 0.5 to 2 GeV/c, proton identification is done by EMcal-time-of-flight. Second, from 3.5 up to 6.5 GeV/c, proton is identified by veto-AEROGEL with additional requirement as a charged track (but not as a photon). From 3.5 up to 6.5 GeV/c, veto-RICH as well as veto-AEROGEL is better to reject background.

## 1.2.4 PID with AEROGEL, RICH and TOF

In addition to RICH, proposed AEROGEL, and EMCal-time-of-flight, additional TOF allows to enrich PID capabilities. The schematic diagram for PID with AEROGEL, RICH and TOF is shown in Fig. 6.

As a whole, charged pion can be identified from 0.5 to 3.5 GeV/c and from 5.5 to 10 GeV/c (as high as momentum can be measured and statistics allows). Kaon and are identified from 0.5 to 3.5 GeV/c, and then 5.5 to 6.5 GeV/c. (Anti-)proton are identified from 0.5 to 6.5 GeV/c. Those momentum range is based on (I) the TOF resolution is 100 ps, and (II) the AEROGEL ( $n = 1.0114$ ) threshold is at 10 % of the maximum number of photoelectrons.

One should need additional consideration when only veto logic is used for AEROGEL and RICH counter in proton identification. If these are needed as a trigger, an additional trigger logic to identify as a charged track is required to reject photon.

### Note

To reduce the gap between 3.5 GeV/c (for pion and kaon) and 5.5 GeV/c, it is needed either (i) RICH uses higher index of gas than 1 atm of  $CO_2$  ( $n = 1.00041$ ) in order to make the 5.5 GeV/c down, or (ii) separation with AEROGEL according to the pulse height (for momentum range more than 10 % of maximum number of photoelectron) is possible to make the 3.5 GeV/c up. And the region above 6.5 GeV/c (for kaon and proton), the method (ii) is needed.



With TOF AEROGEL : (n=1.0114, threshold= 10% of Max. Np.e.)

Momentum [GeV/c]	0.5	1.	2.	3.	4.	5.	6.	7.	~10. (momentum limit)
$\pi$		TOF		AEROGEL			RICH		
$K$		TOF		AEROGEL			RICH		
		TOF(proton)		AEROGEL					
$p$		TOF		AEROGEL			RICH		

Figure 6: PID capabilities with AEROGEL, RICH and additional TOF. Aerogel is based on  $n = 1.0114$  with threshold at 10 % of maximum number of photoelectrons.

Please note that in Fig. 1, the threshold is raised to some 50 % of maximum number of photoelectrons.

#### Pion identification

It is done first by TOF, from 0.5 GeV/c, up to 2.5 GeV/c. Then AEROGEL covers pion identification from 1 to 3.5 GeV/c (when kaon fires AEROGEL). There is overlap between 1 to 2.5 GeV/c, which allows to make cross check. Above 5.5 GeV/c, RICH takes care pion identification up to the highest momentum, where statistics and momentum measurement allows, and where it is less than 17 GeV/c (where kaon begins to contaminate into pion for RICH).

#### Kaon identification

First, from 0.5 to 2.5 GeV/c, kaon identification is done by TOF as same way as pion. Second, from the 2.5 to 3.5 GeV/c, kaon PID is done veto-AEROGEL with TOF as non-(anti-)proton. Third, from 5.5 up to 6.5 GeV/c (when proton is contaminated into kaon), kaon PID is done by veto-RICH and AEROGEL.

#### Proton identification

First from 0.5 to 4.2 GeV/c, proton identification is done by TOF. Second, from 3.5 up to 6.5 GeV/c, proton is identified by veto-AEROGEL with additional requirement as a charged track (but not as a photon). From 3.5 to 6.5 GeV/c there is overlap by the two kinds of measurements. From 3.5 up to 6.5 GeV/c, veto-RICH as well as veto-AEROGEL is better to reject background.

## 2 Mechanical design

### 2.1 Cell design

The acceptance of the Aerogel counter is planned to cover about  $4 \text{ m}^2$  at radial distance of  $\sim 4.5 \text{ m}$  from the beam line between pad chamber 2 (PC2) and 3 (PC3) at mid-rapidity (west arm sector 1 : W1) as shown in the left panel in Fig. 7. Each counter cell (Aerogel part) is about  $22(z) \times 11(\phi) \times 12(r) \text{ cm}^3$ , which makes  $16(z) \times 10(\phi)$  cells in total and is oriented with respect to the beam direction as shown in the right panel of Fig. 7.

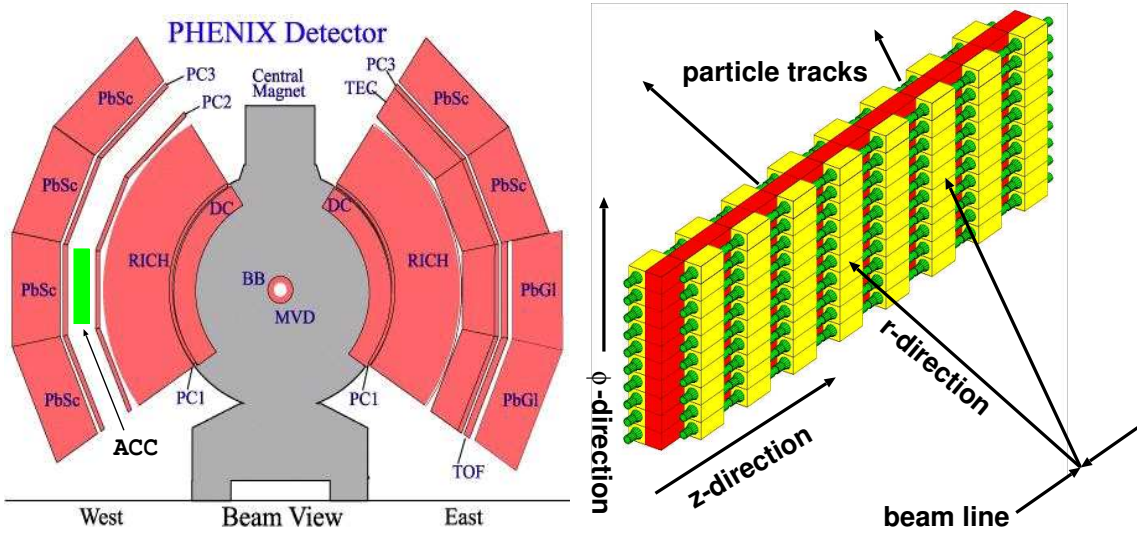


Figure 7: The aerogel detector in the west arm between pad chamber 2 (PC2) and 3 (PC3) in the W1 sector (left) and the aerogel detector structure and orientation with respect to the beam line (right) are shown.

A single cell of the aerogel counter is shown in the left panel of Fig. 8. One cell consists of 3 parts, the aerogel part (shown in red), an integration air gap (shown in yellow) and 2 PMTs (shown in green) located on the side surfaces of the integration air gap as shown in the figure. In order for the aerogel part of all cells to be located in the same plane, every other cells along the z-direction is flipped in the radial direction. This means that for half of the cells, particles from the interaction vertex would enter the aerogel cell first, then go into the integration air gap. For the other half of the cells, particles go through a cell in opposite way (the integration air gap first). Based on beam test results, which will be discussed in following sections, this integration type cell (with air gap) including the size and the shape of the cell has been chosen for its very uniform position dependence compared to the Belle-type design (without the integration air gap). The latter design which was discussed as one of the options in the letter of intent. The right panel in Fig. 8 shows the prototype aerogel counter cells used during the run3-pp. The final design of the cell is very similar to what is shown in this photo. The aerogel, the integration air

gap and 2 PMTs will all be in one thin Aluminum box and the PMTs will be fixed to the lid. The LED for the single photon calibration will also be attached the lid.

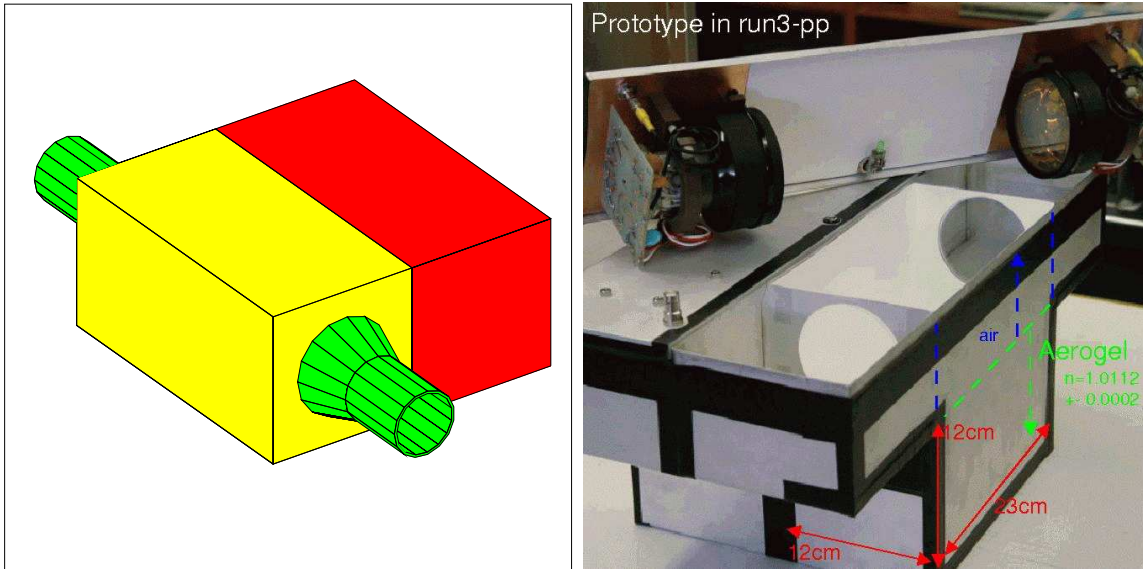


Figure 8: Aerogel detector single cell (left) and prototype cells used in run3-pp (right).

### 2.1.1 Silica Aerogel

For the combined performance of PID with TOF, RICH and the proposed Aerogel cherenkov counters, refractive index of the additional cherenkov radiator needs to be at around 1.01, which is almost the lower end of achivable index even with the silica aerogel. We have chosen hydrophobic silica aerogel SP-12M (Matsushita) for this project. Essential manufacturing method has been transfered from KEK-Belle experiment. Stability and performance of the hydrophobic silica aerogel has been well demonstracted by the KEK-Belle experiment. SP-12M is a silica aerogel with lowest refractive index which is commercially available at this time. Parameters of SP-12M is shown in the table 1. 3000 tiles of SP-12M have been delivered to Tsukuba already and the final prototype using SP-12M has been evaluated and proved to provide enough p.e. ( $>14$ ) at KEK.

Table 1: Parameters for silica aerogel SP-12M (Matsushita)

Refractive Index	$1.0114 \pm 0.0008$
Density [g/cm <sup>3</sup> ]	0.04
Transmission for 10 mm thick	64% (400nm), 88% (550nm)
Size [mm]	$112.5 \pm 1 \times 112.5 \pm 1 \times 11.0 \pm 0.5$

### 2.1.2 Photomultiplier Tube R6233-01HA (Hamamatsu)

We have chosen 3 inch photomultiplier tube R6233-01HA (Hamamatsu), which has 8 stage dynode structure and gain of  $5 \times 10^6$  at 1500V. One p.e. peak is visible as seen in Fig. 9, this PMT is suitable for photon counting.

The parameter of the PMT is tabulated in Table2.

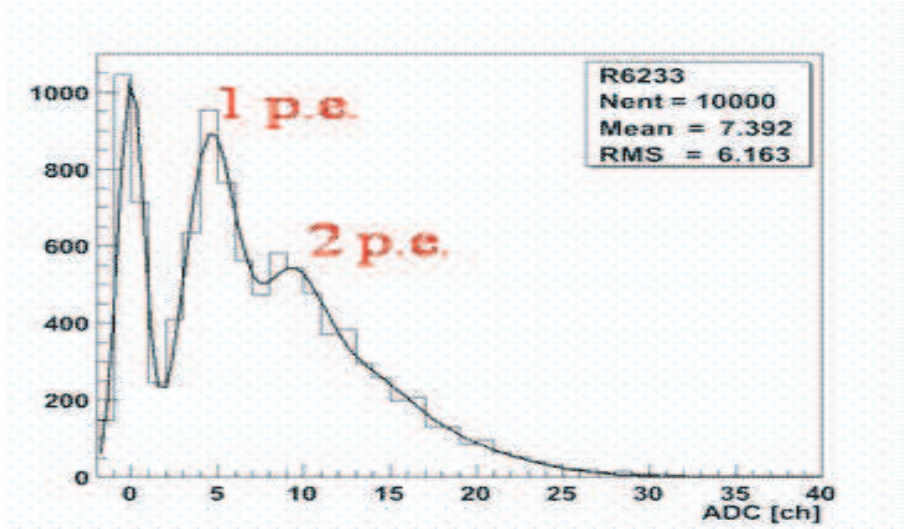


Figure 9: Pulse height (ADC) distribution of R6233. Clear one photo-electron peak is seen.

Table 2: Parameters for photomultiplier tube R6233-01HA (Hamamatsu). Note (\*1); obtained with a voltage distribution ratio of 2-2-1-1-1-1-. For this project, we use the voltage distribution ratio of 1-1-1-1- in order to obtain higher gain, more than  $5 \times 10^6$  at 1500V.

Spectral response [nm]	300 - 650
Peak Wave Length [nm]	$420 \pm 30$
Photocathode	Bialkali
Typical Q.E.	30%
Window	Borosilicate glass
Dynode structure	8 stages
Diameter [mm]	$76.5 \pm 0.8$
Effective Diameter of photocathode [mm]	70 MIN.
Length [mm]	$100 \pm 1$
Weight [g]	145
Max high voltage [V]	1500
Gain (*1)	$2.7 \times 10^5$ at 1000 V
Anode Sensitivity (*1) [A/lm]	> 30
Rise time [ns]	6.0
Transit Time [ns]	52

### 2.1.3 PMT Base

**Circuit diagram** A circuit diagram of a PMT base is shown in Fig. 10. The PMT base is composed of 12 metal-film resistors (R1 - R12), 4 ceramic capacitors (C1 - C4) and a glass-epoxy P. C. board. R1 - R11 are connected in series seen from the high voltage input. The input high voltage is mainly divided by R2 - R11 since R1 has quite low resistance as compared with other resistors. R2 - R12 are the same. A photomultiplier tube (PMT) has 11 leads as shown in the figure. The divided high voltages are supplied to 10 of the leads, and the remaining one is the output terminal of the signal. R12 takes the output over the ground for protection. R1 is also a protector. C1 - C3 keep the divided voltage ratio between leads of a PMT in the case of the high signal rate, and C4 works as a noise canceller. Semi-flexible leads of the PMT are installed to the PMT base by soldering directly.

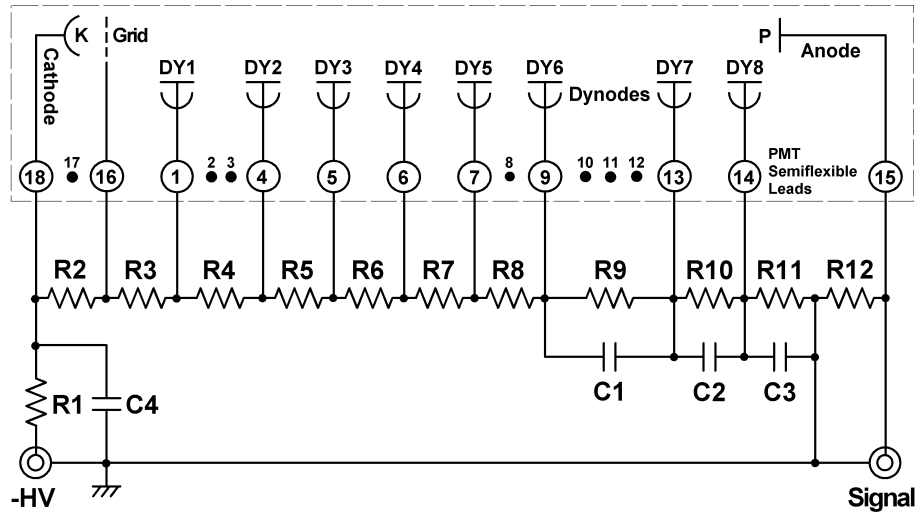


Figure 10: A circuit diagram of the PMT base.

**P. C. board** The P. C. board of the PMT base is a one-pattern-layer glass-epoxy board. A thickness and a size of the P. C. board are 1.6 mm and 80 \* 75 mm<sup>2</sup>, respectively. A layout pattern of the conductor (black area) and a location of parts are shown in Fig. 11 and Fig. 12, respectively.

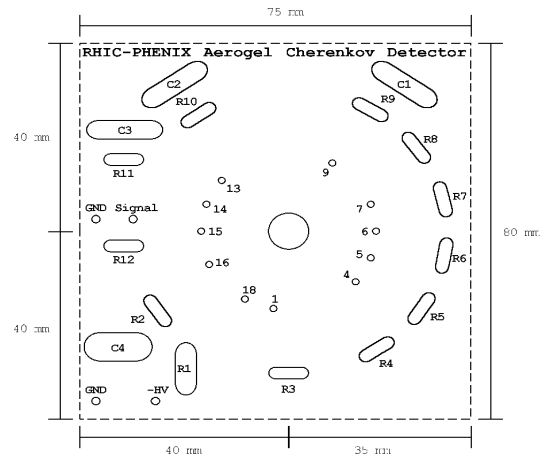
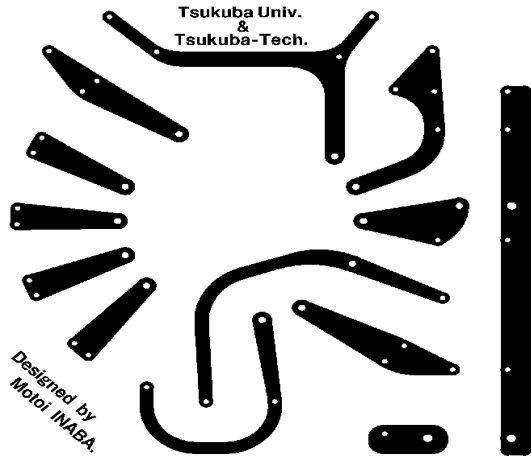


Figure 11: A layout pattern of the conductor on the PMT base. Figure 12: A location of parts on the PMT base.

**Parts** Table 13 is the parts list of a PMT base. All resistors and all capacitors are coat-insulate fixed metal film resistors and high voltage ceramic capacitors, respectively. If the maximum operating voltage of a PMT (1500 volts) is supplied to the PMT base, each voltage that is divided by resistors would be 100 volts. The maximum working voltages of R1 and R2 - R12 are 350 volts and 250 volts, respectively, and their dielectric breakdown voltages are twice of their maximum working voltages. In the case of the operation under the maximum voltage of a PMT, the current that flows through the PMT base is estimated to be 220 microamperes. Therefore, the maximum power consumption of one resistor for the voltage dividing would be only 33 milliwatts. The power consumption of other resistors becomes smaller than resistors for the voltage dividing if the stable high voltage is supplied to the PMT base. The maximum working voltages of C1 - C3 and C4 are 500 volts and 3150 volts, respectively. The resistors are arranged on the conductor side of a PMT base, and the leads of the PMT and capacitors are connected to the other side as shown in Fig. 14.

Part Name	Value	Kind	Type	Maximum Working Voltage	Dielectric Withstanding Voltage	Power Rating
R1	10 k $\Omega$	Coat-Insulate Fixed Metal Film Resistor	MF 1/2	350 V	700 V	1/2 W
R2 - R11	680 k $\Omega$		MF 1/4	250 V		1/4 W
R12	200 k $\Omega$		MF 1/4	250 V		1/4 W
C1 - C3	10 nF	High Voltage Ceramic Condenser	DD1464E103P500	500 V		
C4	4.7 nF		DEBE33F472ZA3B	3150 V		

Figure 13: Parts list.



Figure 14: A photograph of a PMT with the PMT base.

**Test of the PMT base** A circuit diagram of a PMT base is shown in Fig. 10. The PMT base is composed of 12 metal-film resistors (R1 - R12), 4 ceramic capacitors (C1 - C4) and a glass-epoxy P. C. board. R1 - R11 are connected in series seen from the high voltage input. The input high voltage is mainly divided by R2 - R11 since R1 has quite low resistance as compared with other resistors. R2 - R12 are the same. A photomultiplier tube (PMT) has 11 leads as shown in the figure. The divided high voltages are severally supplied to 10 leads of them, and the remaining one is the output terminal of the signal. R12 takes the output over the ground for protection. R1 is also a protector. C1 - C3 keep the divided voltage ratio between leads of a PMT in the case of the high signal rate, and C4 works as a noise canceller. Semi-flexible leads of the PMT are installed to the PMT base by soldering directly. The PMT base has been tested for three properties: (a) electric non-conductance of the P. C. board, (b) the idling current and (c) the long-sustained stability.

(a) Electric non-conductance of a P. C. board

The electric non-conductance of a P. C. board is the very important requirement for operation of a circuit under high voltage since a leakage current which flows on a P. C. board sometimes causes the serious problems. Conditions of the electric non-conductance are shown as follows. For the test, all leads of a PMT were disconnected and all of resistors and capacitors were removed from the P. C. board. During a one-hour test, the current that flows on a P. C. board were kept at less than 0.0 microamperes (the minimum range of a measuring device), and no smoke, no heat and no electric spark were detected on the P. C. board.

Test conditions

Date: 21 April, 2003.

Temperature: 22 degrees C.



Humidity: 47 Operating voltage: - 3246 V.  
 High voltage module: RPH-30 No.023.  
 Current measuring device: HP-2378A-3531J26561.

Test results for one hour:

Measured current: less than 0.0 microamperes.  
 No smoke, no heat, no spark were detected.

(b) Idling current

From the test results of electric non-conductance of the P. C. board, the current and power consumption of a PMT base can be estimated by the input voltage and the value of resistors in the series connection. The measured currents were compared with estimated values. All PMT leads were disconnected from the PMT base.

Test conditions

Date: 21 April, 2003.  
 Temperature: 22 degrees C.  
 Humidity: 47 Operating voltage: from - 1000 to - 3247 V.  
 High voltage module: RPH-30 No.023.  
 (A current is also measured by a current-meter of the high voltage module.)

Operating voltage [V]	Idling current [ $\mu$ A]	Comments
-1000	304	Typical operating voltage of the PMT
-1500	457	Maximum operating voltage of the PMT
-2000	609	
-2500	762	
-3000	914	
-3247	989	Maximum output voltage of the H. V. module

Figure 15: Idling current.

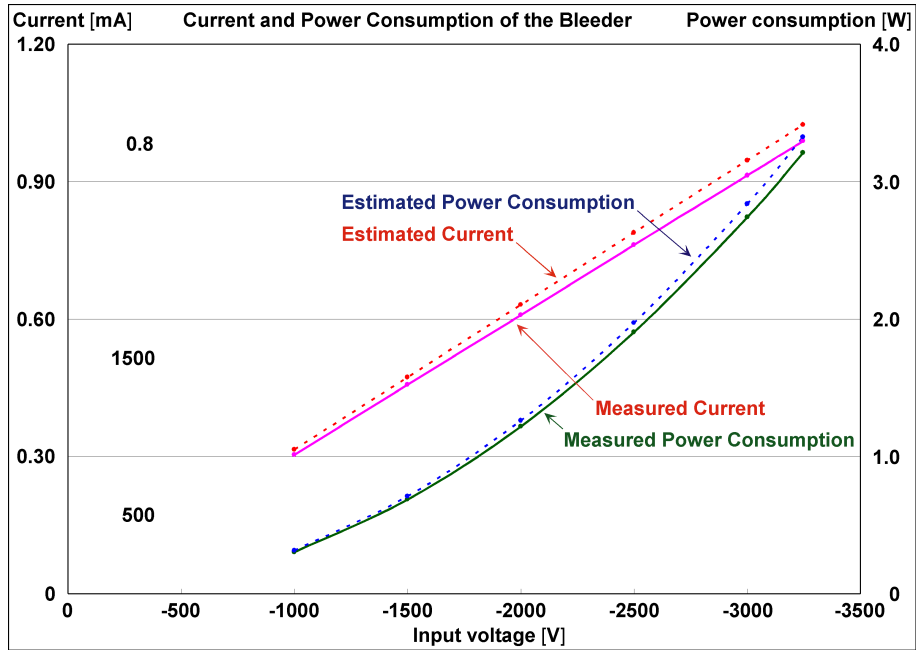


Figure 16: Idling current and power consumption of a PMT base.

(c) Long-sustained stability The stability of a PMT base has been checked during a 6-hour test. For the first one hour, 2500 volts were supplied to the PMT base. After that, the supply voltage was raised to 3200 volts and kept there for 5 hours. The current that flowed through the PMT base was quite stable for 6 hours as shown in Fig. 17, and no smoke, no heat and no electric sparks were detected

Test conditions:

Date: 03 March, 2003.

Temperature: between 21.2 and 21.4 degrees C.

Humidity: 31

Test results

Idling current remained constant.

(767 micro A at 2500 volts)

(989 micro A at 3200 volts)

No smoke, no heat and no spark were detected.

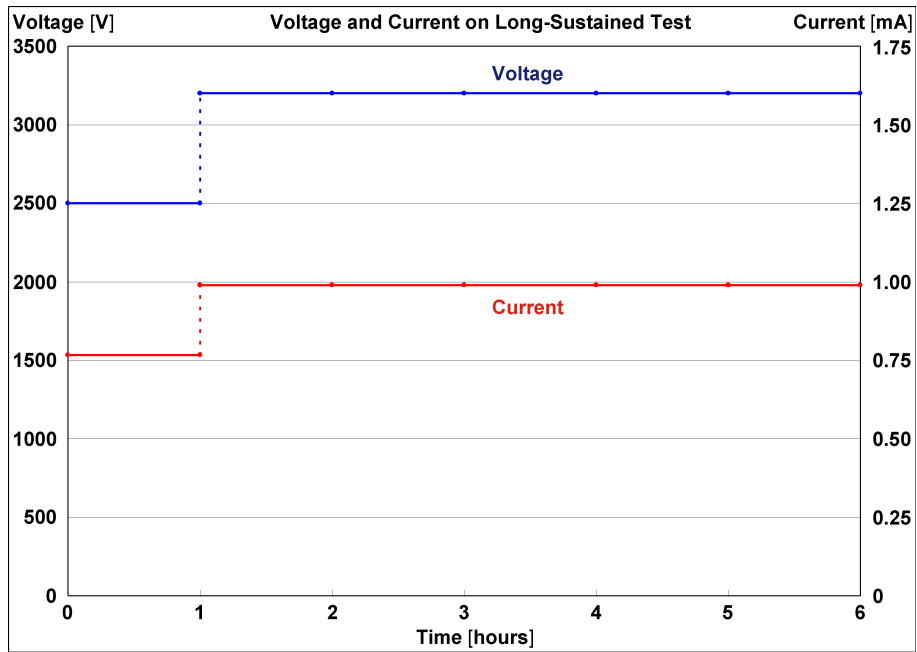


Figure 17: Long-duration stability of the PMT base.

### 2.1.4 Mu-metal Shield for PMT

**magnetic field at aerogel counter** The magnetic field in the space between PC2 and PC3 at W1 sector on the West carriage where the aerogel counter will be installed was measured on Feb./26/2003, 9A.M. The magnitude was from 2G to 8G.(Table3) The measurement was done by insertion a probe when the PHENIX Central Magnet was on full field.

PC2-side (inner) [Gauss]						
	South			North		
	edge	Middle	z=0	z=0	Middle	edge
Top	6.9	2.3	4.5	3.8	7.9	7.5
Middle	7.0	3.2	5.1	3.8	7.8	7.7
Bottom	6.1	2.8	4.5	3.9	6.9	7.6
PC3-side (outer) [Gauss]						
Top	6.8	1.9	2.8	2.9	4.4	4.8
Middle	5.6	1.6	2.1	2.2	4.5	4.3
Bottom	5.3	1.6	1.9	2.1	3.9	4.2

Table 3: Integrated magnetic field strength,  $|B|$ , between PC2 and PC3 on the west where the aerogel counters will be installed.

**Measurement condition** In order to test the performance of mu-metal shields for PMTs, we employed a Helmholtz coil. The radius of the Helmholtz coil is 17.5 cm. Figure18 shows the magnetic field distribution between the coils. The x axis is along the direction from one coil to the other. While  $|B|$  is 10.0 Gauss at the center of Helmholtz coil  $(x,y,z)=(0,0,0)$ ,  $|B|$  in the area which is approximately 5cm from the center is  $10.0 \pm 0.5$  Gauss. When the mu-metal shields were tested using the Helmholtz coil, the photocathode of the PMT was placed at center of the Helmholtz coil. Thus the magnetic field at the PMT location was sufficiently uniform for following shield measurements. The value of the PMT high voltage during the measurement was -1500 V. Number of photoelectrons was around 20 using LED to emit light to PMT photocathode. Number of photoelectrons,  $n$ , was calculated from Poisson fit to ADC distribution by following equation.

$$P(n) = \frac{(\bar{n})^n}{n!} \exp(-\bar{n}) \quad (2)$$

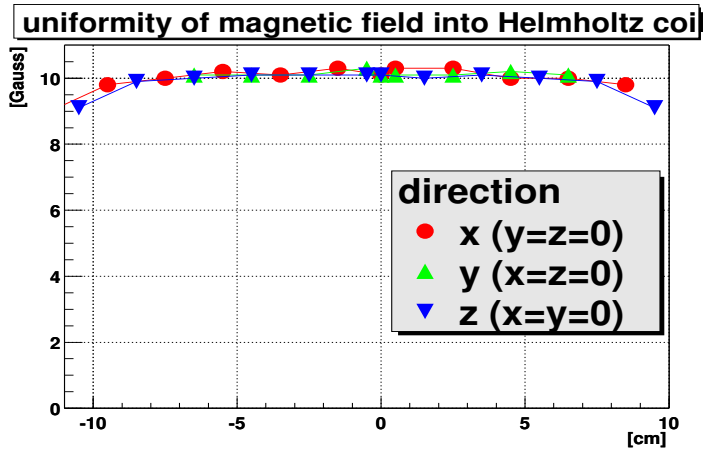


Figure 18: Position dependence of the B-field in the Helmholtz coil.  $(x,y,z)=(0,0,0)$  is the center.

**Shield test** Since the magnitude of magnetic field at PHENIX is 2-8 Gauss, we tried to get a shield which protects PMT up to about 15 Gauss. Using the Helmholtz coil, the performance of the shields was tested under various magnetic field strengths. The direction of the field for these tests is defined by Figure 19. First, the PMT was tested without any mu-metal shields (Figure 22 - Figure 25). The ADC output normalized at 0 Gauss goes to 20% at 4 Gauss vertical B-field. It is obvious that the PMTs needs some shielding from Phenix's magnetic field. Next, three different length (4cm, 8cm, 12cm)

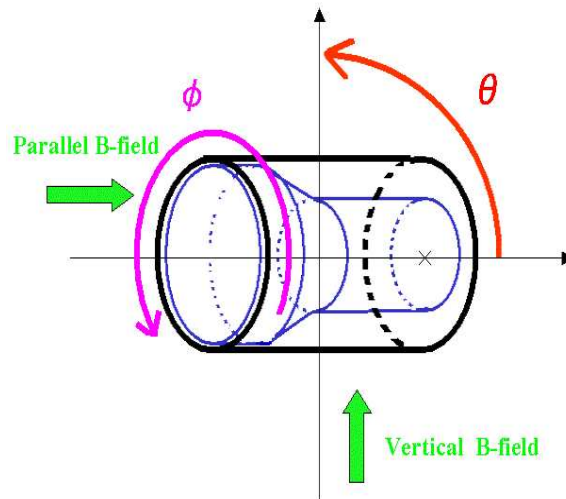


Figure 19: Definition of the direction to PMT

× two different thickness (0.2mm, 0.5mm) of mu-metal shields were tested. Compared

with the number of photoelectrons, the normalized ADC at 0 Gauss decreases at smaller magnetic field. Namely, the number of photoelectrons goes down after the gain of PMT begin to decrease while increasing magnetic field (Figure 20 - Figure 21).

The results in Figure 20 - Figure 25 can be integrated into following two statements. One is that 4cm-length shield insufficient even at the 0.5mm thickness. The other is that 0.2mm-thickness shield does not provide sufficient shielding even when the length is 12cm. In order to get enough shielding against a 15-Gauss B-field, 8cm-length  $\times$  0.5mm-thickness are necessary. Especially pointing out number of photoelectrons, 8cm-0.5mm shield is almost holding the number until 15 Gauss even the rate of ADC normalized at 0 Gauss slightly going down.

More studies on the 8cm-length  $\times$  0.5mm-thickness shield were done. First, the PMT was tested in fields is from zero to 40 Gauss (Figure 26). The results show that the ADC output decreased by half at 20 Gauss. Secondly, measurements were done with the PMT at various angles  $\theta$  to the magnetic field, see Figure 19. The test results show that the shield works effectively at any angle (Figure 27 - Figure 28). Moreover, rotating PMT in the  $\phi$  direction was tested, see Figure 19. The shielding does not change appreciably under PMT rotation. Therefore, a mu-metal shield which has 8cm-length and 0.5mm-thickness was selected for the aerogel counter PMTs.

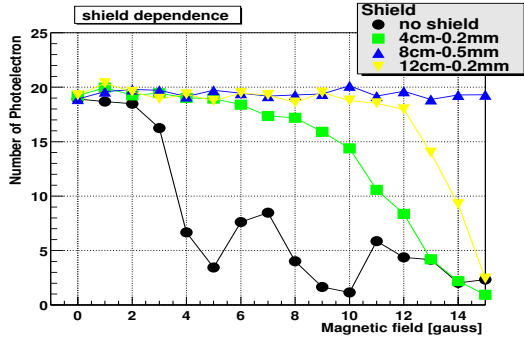


Figure 20: Number of photoelectrons on vertical B-field.

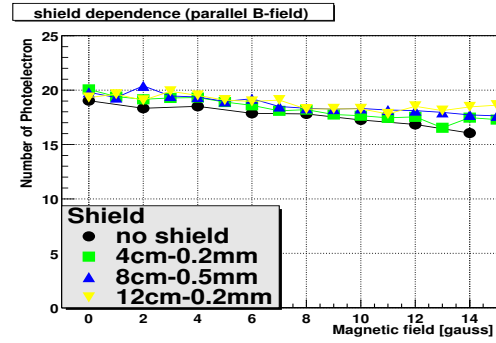


Figure 21: Number of photoelectrons on parallel B-field.

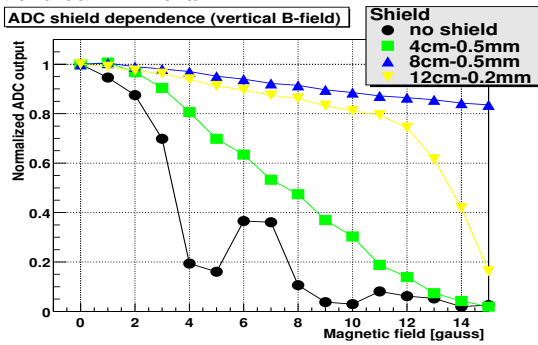


Figure 22: Normalized ADC output at  $|B|=0$  on vertical B-field.

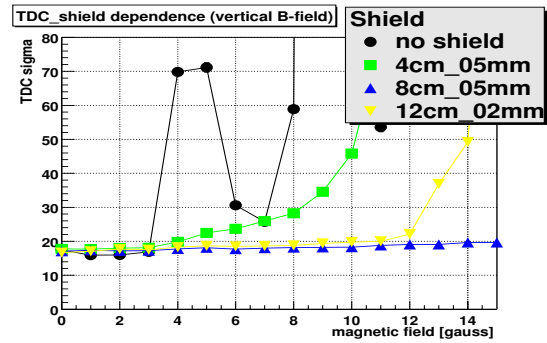


Figure 23: Sigma of TDC on vertical B-field.

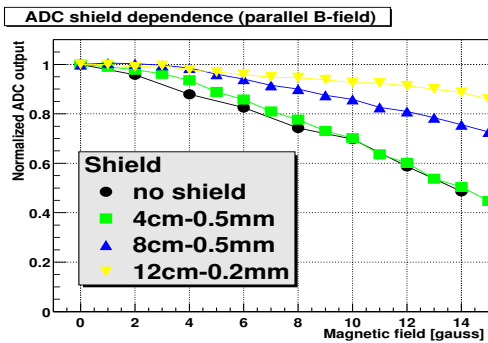


Figure 24: Normalized ADC output at  $|B|=0$  on parallel B-field.

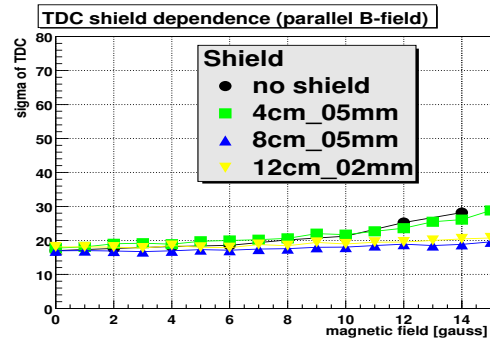


Figure 25: Sigma of TDC on parallel B-field.

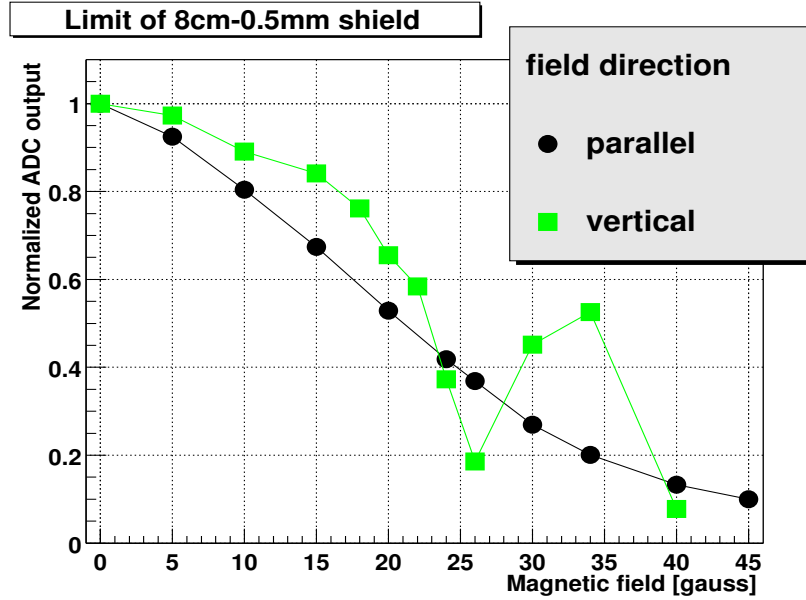


Figure 26: Normalized ADC output at 0 Gauss on vertical and parallel B-field.

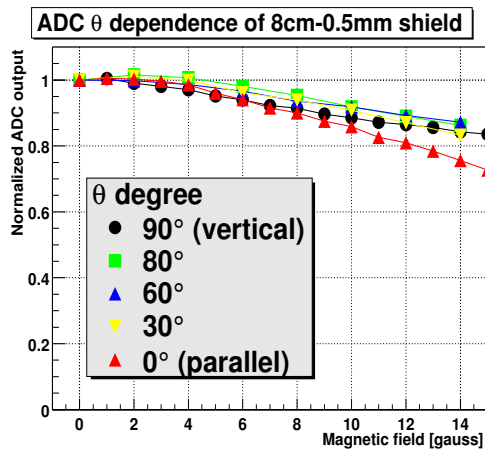


Figure 27: Normalized ADC output at 0 Gauss at several angle w.r.t. the B-field.

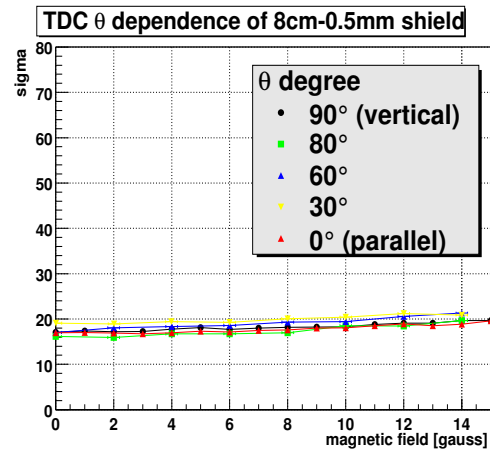


Figure 28: The TDC sigma under several angles w.r.t. the B-field.



### 2.1.5 Reflector

**Reflector Selection** The inner surface of the counter box should be covered with highly reflective material, since most photons may undergo numerous reflections prior to reaching the photocathode. In order to select the best reflective material for Cherenkov light collection, we tested 8 samples (Goretex, Lumirror, Tyvek, Tetratex, Millipore, Aluminized mylar, Black paper) during the beam test. Using the exponential behavior of Belle type (the aerogel tiles are contained in a diffusion box viewed by two PMTs, attached directly on the surface of the aerogel at the both sides), we compared the light collection efficiencies of the samples. The measurement results are summarized in Table 4. The number of photoelectrons ( $N_{pe}$ ) and the attenuation length ( $N_{pe}$  decreases exponentially with the distance from PMT. the length is the slope of that function.) correspond in light collection. Goretex sheet is found to have the highest light of all reflector materials tested. The light yield at the center was improved by a factor of 6 (from “Black paper” to “Goretex”). (For detailed information of Goretex, see the next section.) We will use the Goretex sheet as a real reflector. For any counter geometries, reflector material was an important component of the light collection system.

Reflective material	Thickness [ $\mu\text{m}$ ]	$N_{pe}$ for light velocity particles	Attenuation length (cm)
Goretex	430	28	6.6
Lumirror	190	24	6.8
Tyvek (double layers)	260	23	6.2
Tetratex	200	22	6.1
Millipore	160	20	-
Tyvek (single layer)	130	17	5.2
Al mylar	100	14	4.8
Black paper	210	5	2.0

Table 4: Comparison of the tested reflectors.

**Properties of GORETEX** The DRP reflector (we call “Goretex” simply) is a porous, polytetrafluoroethylene (PTFE) sheet (Manufacturer: W.L.Gore & Associates, Inc.). Due to the microporous structure, high reflectance and high diffuseness can be achieved. Light reflects and refracts from fiber to fiber within this structure.

The reflectance of Goretex sheet material was measured as a function of wavelength using a reflectance spectrometer. We checked the effect of backing material on reflectance.

The result (relative to the reflectance of Spectralon) is shown in Figure 29. The results show that the reflectance is mostly independent on the backing material, from 250 nm to 800 nm. The sensitive range of the R6233-PMT is from 300 nm to 650 nm. In the UV region, the reflectance increases slightly. Referring to the absolute reflectance curve, Figure 30 [1], the total reflectance is estimated to be more than 99 % over the wavelength interval.

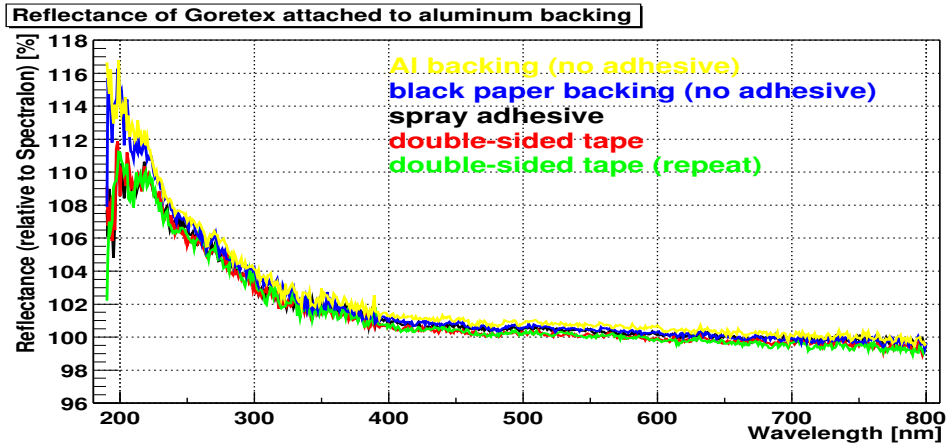


Figure 29: Reflectance of Goretex attached to aluminum backing

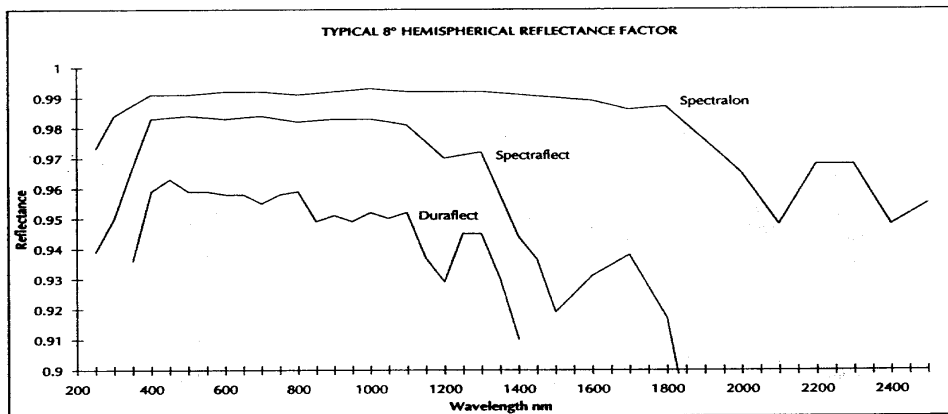


Figure 30: Reflectance of Labsphere Spectralon

Other properties are summarized in Table 5 [2]. Goretex is also radiation hard up to 8.6 Mrad equivalent dose w.r.t. reflectance in the visible range between 425 - 675 nm [3].

Property	Value
Thickness	0.5mm
Thermal conductivity	0.04W/m/K
Water resistance	Highly hydrophobic
UV Exposure	UV-resistant
Dimensional shrinkage	<1%
Durability	Inert, stable

Table 5: Other properties of Goretex

## References

- [1] Labsphere “Reflectance Materials” from Spectralon product Catalog.
- [2] W.L.Gore & Associates, Inc., Product information for DRP Reflector
- [3] S.K. Sahu et al., Nucl. Instr. and Meth. A 384 (1997) 544.

### 2.1.6 Box

The aerogel detector consists of detector cells covering the surface of about  $4 \text{ m}^2$ . The following factors have to be taken into account for the design of the detector cell:

1. the shape of the cell should be such that a wall can be constructed from them with as little dead space as possible;
2. the size of the cell was limited by the following items:
  - by the size of PMT;
  - by the acceptable occupancy of the cell;
  - by size of the available space in the West arm; the way of the secondary particles;
  - by the sizes of produced aerogel pieces. In principle it is possible to cut these pieces, but this is difficult and would lead to additional expense.
3. the aerogel detector should have as small a radiation length as possible;
4. efficiency across the detector surface should be uniform;

The integration-cube type detector cell was chosen as a solution. A photograph of the box is shown in Fig. 31 and drawings of the box are shown in Fig. 32.



Figure 31: View of a box.

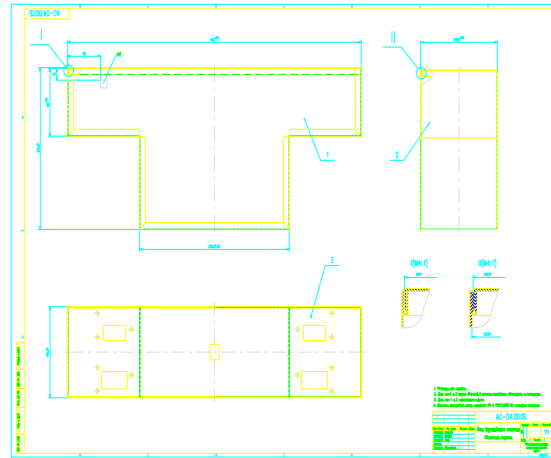


Figure 32: Box drawings.

The box must provide the light protection, provide support for PMTs and protection of the fragile aerogel radiator. After some studies it was found that box itself would be fabricated from aluminium alloy 1530 of 0.5 mm thickness. The lid is fabricated from aluminium alloy 1520 with 0.8 mm thickness. The elemental composition of these alloys are shown in the table.

	content of shown element in %								
alloy	Al	Cu	Mg	Mn	Si	Fe	Zn	Ti	Cr
1520	95.5 – 98	<0.1	1.8 – 2.6	0.2 – 0.6	< 0.4	< 0.4	< 0.2	< 0.1	< 0.05
1530	94.65 – 96.5	<0.1	3.2 – 3.8	0.3 – 0.6	< 0.5	< 0.5	< 0.2	< 0.1	< 0.05

The technology choice for the assembly of the boxes was between epoxy gluing and spot welding. Assembly with epoxy glue provides sufficient strength and light protection. Spot welding does not provide sufficient light-tightness and leads to small deformations. Therefore gluing was chosen for the box assembly.

Prototypes of the boxes were delivered to PHENIX for testing of aerogel cells during p-p part of RUN03.

As alternative cell construction option was the so-called double size box (a box containing two aerogel counters), and some were built.

However, to avoid cross-talk between the two counters situated in the same box, the single-size box was chosen.

An estimate of the radiation thickness of one cell is shown below (calculations are done for a cell with cross section ( $45 \times 12 = 540 \text{ cm}^2$ )) :

- Box(Al) – 500g
- PMT 6233 - 190g x2 – 380 g
- Magnetic shield – 180g x2 – 360 g
- Socket assembly – 156g x2 – 312 g
- PMT-connector to – 170g x2 – 340 g
- totally – 1890 g

The reduced length of one cell is at about  $3.5 \text{ g/cm}^2$  or 0.16 radiation length. Any particle from the event will cross two cell, and total thickness of aerogel detector can therefore be estimated to be 0.3-0.4 radiation length. The contribution in this value from box itself can be estimated as  $< 30\%$ .

**Test of the Cherenkov aerogel counter** A prototype of the Cherenkov aerogel counter was tested at the  $\pi^-$  and  $\pi^+$  secondary beams with momentum  $2.2 \text{ GeV}/c$  produced by proton on Be target during 25-27.06.2003 run at the SPHERE-setup (LHE, JINR).

The purpose of this measurement was:

1. additional test of the position dependence of the number of photoelectrons ( $N_{pe}(X,Y)$ ) across the working aperture of the counter;
2. the measurement of the response of the PMT to direct hits with beam particles (pions and protons);

3. the estimation of  $N_{pe}(X,Y)$  for subthreshold protons;
4. the estimation of the background deposit of Cherenkov's signals from interactions of pions and subthreshold protons with integrating box materials;

Matsushita aerogel type SP-17 ( $n=1.017$ ) was used for tests. For the measurements of coordinate dependence, scintillation hodoscopes were used with resolution 10 mm in Y (vertical, perpendicular to the beam and line connected two PMTs) and X (horizontal).

The obtained results can be explained as following:

1. the average  $N_{pe}$  is 20pe (for PMT1+PMT2). This number is practically independent of X and Y, see Fig.33;
2. the PMT response to direct particle hits, by visible (2-3 times) and strong (10 times) increase of  $N_{pe}$  (Figs.34-35 respectively);
3. the subthreshold protons with  $P=2.2\text{GeV}/c$  give an average  $N_{pe}=0.41$  (R.M.S. =0.15) for PMT1+PMT2.
4. the background Cherenkov's scintillation of pions and the subthreshold protons with integrating box materials give  $N_{pe}=1.96$  (R.M.S.=0.68) and  $N_{pe}=0.71$  (R.M.S. = 0.14) respectively (PMT1+PMT2).

**Present status of the Box production** By 21 July 2003 more than 60 boxes were fabricated. The tests for light-tightness are in a progress now (see Fig.36). In Fig. 37, boxes are being prepared for shipment to BNL.

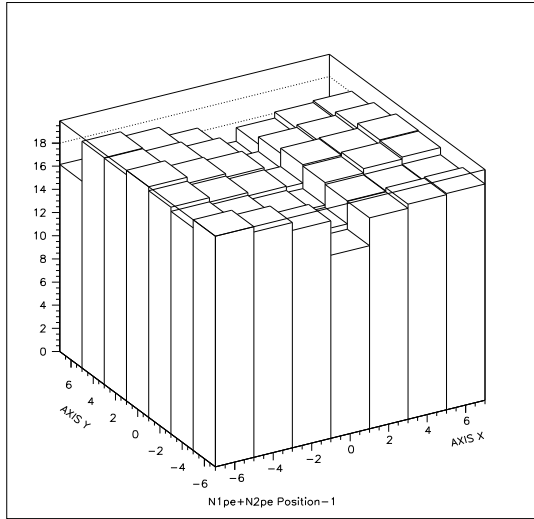


Figure 33: Response vs. hit position of the aerogel Cherenkov counter.

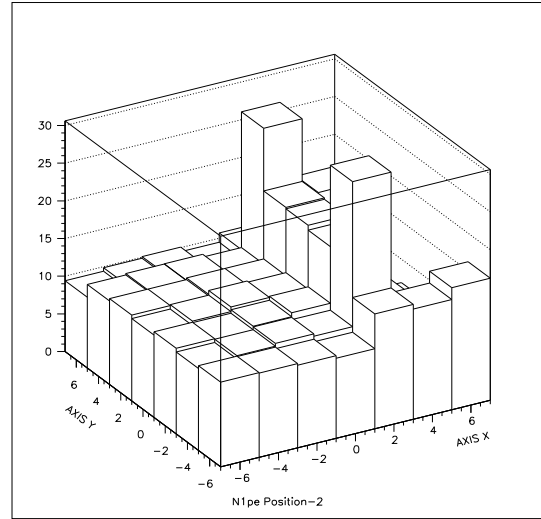


Figure 34: The effect of particles passing directly through the PMT. The PMT's window is situated at  $X = 2$  cm and particles were moving parallel to this window.

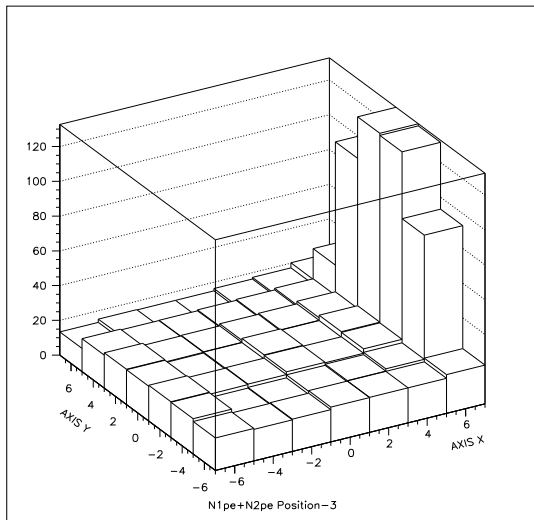


Figure 35: The effect of particles passing directly through the PMT. The PMT's window is situated at  $X = 6$  cm and particles were moving at an angle of about 20 degree.



Figure 36: Testing and improving the box light-tightness.



Figure 37: Boxes being prepared for shipment to BNL.



### 2.1.7 Connectors on Box

There are five connectors on the lid of an Aerogel box. Two of them are signal connectors from photomultiplier tubes (PMTs) and the other two are used for supplying high voltage to PMTs. The remaining one is connected to an LED in the box for calibration. All of connectors have approved flammability ratings such as UL 91V-0 and UL 94V-0. Signal connectors, high voltage connectors, LED connectors are 2-pin Universal MATE-N-LOK, 3-pin Universal MATE-N-LOK and 2-pin Mini-universal MATE-N-LOK series, respectively, produced by Tyco Electronics Corporation. The same type of signal connectors is used for the EMCAL in PHENIX.

**Signal connector** The signal connectors that are connected to PMTs in the box are 2-pin soft-shell connectors. They are composed of a 2-socket right-angle header, a plug housing and its contacts. The connectors are black in color. The material of the header and the housing is Nylon and it has approved flammability ratings of UL 91V-0 or UL 94V-0. The contact pin is made of Phosphor-Bronze and its mating area is plated with Tin. A seal protector made of silicon rubber is used in order to release a strain of the cables at the edge of connectors and to protect the inside of the connector from water and dust. The maximum operation voltage and the maximum current of signal connectors are 600 volts and 19 amperes, respectively.

A set of signal connectors is composed of following five parts (see Appendix B).

643226-1 : 2-Circuit Socket-type Right-Angle Header (Black color).

350777-1 : 2-Circuit Plug Housing (Black color).

350690-3 : Pin Contact (24-18AWG) for 350777.

350547-3 : Pin Contact (20-14AWG) for 350777.

794270-1 : Seal Protector for 350777.

**High voltage connector** The high voltage connectors are the same type as signal connectors mentioned in above section with exception of the number of pins. High voltage connectors have 3 pins in a line and it skips the center pin, i.e. the outside 2 pins are used for supplying the negative high voltage and the ground. High voltage connectors have flammability rating UL 94V-0. The contact material is Phosphor-Bronze and its mating area is plated with Tin, the same as the signal connectors. In order to prevent from misconnection between signal connectors and high voltage connectors, the color of high voltage connectors would be white, contacts of the high voltage header are the pin-type, and a shape of their mating areas is different. Although the maximum operating voltage between each pin pairs and the maximum current to flow per pin are 600 volts and 19 amperes, respectively as specified on the data sheet, the production company guarantees that these connectors are able to withstand operation up to 5 kV in the case of small currents such as driving a PMT base.

A set of high voltage connectors is composed of following five parts (see Appendix B).

1-350943-0 : 3-Circuit Pin-type Right-Angle Header (White color).

350766-1 : 3-Circuit Sealable Plug Housing (White color).

350689-3 : Socket Contact (24-18AWG) for 350766-1.  
350550-3 : Socket Contact (20-14AWG) for 350766-1.  
794272-1 : Seal Protector for 350766-1.

**LED connector** In addition to two signal connectors and two high voltage connectors, one small connector is put on the lid of the Aerogel box for calibration using a blue LED. The connector type is Mini-universal MATE-N-LOK produced by Tyco Electronics Corporation. shell of the connectors is Nylon that has approval of a flammability rate of UL 94V-0. A material of contacts is Brass and its mating area is plated with Tin. On the other hand, the 2-pin right-angle header has contacts made from duplex Brass. The maximum operating voltage and the maximum current are 600 volts and 9.5 amperes, respectively.

A set of LED connectors is composed of following three parts (see Appendix B).

770966-2 : 2-Circuit Pin Right-Angle Header (White color).  
172165-1 : 2-Circuit Plug Housing (Natural color).  
170364-1 : Pin Contact (22-18AWG).

## 2.1.8 LED Calibration System

The Aerogel detector has one LED in each box in order to calibrate the photomultiplier tubes (PMTs). A block diagram of the system is shown in Fig. 38. PPG, GTM and LVPS are the programmable pulse generator, the granule timing module and the low voltage power supply, respectively. The calibration system is composed of 1 PPG, 3 drivers, 20 dividers, 160 LEDs and some signal cables. The LED is located on the side of one PMT and is used for calibration of both PMTs in the box. First, the PPG makes a synchronized TTL signal with the granule timing. Then the driver amplifies the TTL signal for its 8 output channels. Moreover, one output signal from the driver is divided across 8 lines by a divider that is composed of resistors. Each of the five signals from the divider are led to five LEDs by one cable with five twisted-pair lines. Thus one driver drives 80 LEDs at the same time. The pulse width and a height of the output signal are determined by the TTL signal from PPG and variable resistors on the driver board, respectively. The LED intensity can be varied by software and hardware. During bench tests of the driver board, a TTL signal with a pulse width of about 30 ns produced a PMT signal equivalent to 10 photoelectrons. on one PMT.

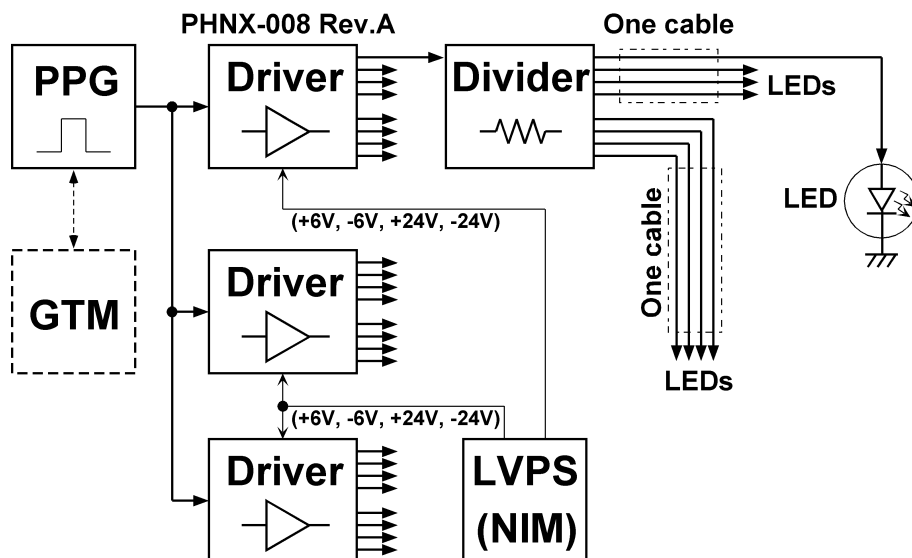


Figure 38: A block diagram of the calibration system using LED.

**Driver** The LED driver for the calibration system of Aerogel detector is the same as the PHENIX TTL driver, PHNX-008. The driver has 8 output connectors (Lemo) and 2 input connectors (Lemo). It is possible to trigger the circuit by positive and negative TTL signals. The pulse width of output signals is determined by the width of the input TTL signal. On the other hand, the pulse height of output signals can be varied arbitrarily. Each output channel has two 10-turn variable resistors on the board for controlling the

high level and the low level of the output pulse separately. The main chip of the driver is an AD811, capable of driving 100 mA at up to +12 volts on each channel. It needs low voltages of +6, -6, +24, -24 volts and the NIM crate is suitable for this requirement. A circuit diagram of the driver is shown in Fig. 39.

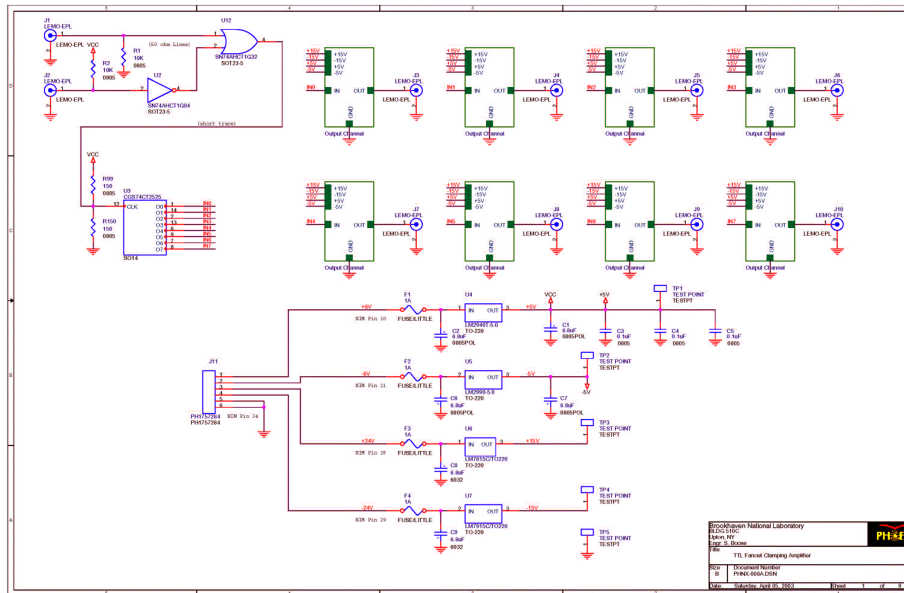


Figure 39: A circuit diagram of the LED driver.

**Divider** The divider is composed of resistors and connectors as shown in Fig. 40. The input and output connectors are Lemo and Category-5 network connectors, respectively. The input signal is divided to five signals by resistors. No power supply is required for its operation.

**LED** The calibration system uses blue 160 LEDs that have intensity of 665 mcds under the forward direct current supply. A peak wavelength is about 468 nm. The diameter of the LED is 3 mm and it has clear body. Specification of the LED is shown in Fig. 41 It consumes about 20 mA under forward voltage of 3.4 volts.

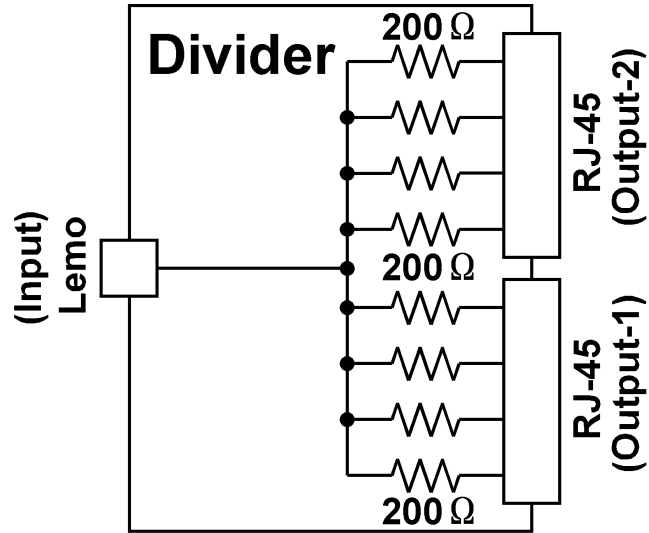


Figure 40: A circuit diagram of the divider.

<b>Type</b>	<b>E1L33-3B</b>
<b>Product company</b>	<b>Toyoda Gosei Co., Ltd</b>
<b><math>\lambda_p</math> [nm]</b>	<b>468</b>
<b>D [mm]</b>	<b>3.0</b>
<b><math>I_v</math> [mcd]</b>	<b>665</b>
<b><math>V_f</math> [V]</b>	<b>3.4</b>
<b><math>I_f</math> [mA]</b>	<b>20</b>

Figure 41: Specification of the blue LED.

### 2.1.9 Gas Flow

**Purposes** The purposes of gas flowing are as follows:

1. Purging outgas  
The aerogel which will be used is hydrophobic. However, the aerogel might still be damaged by the outgassing of the chemicals in the box. For protection of the aerogel, purging of these gases is necessary.
2. Non-flamability  
Nitrogen gas excludes the components from burning while the gas is flowing.
3. Cooling  
Because of the small power dissipation of the PMT base, gas flow is not necessary for cooling. (See Appendix A) for heat load measurements and calculations.)

**Requirements** The requirements for the gas system are as follows:

1. Gas delivery system  
The system consists of 160 cells. Groups of 10 cells are connected in series to form a chain, and 16 chains are connected in parallel. Each cell has inlet/outlet connectors at the ends. Gas inside the cell flows through the small gap between the PMT and the inner box, and into the integration cube.  
It is necessary to flush out the air with nitrogen before turning high voltage on, to reduce the effect of the air's humidity.
2. Clean gas  
The gas should be clean and dry in order to maintain clean surfaces on the aerogel tiles and the reflector sheets. Light collection performance will be damaged by any dust accumulation on these surfaces.
3. Light and air tightness  
The gas tubes and connectors should be light and air tight. The color is mat black. One option is to have a piece of tube (pig-tail) on the inside which is black.
4. Flow rate  
The flow rate will be relatively low, just enough to purge the volume. Adequate purging time is 3~4 hours, that is, a maximum of ~200 liters per hour is needed. We may decide to have a bit more as a reserve to compensate for gas leakage from the boxes.

Type of Gas	dry and clean Nitrogen ( $N_2$ )
Pressure	ambient air pressure
Flow Rate	800 liters per hour (temporary)
Gas Volume	688 liters
Hazards	Non-flammable

Table 6: Requirements of the gas system

### 2.1.10 Performance

**Beam Test** A number of prototypes were tested in beam lines pi2 and T1 at KEK-PS. The prototypes were configured with different refractive indices of aerogel, arrangement of aerogel tiles, reflective materials, number, kind and location of the photomultipliers. The aim of the beam tests was to understand the design factors in order to optimize the light yield, uniformity of response and to estimate backgrounds. Based on these beam test results, we optimized the final design of the counter.

The beam composition in the test beam was mainly pions and protons, in the momentum range 0.3 - 2.0 GeV/c. Particle separation was obtained by applying the proper cuts to the TOF spectrum, and to correlated response between two gas Cherenkov threshold counters. Figure 42 shows a scatter plot of pulse height from an aerogel counter versus TOF value at 2.0 GeV/c. The refractive index of aerogel is 1.011. From the differences of TOF, particles can be identified. Clear particle separation is demonstrated.

Typical pulse height spectra for 2.0 GeV/c pions and protons are compared in Figure 43. Pions (above threshold) and protons (below threshold), being identified by TOF, show clear difference in the aerogel. Pions show a clear signal while protons give mostly pedestals and low-rate single photoelectrons. With the beam composition at the test beam, the pion identification efficiency is 99.5 % and fraction of protons being misidentified as pions is 0.5 %, with the threshold set at 1.5 p.e.

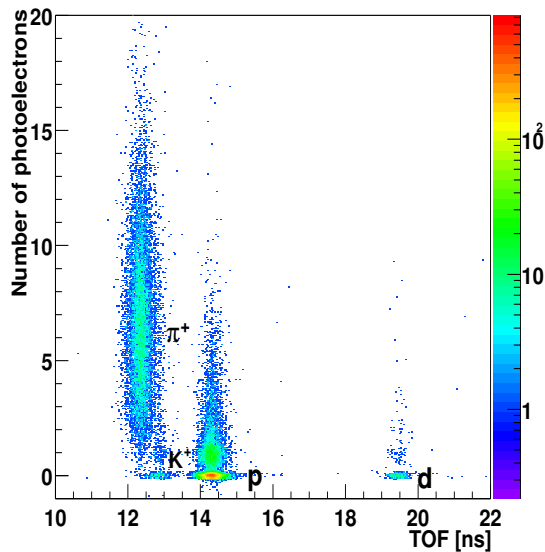


Figure 42: Scatter plot of pulse height per PMT versus TOF at 2.0 GeV/c. The particle identity can be deduced by the TOF differences ( $\pi^+$ ,  $K^+$ , p, d, from left to right).

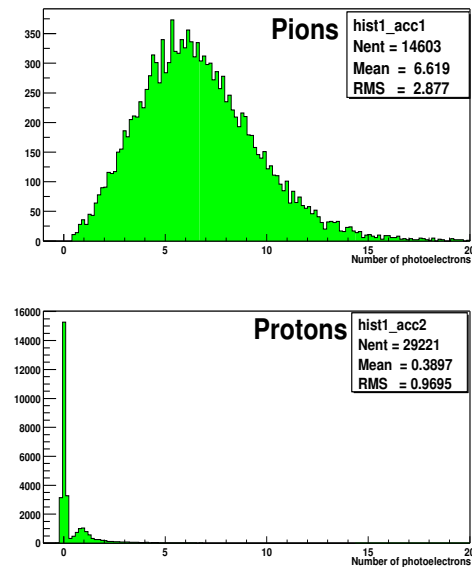


Figure 43: Pulse height spectra in units of photoelectrons from one PMT for 2.0 GeV/c pions (above threshold) on the top and protons (below threshold) in the bottom.



Light yields were measured by changing the momentum of the incident pions which was incident onto the center of the aerogel volume. The refractive index of aerogel was 1.017. Figure 44 shows the result of the measurement. When the beam polarity was changed, almost the same values were obtained and plotted in the same figure. The dependence of light yield on momentum is well described by the theoretical curve. This consistency ensures that the light we measured originated from the Cherenkov radiation.

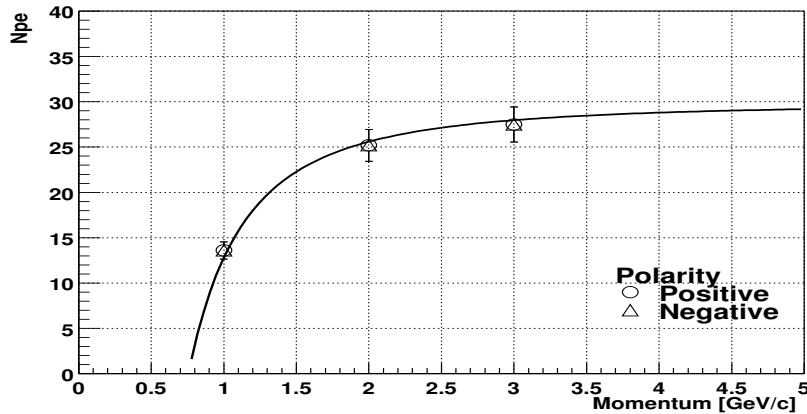


Figure 44:  $N_{pe}$  for pions versus momentum (Belle type,  $n=1.017$ ). The curve represents the theoretical fit.

**Integration Cube Type** Figure 45 shows a schematic drawing of the final prototype. Cells are covered with mylar-Goretex laminate, where the Goretex is highly reflective and diffusive material. Each set of aerogel cells is then loaded into each Aluminum box.

Light coming out of the aerogel is integrated in the air space behind it called “integration cube”, and detected by two PMT’s. Having the integration cube behind the aerogel, unscattered cherenkov light as well as light scattered in the aerogel has a good chance of reaching one of the PMTs. The arrangement using this ‘integration cube’ is found to be effective in producing a uniform response of the detector with respect to incident position of the particles.

Figures 46 ~ 49 show light yield uniformity of the Integration Cube type. Light yield per PMT varies less than 40% over the cell surface, while the total light yield stays constant within 10%. The dip in the distribution at the center in Figure 46 is due to the gap between aerogel tiles. Figure 47 however has clear peak at the center. This is explained as direct hits on the calibration LED. (At the momentu of Figure 5, the LED was not installed.) For the actual experiment, the LED will be placed in the corner.

During the assembly of Integration Cube type counters in the PHENIX detector, the units will alternately face forward or backward, see Fig. 2. This is done in order to minimize dead space between aerogel, and to have the aerogel volume in one plane at the same radius. In this configuration, particles enter backwards-facing cells in the reverse

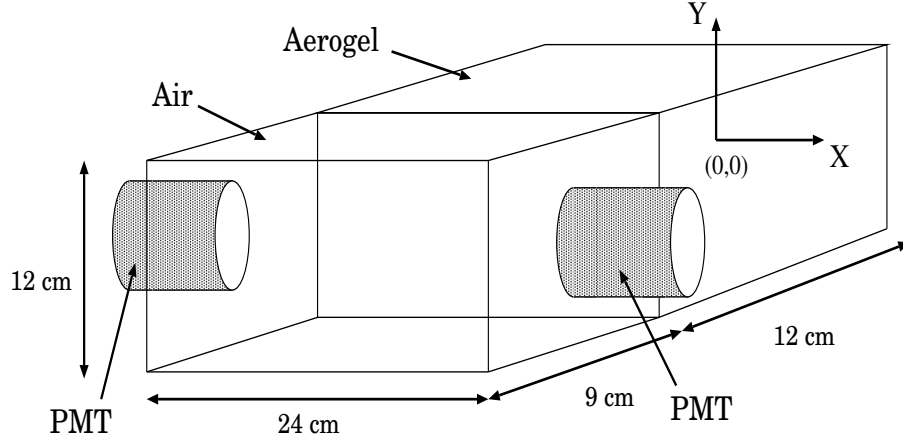


Figure 45: Schematic drawing of Integration Cube type.

direction. We observed less than 10% difference between two cell orientations: PMTs downstream or upstream (Figure 50). This rather small difference suggests that most of photons in the integration cube do not have directionality already, which is again consistent with the diffusive optical property of the aerogel.

Light yield dependence on the aerogel block cross-section and thicknesses is summarized in Table 7. In the final design the depth of aerogel is set to 12cm, the lateral cell size set to double the aerogel tile size ( $11 \times 22 \text{ cm}^2$ ).

Cross Section ( $X \times Y, \text{cm}^2$ )	Aerogel [cm]	Integration [cm]	$N_{pe}$ (PMTs downstream)	Attenuation Length [cm]
15 x 15	12	12	17	67
15 x 15	12	9	18	44
15 x 15	9	9	15	44
15 x 15	9	6	13	32
22 x 12	12	9	15	38
22 x 12	9	9	13	28
22 x 12	8	13	13	42

Table 7: Combination test of cross-sectional size and thicknesses (Aerogel, Integration cube) of the cell.

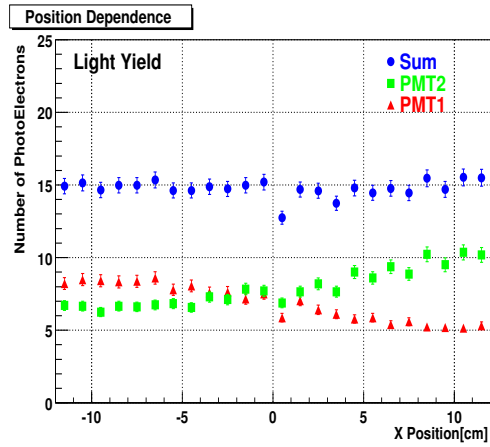


Figure 46: Position dependence of  $N_{pe}$  as a function of  $x$  at  $y = 0$  cm (PMTs downstream).

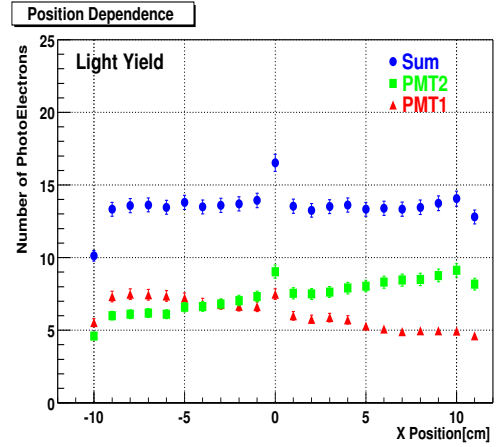


Figure 47: Position dependence of  $N_{pe}$  as a function of  $x$  at  $y = 0$  cm (PMTs upstream).

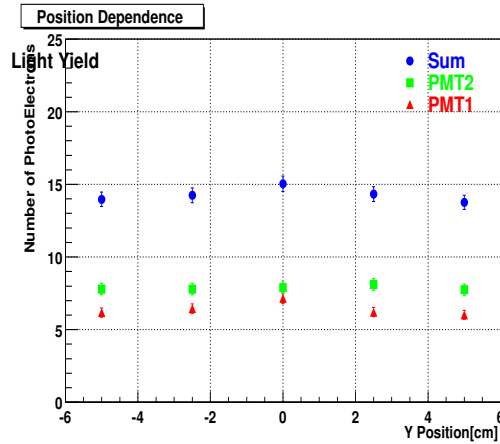


Figure 48: Position dependence of  $N_{pe}$  as a function of  $y$  at  $x = 0$  cm (PMTs downstream).

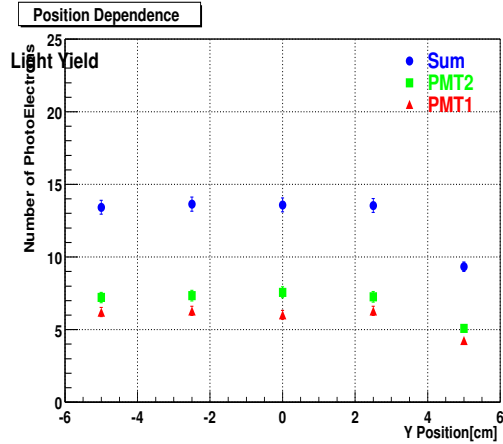


Figure 49: Position dependence of  $N_{pe}$  as a function of  $y$  at  $x = 0$  cm (PMTs upstream).

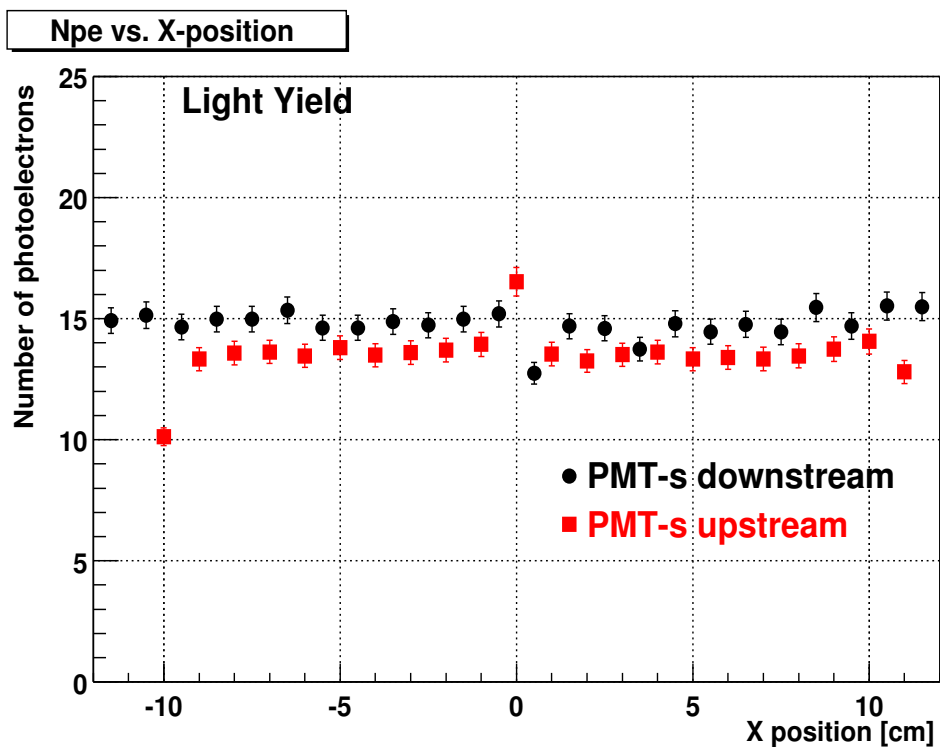


Figure 50: Comparison of  $N_{pe}(\text{sum})$  between orientations with PMTs downstream and upstream.

**Background Estimation** It is important to estimate backgrounds because background processes produce a signal even for an incident particle with momentum below the Cherenkov threshold, causing a misidentification of K as  $\pi$ . Indeed in Figure 42 with Z-axis in log-scale, upper tails of each cluster are observed (It is clear especially for pions and protons due to high statistics). The long upper tail of the histogram produced by below-threshold protons is also observed in Figure 51 which is the same distribution of Figure 43 (bottom) in log-scale. Such tails represent backgrounds for the Cherenkov signal detection. We have studied the response of the counter to below-threshold particles. At 2.0 GeV/c, for a run in which  $N_{pe}$  for  $\beta = 1$  pions is equal to 16.2 p.e. from both PMT's, we found a background of 0.4 p.e. induced by below-threshold protons. The background can be attributed to several different sources. For example,  $\delta$ -rays, scintillation light produced in either aerogel or reflector, Cherenkov light produced in reflector, interactions in the upstream counters, contamination of above-threshold particles and so on.

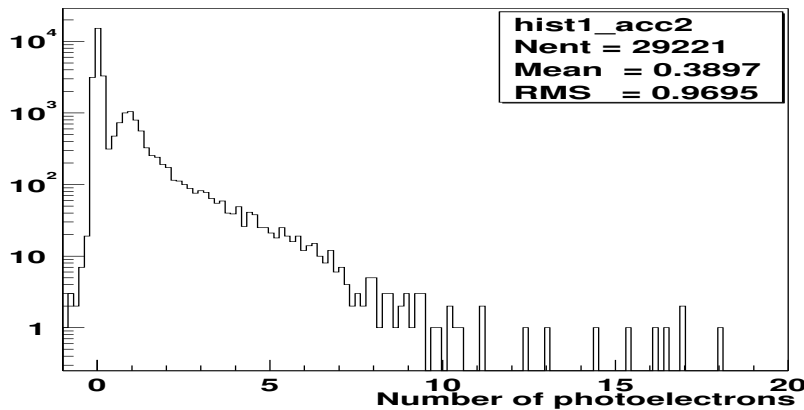


Figure 51: Pulse height spectrum of one PMT in units of photoelectrons for 2.0 GeV/c protons (below threshold).

**Background Rejection** By requiring a coincidence between signals from both PMTs in the same cell, we can reject the background due to particle hits on the PMT glass windows and/or electron kick-off on the photocathode. Moreover, we have another rejection method: using timing information of the pulses

(typical timing resolution ;  $\sim 1$ ns) from PMTs. This type of background is self-detectable by the aerogel counter itself. Figures 53 and 54 are example cases: in Figure 53, individual PMT can select the Hit-on-PMT events with prompt timing and extraordinary pulse height. Figure 54 shows that the pulse height of one-side PMT is not affected when particles hit the opposite-side PMT (triggered by timing information). The measured dependence of the timing peak of both PMTs on the incident position is plotted in Figure 52. Time-zero point is defined as the time of the hit on the PMT window. Hits close to one of the PMTs result in  $\sim 2$  ns timing difference as measured by individual PMTs. Timing

measurement could possibly be used for position resolution better than the counter size. They are also delayed compared to the time of the direct hits by  $\sim 8$  ns, which is the propagation time of Cherenkov light from emission point to photocathode.

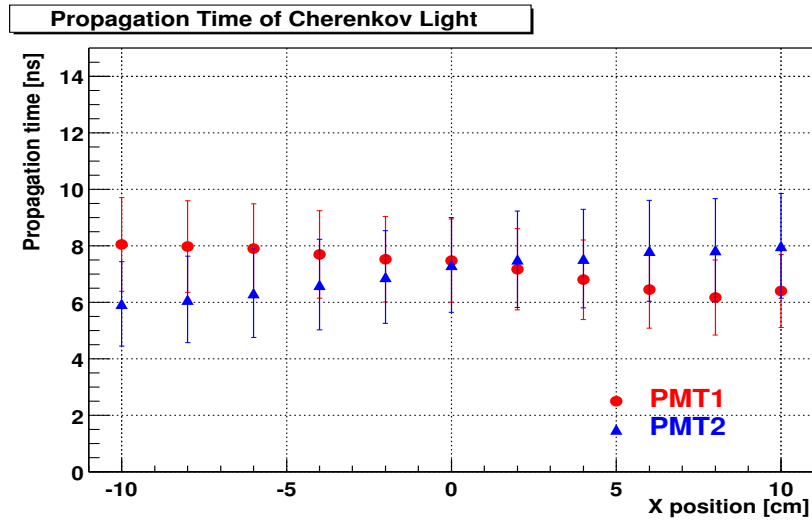


Figure 52: Propagation time of both PMTs as a function of the incident position X.

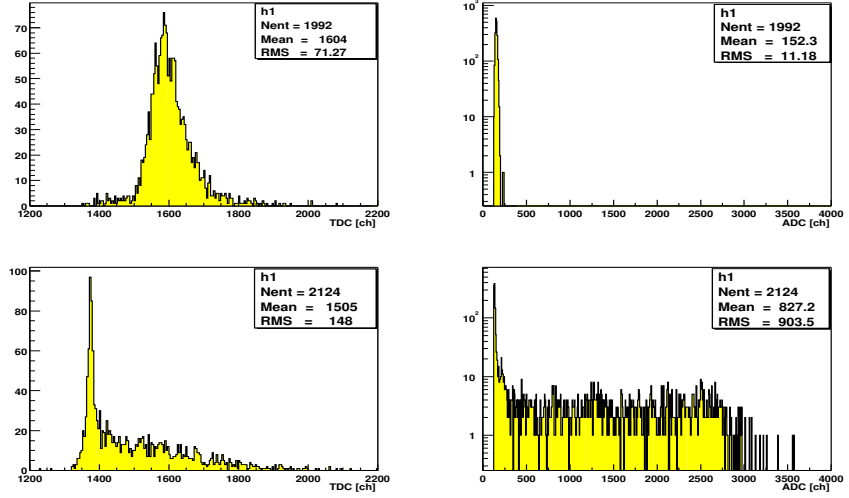


Figure 53: Different response of TDC (left) and ADC (right) distributions of the same PMT. Upper panels at x=-2cm, lower panels at x=-12cm.

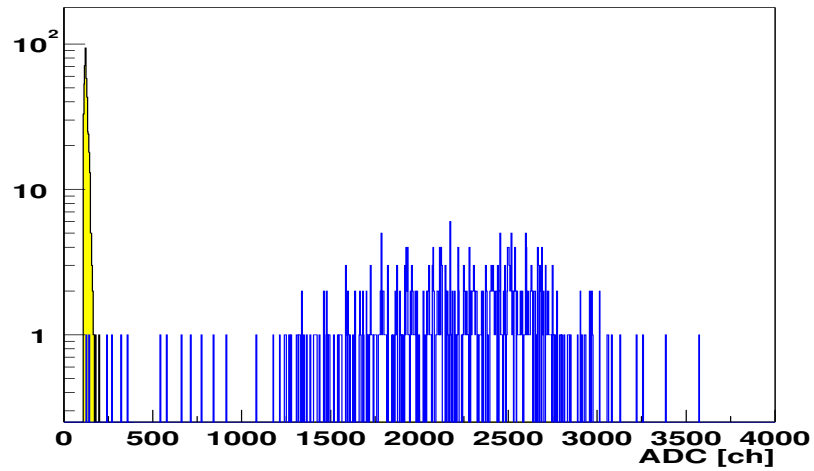


Figure 54: ADC distributions of the hit-side PMT (blue) and the opposite-side PMT (yellow).

## 2.2 Assembly

The Aerogel detector cells are assembled in two steps: (1) cells built of mylar-Goretex laminate are loaded with aerogel tiles; (2) these cells are then loaded into 0.5 mm thick Al safety and light insulating boxes; (3) the photomultipliers are attached to the box lid which is constructed as a sandwich of pc-board carrying the PMT supports and connectors, black light protecting clothe and 0.5 mm Al with prefabricated openings for connectors. When fully assembled the detector cells are subjected to light leak, HV and noise testing. Only those cells passing these tests are used in assembling the detector.

The Aerogel detector cells are assembled into two arrays containing 80 cells each, 8 cells wide (Z direction) and 10 cells high (Y direction). The cells are attached to vertical support straps hung from the array backbone, which is supported by two trolleys riding on the horizontal I-beam of a rolling A-frame (Fig. 55).

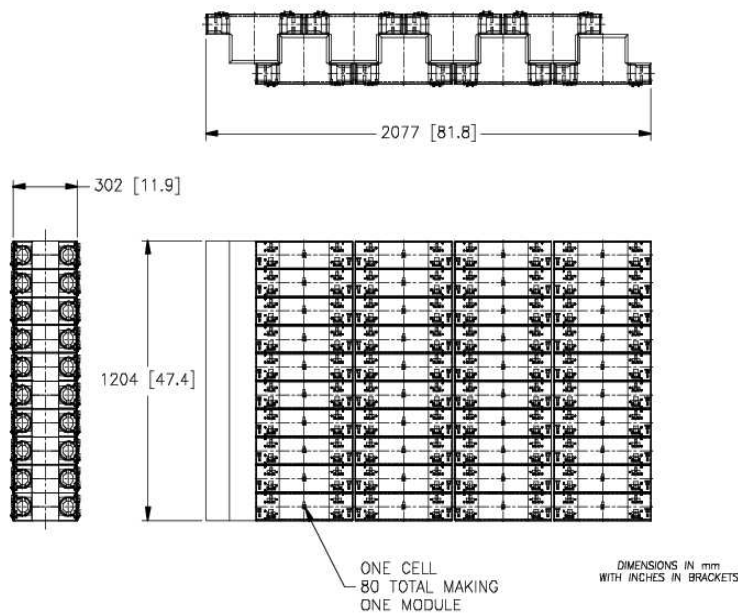


Figure 55: 80-cell Array of aerogel counters. Two Arrays of this kind will be constructed in Aerogel Detector assembly area. Each Array will be independently tested for light leaks, HV and readout problems prior to the installation into West PHENIX carriage.

Once assembled, the 80-cell array is always supported from above by an I-beam. The A-frame I-beam is detached from its rolling stanchions to serve as a lifting fixture during installation.

While supported on the A-frame, the cells are cabled, tested and light sealed. Cable trays run in Z across the top of the array with all cables running to the +-z end of the



array to the top of the pre-amp box. Cables are coiled and attached to the array end for installation

## 2.3 Integration

**Installation** Once installed in the west carriage, the two 80-cell arrays are supported by a 14 foot long I-beam spanning the entire space (in Z direction) between the aluminum towers, and attached to the towers. Installation is performed by rolling the array from the lift I-beam onto the support I-beam. A temporary transition rail is attached to the tower to permit the array to roll through the tower. Since installation is expected after the east carriage is returned to the IR, the arrays will be rolled into the IR on it's A-frame until accessible by the IR crane (see Fig. 56).

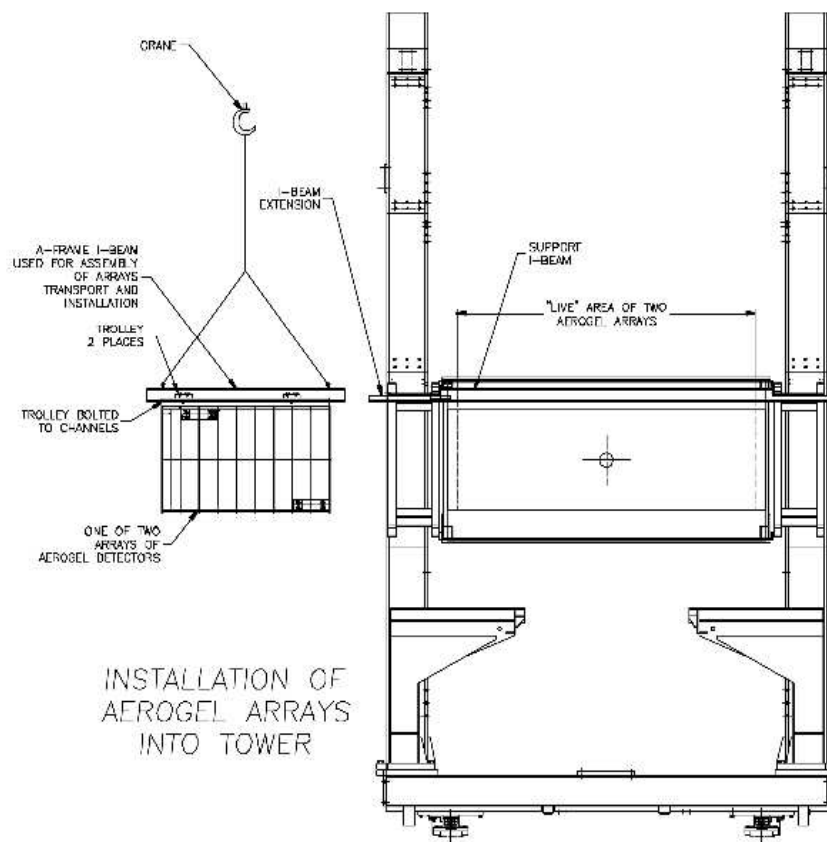


Figure 56: Installation of the Aerogel Array into PHENIX West Carriage. Only one array of 80 towers is shown. Trolleys are temporary supported from the I-beam used to carry the Array's structural elements during assembly phase.

The north and south arrays are both installed from the south end of the west carriage.

Once the arrays are in the carriage, the support I-beam will be raised up by jacking screws to get the structural aluminum and cables as close to the edge of the EMCAL acceptance as possible.

After mechanical installation, the cables will be run into the racks and connected to complete the installation.

**Infrastructure** Two new rack platforms are being fabricated which will mount on the sides of the west carriage adjacent to sector W1, with access by ladder. These are designed to accommodate two racks each and provide personnel access to the front of the racks and to the end of the Aerogel array with the pre-amp box. They will also be used during installation and cabling. The plan is for each new rack platform to have one wide rack and one narrow rack with appropriate services.

**Detector Access** Once installed, there is no access to the Aerogel detector cells. They are effectively trapped between PC2 and PC3 and unreachable. Removal of the Aerogel array involves reversing all the installation steps, including disconnecting and coiling cables.

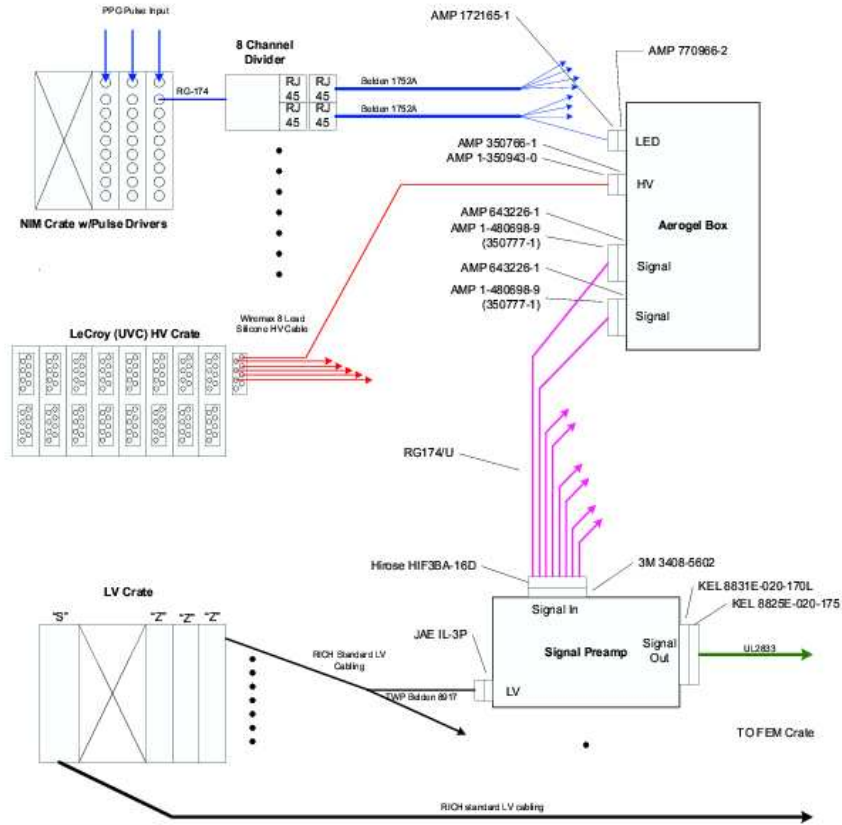
In order to provide access to the back (west end) of the new racks, the window washer previously used to access the back of the EMCAL will be replaced with a new set of different length stages that will provide access all across the back at the necessary levels. These stages will also raise up out of the way when the carriage is retracted. When in place, they will be at fixed height with simultaneous access to all EMCAL levels without requiring use of harnesses. Access to these stages will require two more ladders and another small platform at the sector W2 level.

**Integration with PHENIX Infrastructure** The Aerogel Detector when installed into the PHENIX West Central Arm will need the following services: - Low Voltage power, to power the preamplifiers located in the boxes on the south and north sides of the detector; - High Voltage power for the photomultipliers; - Dry and clean nitrogen gas for purging the detector volume. Power to detector will be provided from crates located inside the second level racks, gas flow to the detector will be controlled from the PHENIX gas mixing house.

All currently known communication lines and interconnects between detector and PHENIX infrastructure are shown in Fig. 57.

**Aerogel Cables and Connectors (One Side)**

July 2003



Steve Boose

Figure 57: Integration diagram for the PHENIX Aerogel detector. Only one of two arrays is shown.

### 3 Readout Electronics

The readout electronics of the Aerogel Cherenkov Counter (ACC) are described in this section. The electronics consist of 3 parts: preamplifier, front-end electronics (FEE), and trigger circuits.

The ACC will be installed in the West arm of the PHENIX detector system and it is separated into north and south halves. The north and south halves are constructed symmetrically. Each half has 80 segments and each segment has 2 PMTs. Thus, there are 160 channels of PMT in each half. Each of the signals is led to the front-end electronics (FEE), which are placed on the north and south sides of the west arm, via preamplifiers and cables.

A schematic view of the electronics and wiring is shown in Figure 58 and Figure 57.

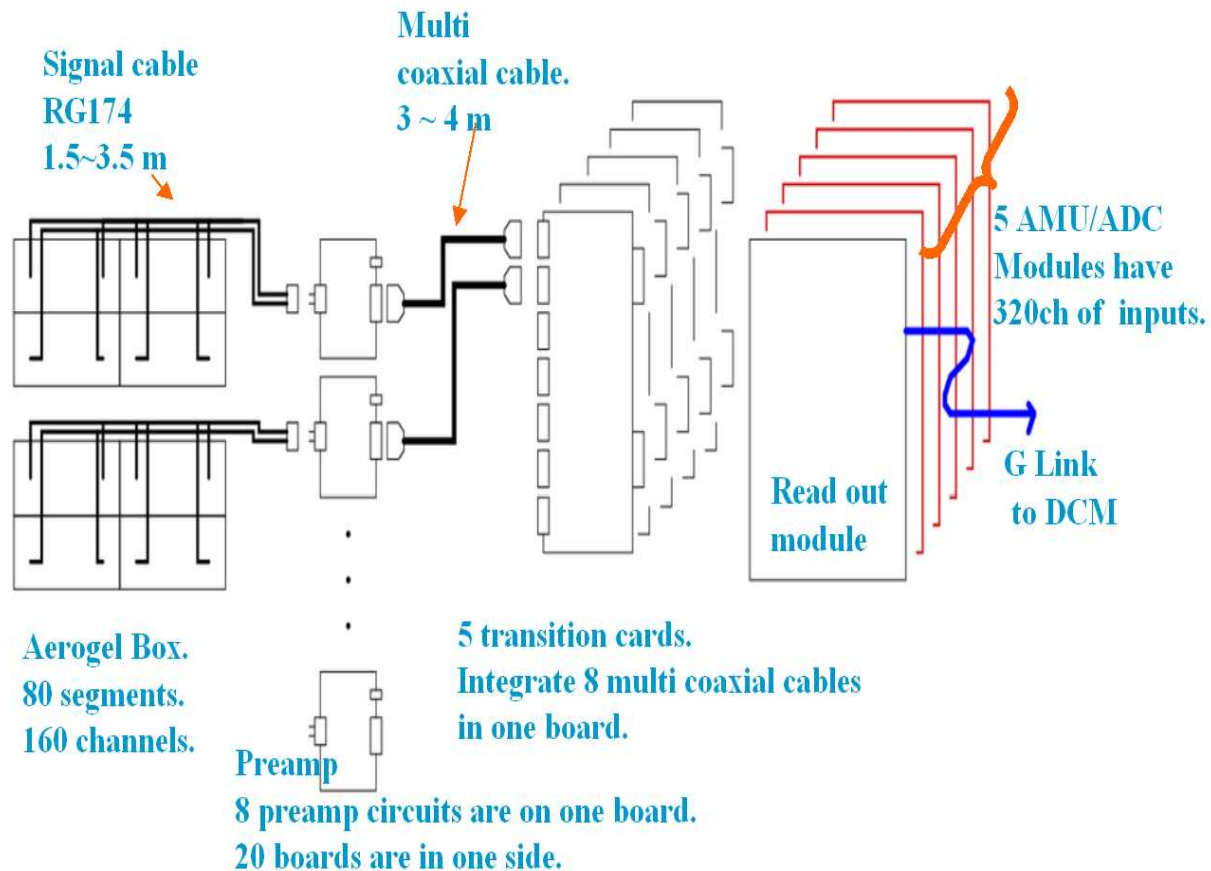


Figure 58: Schematic view of the readout electronics for one half of the Aerogel Cherenkov Counter.

The PMT signals are transferred to preamplifiers via RG174/U coaxial cables. These cables have various lengths from 1.5 m to 3.5 m to match the difference in location of each cell. The cables run vertically on the surface of the ACC, and then horizontally in

a cable tray which is placed at the top of the ACC.

The preamplifier cards and their shield boxes are attached to the side of the ACC. One preamplifier card has 8 channels and 20 preamplifier cards are used on one side. Amplified signals are sent to FEE via HITACHI-UL2833 cables. One UL2833 cable has ten fine coaxial cables and eight of these are used for one preamplifier card.

Signals enter the FEE from the back plane and are converted into digital data on a front-end board. Data packets are sent to the Data Collection Module via G-Link fibers. The FEE is the same as that of the RICH, except for one board, the transition card. One front-end board of FEE has 64 channels. So, eight UL2833 cables are connected to one board. For this purpose, a transition card is used at the backplane. This transition card is modified from the original RICH board to have suitable connectors for the UL2833 cables.

### 3.1 Preamplifier

#### 3.1.1 Electrical Design

The preamplifier circuit is designed to meet input dynamic range for FEE and to keep signal/noise ratio high. The circuit design of preamplifier is shown in Figure 59. It is a non-reverse and voltage sensitive type preamplifier. The circuit is required high speed to match the input signal. Therefore, a AD8009 op-amp chip is used since its bandwidth is 1.0 GHz and slew-rate is  $5500\text{V}/\mu\text{s}$ . The gain of the circuit is 4.5, which is determined by two resistors,  $R1 = 1.2\text{ k}\Omega$  and  $R2 = 150\ \Omega$ . The calculated gain with two resistors is 9.0 and a resistor on the output divides the signal to half with coaxial cable. Thus, its gain of output to input becomes 4.5.

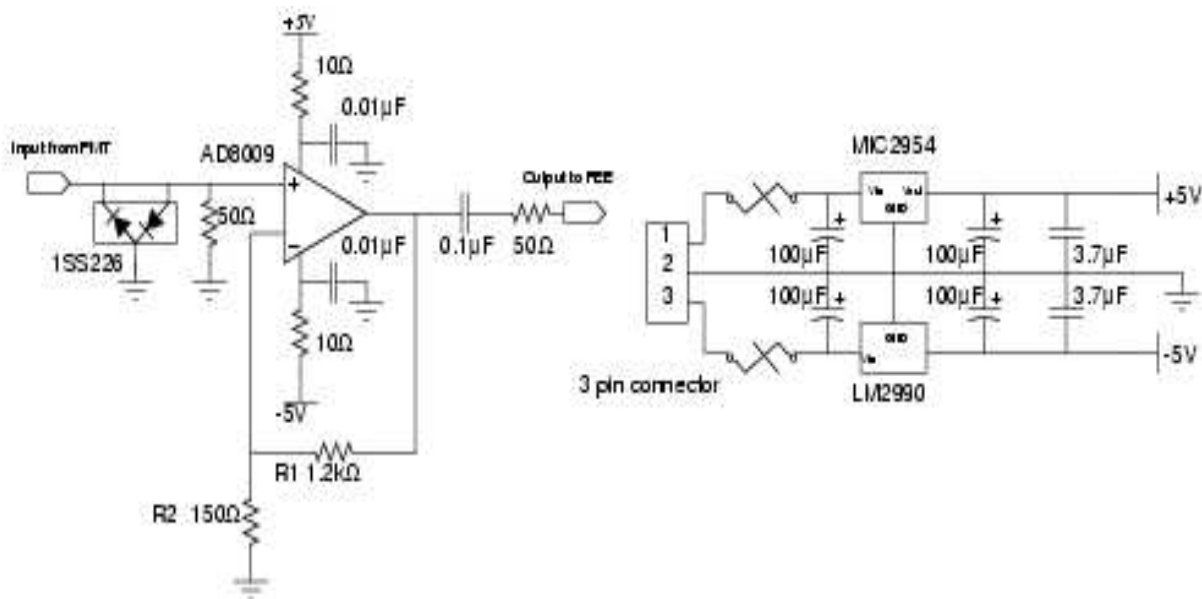


Figure 59: Circuit design of preamplifier and power supply

Table 8: Specification of parts on Preamplifier

parts	part name	specification	
Op-amp	AD8009	Slow-rate	5500 V/ $\mu$ s
		Band Width	1.0 GHz
		Current Consumption	14 mA
Regulator	MIC2954	$V_{out}$	+5 $\pm$ 0.5 V
		Dropout Voltage	0.6V
	LM2990	$V_{out}$	-5 $\pm$ 0.5 V
		Dropout Voltage	0.6V
Diode	1SS226	Forward Voltage	1.2 V

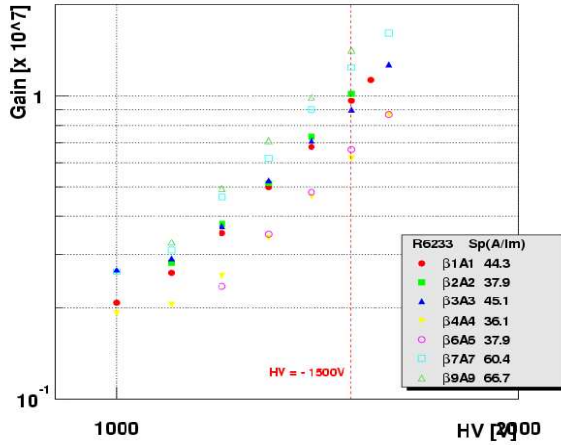


Figure 60: Some PMTs gains according to High Voltage.

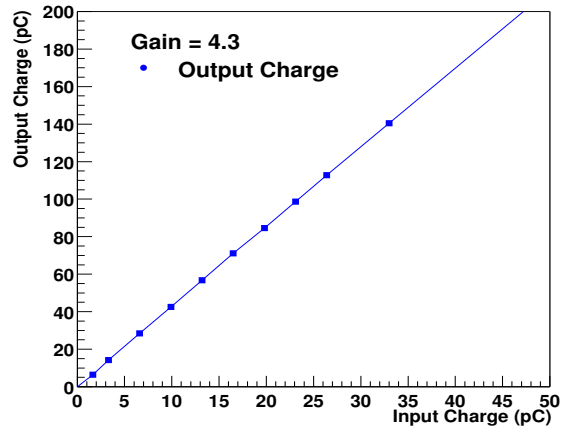


Figure 61: Plots of charge for input pulse and output pulse from preamplifier according to input charge

The reason of the design value of the gain is described below. The gain of the PMT is about  $5 \times 10^6$  when a high voltage of 1500 V is applied to the PMT. This is the lowest gain among all tested PMTs. The gains of all PMTs can be adjusted to this lowest value by adjusting the high voltage. Figure 60 shows some examples of PMT's gains with its sensitivity of positive pole (Sp) according to High Voltage, and the minimum Sp among PMTs is 30 A/W. Assuming this gain of the PMT, one photo-electron signal correspond to 0.8 pC. Here, it is required that the maximum photo-electrons is 50 and 50 photo-electron correspond to 40 pC. On the other hand, FEE's dynamic range of input is 0 to 160 pC. Thus, the gain of factor 4 is required. To have some margin for this calculations, a gain of 4.5 is chosen. This gain is sufficient for the cherenkov light signals, since the observed mean number of photo-electrons is 7 with a 2 GeV/c pion beam.

Figure 61 shows plots of amount of charge observed by ADC for the output signal as a function of the input charge. Good linearity was obtained in the range of input charge

from 0 to 40pC. The measured gain is about 4.3.

The circuit is driven by +5 V and -5 V. These voltage are supplied through two regulators which are shown in Figure 59. These two regulators, MIC2954 and LM2990, are low dropout type regulators. The main Low Voltage power supply (LVLP) supplies the original voltage of  $\pm 6.5$  V. The voltage is dropped at the regulators. They have a 1A fuse before regulators on the each board. The operating current was measured to be 0.11-0.12 A. Assuming all of voltage and current is converted to heat, the generation of heat is  $6.5 \text{ V} \times 0.12 \text{ A} \times 1 \text{ s} \times 2 = 1.5 \text{ W}$  per card. The total heat is 30W for the each side. All preamplifier cards are located in the open air at the side of the detector. Thus, this heat can be removed by the ambient air.

The LVLP is shown in Figure 62; it is the same as the RICH's LVLP. One LVLP module is placed on the each side. It has 8 channel and one LVLP channel can supply 25 W power. For this detector, one channel supplies the power for 5 preamplifier cards. Each preamplifier card uses +6.5 V and - 6.5 V. Each of these uses 0.75W. Thus, 5 preamplifier cards dissipate 3.75W for each voltage. It is significant lower than the maximum power of the LVLP channel.

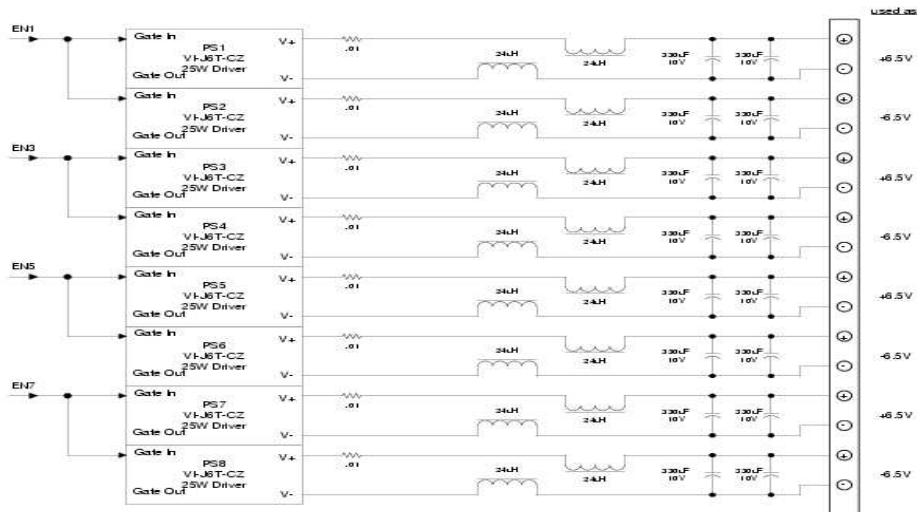


Figure 62: Diagram of LVLP for Aerogel Counter

### 3.1.2 Mechanical Design and Location

The preamplifier card is assembled into a shield box. The shield box is shown in Figure 63. The box has three large squared holes for the input, output and power supply connectors on the side. The box is put on the side of the detector by two screws. The top and bottom surfaces of the box consist of mesh plate to avoid the overheating of the preamplifier card.

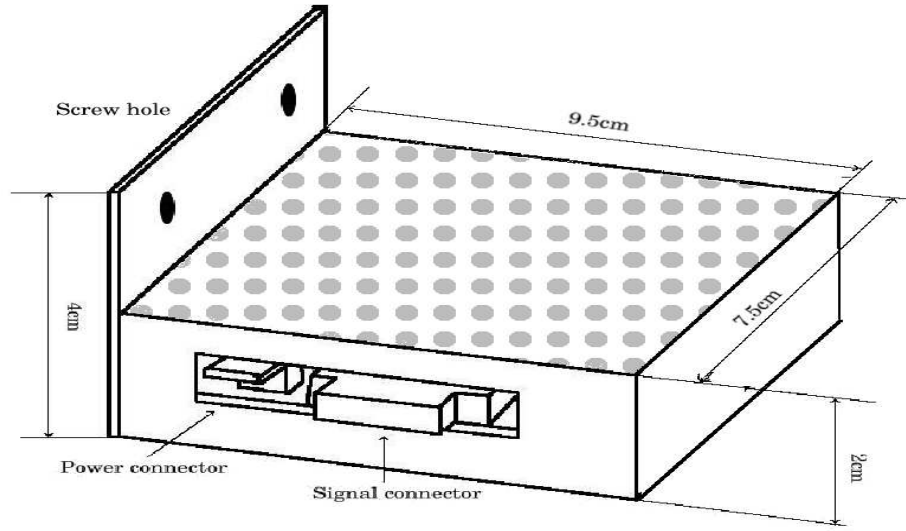


Figure 63: Box design of preamplifier

The preamplifier boxes are placed on the side of the detector. Figure 64 shows the top view of the side part of the detector. The boxes and cables are placed in the space of  $11\text{cm} \times 22\text{cm}$ , which is shown as a mesh part in Figure 64.

Figure 65 shows the schematic view of the arrangement of the preamplifier boxes and cables. The lowest preamp box starts at 50mm above bottom of side board, i.e. lowest row of M3 holes will be 65mm above the bottom. Vertical pitch is 50 mm, so the bottom of the highest box is 1000mm above bottom. Two M3 screws are used to attach each preamp box.

### 3.1.3 Cables

**cable between PMT and preamplifier** The requirements for the cable between PMT and preamplifier are  $50 \Omega$  impedance, small absorption and small size. To reduce the amount of matter in the acceptance region, a small cable is preferable.

We have two candidates, RG58C/U and RG174/U. The diameter of RG58C/U is 5.0mm and it has good signal transfer characteristics. The RG174/U cable is smaller, with 2.8mm diameter. The absorptions of the both cables are tested as a function of the cable length and the result of RG174/U is compared to the result of RH58C/U.

The test result is shown in Figure 66 and 67. The output charge as a function of cable length is shown in the figures. Red and blue sign represent RG174 and RG58 cables, respectively. Figure 66 and Figure 67 are for an input charge of 3 photo-electrons and 10 photo-electrons, respectively. In the length range from 1.5 m to 3.5 m, which corresponds to real cable length, both cables show the same absorption. Therefore, we have chosen the RG174/U cable.



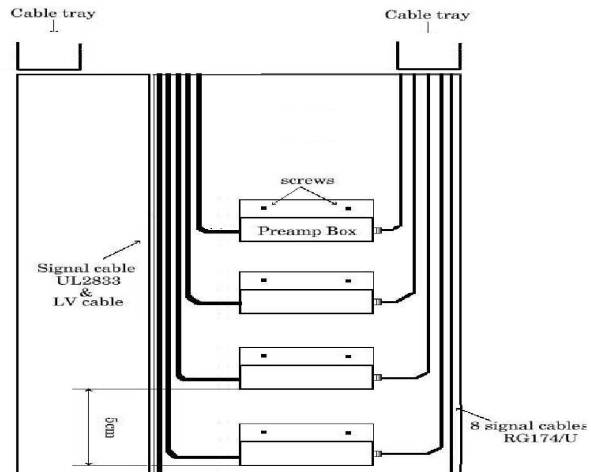
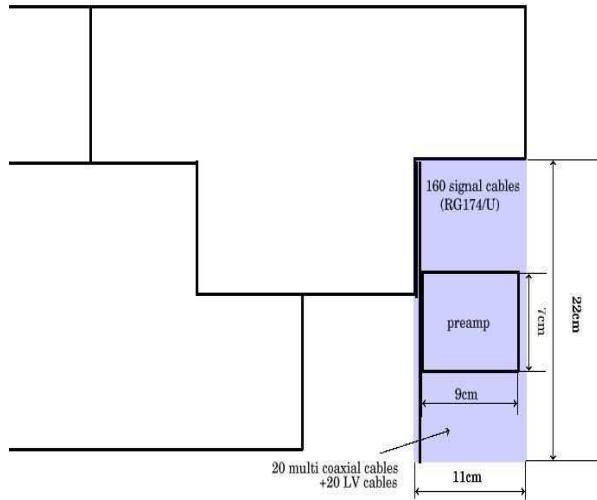


Figure 64: Preamps location. Top view of Aerogel Counter

Figure 65: The box design of preamplifier

**cable arrangement between PMT and preamplifier** Signal cables from PMTs run vertically on the surface of the detector and horizontally in the cable tray which is placed at the top of the detector. There are two cable trays on the top of the detector. 80 cables are placed in each tray. Since we would like to run signal and HV cables in the cable trays on both sides, we need a separator in a cable tray.

We have estimated the total cross sections of signal cables below. Signal Cables have an area of 30mm width x 24mm height = 720 mm<sup>2</sup>. The diameter of RG-174U is 2.5mm and it is assumed that 3mm x 3mm square space is per cable. The number of cables is 80 and 10 cables x 8 layers is assumed. 9 cables per one layer correspond to 30mm width and 8 layers correspond to 24mm height.

The cable arrangement and assignment of the channels are shown in Figure 68. One preamplifier has 8 channels and it services 4 segments of the detector. To reduce the timing difference among these 8 channels, neighboring segments are selected for 8 channels. Actually, the AMU/ADC chip on the FEE handles the 8 channels at the same timing. Thus, the time difference among 8 channels should be reduced. Also, this channel assignment is chosen to reduce the influence of cross talk.

**cables between preamplifier and FEE** To cope with high channel density in the input part of the FEE, small coaxial cables have to be used. For this purpose, UL2833 cable is chosen. The UL2833 cable has 50Ω impedance and 10 channels per cable. The specification of UL2833 is listed in Table 9.

The performance of UL2833 was tested. The output charge is measured after 5m length of UL2833. The input pulse has risetime of 10ns and width of 30ns, to represent

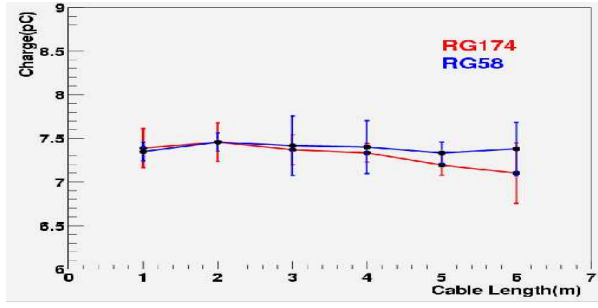
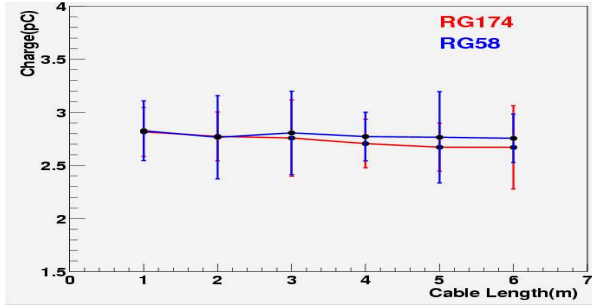


Figure 66: The output charge as a function of cable length is shown in the figure. Red and blue sign represent RG174 and RG58 cables, respectively. The input charge corresponds to 3 photo-electrons.

Figure 67: The output charge as a function of cable length is shown in the figure. Red and blue sign represent RG174 and RG58 cables, respectively. The input charge corresponds to 9 photo-electrons.

Table 9: Specification of UL2833 cable

list		unit	specific
Number of cables		-	10
Conductor	diameter	mm	0.31
Insulator	diameter	mm	0.89
Sheath	diameter	mm	5.7
Impedance		$\Omega$	$50 \pm 5$
Fireproof		-	Pass UL VW-1 test

a fake PMT signal. Figure 69 shows the output charge as a function of the input charge. Figure 69 shows the ratio of the output charge over the input charge as a function of the input charge. The absorption of charge is less than 2% and this is low enough for the detector.

The pulse shape of the output of UL2833 is also checked. Figure 71 and Figure 72 shows the output pulse after UL2833 cable and the transition card. The cable lengths for Figure 71 and Figure 72 are 1 m and 5 m, respectively.

The ratios of the output pulse height over the input pulse height are 85% and 80% for 1 m and 5 m, respectively. Still, the pulse height is sufficient for the determination of timing information and trigger information.

### 3.1.4 Cross Talk

Cross talk through cables, preamplifier and transition card were measured. The setup of the measurement of cross talks is shown in Figure 73. Signals to represent the output of a PMT are generated as a input of this test. Their risetime is about 10 ns. The generated pulses enter the preamplifier card after passing through coaxial RG174/U cable. Amplified

signals were sent to the transition card via multi-coaxial UL2833 cable, and the output signal from the transition card was observed by oscilloscope. Together with this signal, signals of other channels were observed.

The results are shown in Figure 74 and Figure 75. These figures show the scope traces of output signals from transition card. The lower trace in the picture is the cross talk in the neighboring channel. In those picture, the signal pulses correspond to about 10 photo-electrons and 50 photo-electrons for Figure 74 and Figure 75, respectively. The cross talk is generated mainly around output of preamplifier, signal cables, and transition card. Before preamplifier the pulse is smaller than amplified signal, so it dose not affect the other channels much. To a large extent, only the immediate neighboring channel of the signal channel is affected.

The cross talk is less than 3 % of signal pulse in both cases. This is low enough to be ignored in the trigger circuit, because the pulse hight of 2 mV, which is the most likely cherenkov signal (10 photo-electrons), corresponds to 0.1 photo-electrons and the threshold of the aerogel trigger should be 1 photo-electrons. Also, crosstalk signals are bipolar signals, so they carry no charge.

## 3.2 Front End Electronics

Front End Electronics is basically the same as the RICH FEE [1], except for the transition card. Charge and timing information of PMT signals are measured by the FEE. The block diagram of FEE is shown in Figure 76.

The FEE for the each detector half consists of one controller board, five AMU/ADC boards and one readout board. Here, one AMU/ADC board has 64 channels. Thus, three AMU/ADC boards are enough for one detector half. However, one readout card requires five AMU/ADC boards to work properly. Therefore five AMU/ADC boards are installed each detector half. If we use zero-suppression, this should not affect the data volume.

The Controller Module performs all of the functions associated with front-end electronics control, command interpretation/execution, and communication. The Controller Module is connected to Master Timing Module (MTM) via G-link fiber and receives timing information from the MTM. From the timing information, a Clock Distributor daughter Board (CDB) on Controller Module generates system clocks which are provided to FEE modules to synchronize them. In addition to the timing information, the Controller Module also provides data taking signals and controls the data taking.

Sixty-four channels of PMT signals are separately digitized in a single AMU/ADC board. There are two kind of ASIC chips on AMU/ADC board [2]. One is the AMU/ADC chip comprising 32 channels of 64-cell analog memory and a Wilkinson 12 bit Analog-to-Digital Converters. The another is the Integrator/TAC chip, which has eight Charge Integrating Amplifier and Time-to-Amplitude Converter (see Figure 77. Amplified signals from preamplifier are fed into AMU/ADC Modules via the backplane after passing through the Transition Card. The data which are stored in the AMU are converted to digital data and sent to Readout Module under the control of the Controller Module.

The Readout Module collects data from AMU/ADC Modules via a 32 bit Separate

Bus, and the formatted data are sent to the Data Collection Module via G-Link fiber.

### 3.3 Level-1 Trigger

Signals from the detector can be used to select high-pT particles as a part of ERT level-1 trigger in p-p and d-A collisions. For Au-Au collisions, we will use the level-2 trigger.

The Aerogel level-1 trigger will be implemented as a newly constructed circuit, because the RICH level-1 trigger board can not be used for this purpose. The trigger circuit will be installed before Run-5. The current plan is described below.

The current plan of the trigger circuit is shown in Figure 78. In the first stage, the signal from the preamplifier is received by one op-amp as a buffer to avoid a reflection of the signal. The signal is split in two parts after the op-amp. One is for the trigger circuit and one is sent to the FEE to measure charge and timing information. The input for the trigger circuit has a high impedance and almost all of the signal charge is led to the FEE.

The signal for the trigger circuit is discriminated to produce a digital pulse. The threshold of this discriminator can be set externally via a DAC chip. The signals of the two PMTs in one segment are in coincidence with each other. It should be noted that the position dependence of the light yield is very weak and we can discriminate the signals from each PMTs separately.

A further trigger circuit is needed after this circuit. For example, one trigger tile should have an area of  $22\text{cm}\times 44\text{cm}$ , to match the trigger tile size of the RICH and the EMC. This area corresponds 4 segments of the aerogel counter. Thus, we should have another layer of logic on the trigger board or LL1 board.

Further detailed simulation studies are needed to determine the logic of the aerogel trigger.

## References

- [1] Y. Tanaka *et.al.*, NIM. **A455** (2000) 476-588.
- [2] A.Wintenberg *et.al.*, “A CMOS Integrating Amplifier for the PHENIX Ring Imaging Cherenkov Detector”, IEEE Transaction on Nuclear Science, 45(1998), 758.

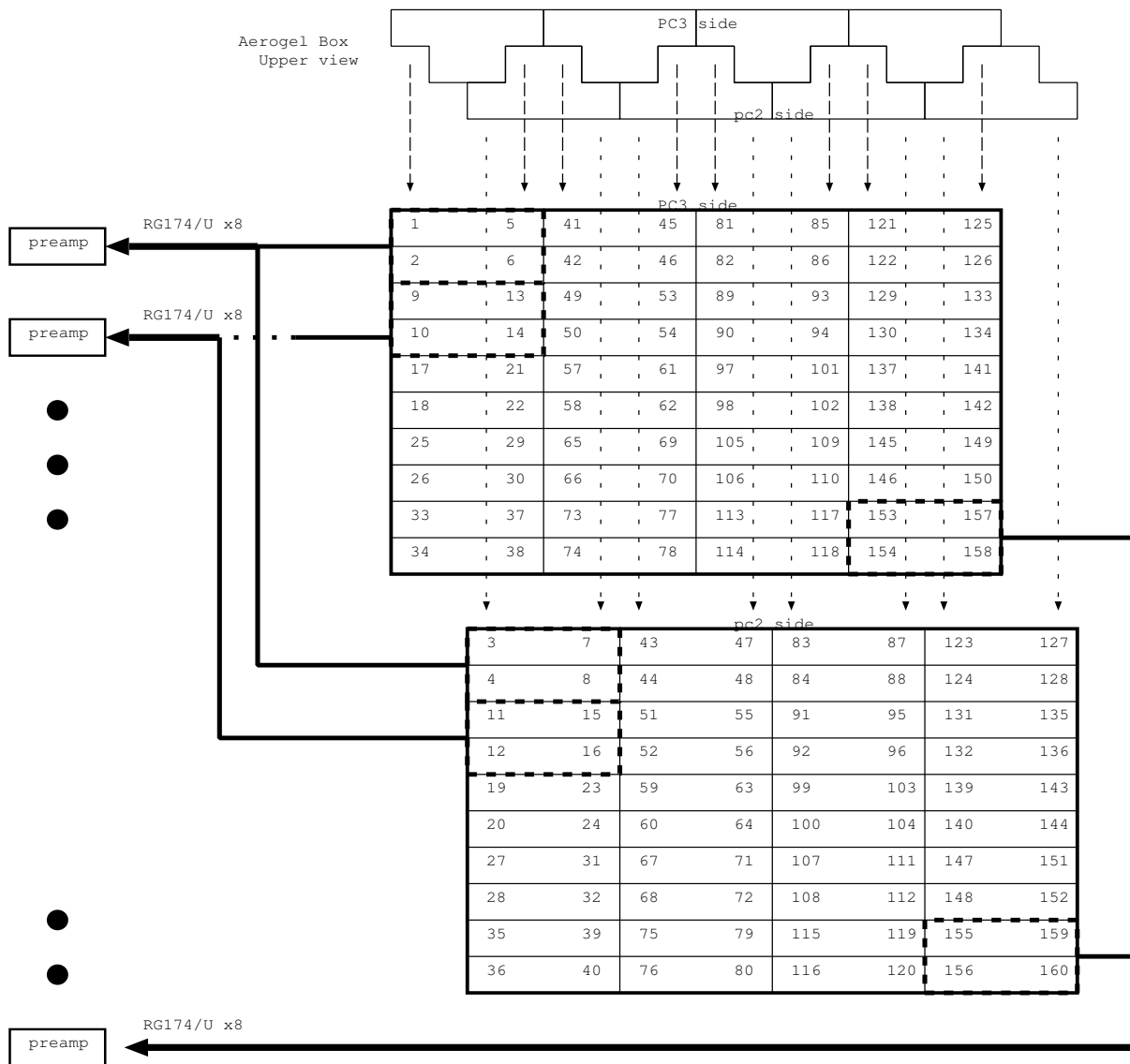


Figure 68: Numbering of signal cables

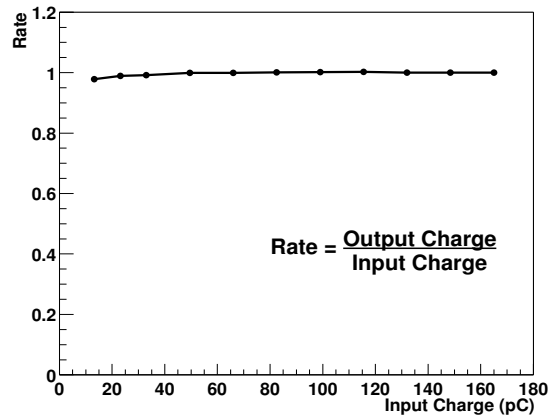
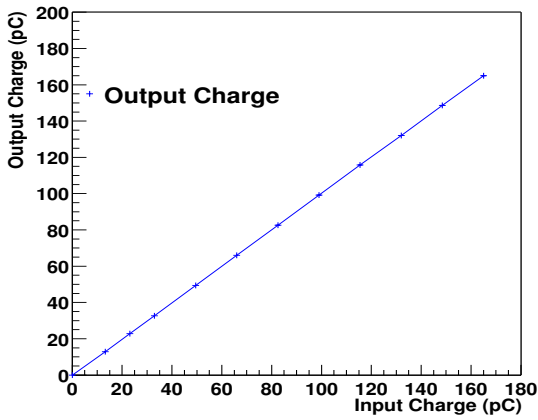


Figure 69: Plots of output charge after Figure 70: Ratio of output charge after UL2833 cable at 5m related to input charge UL2833 cable to input charge

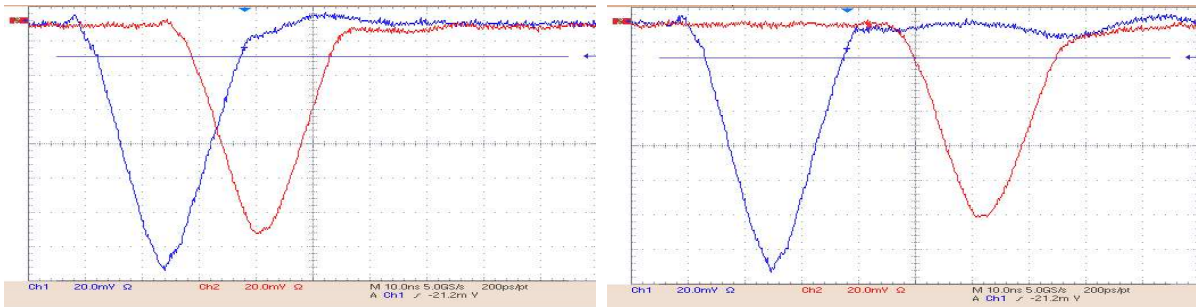


Figure 71: Output pulse after Transition Card and UL2833 1m Figure 72: Output pulse after Transition Card and UL2833 5m

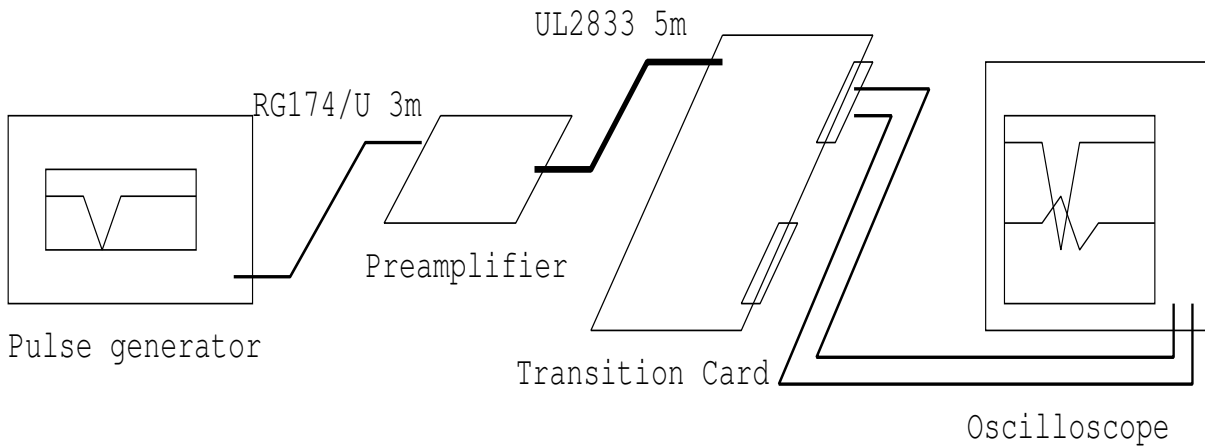


Figure 73: Block diagram of the setup to observe crosstalk

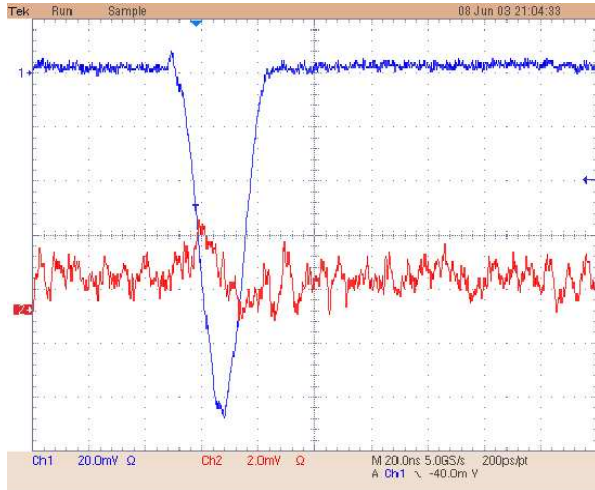


Figure 74: Picture of output pulse with the next channel of the signal channel. Output pulse has 130 mV pulse height and cross talk has 2 mV pulse height.

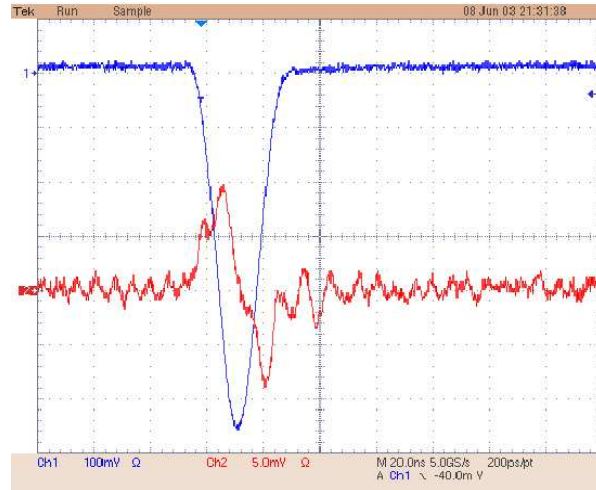


Figure 75: Picture of output pulse, together with the channel neighboring the signal channel. The output pulse has 650 mV pulse height and cross talk has 10 mV pulse height.

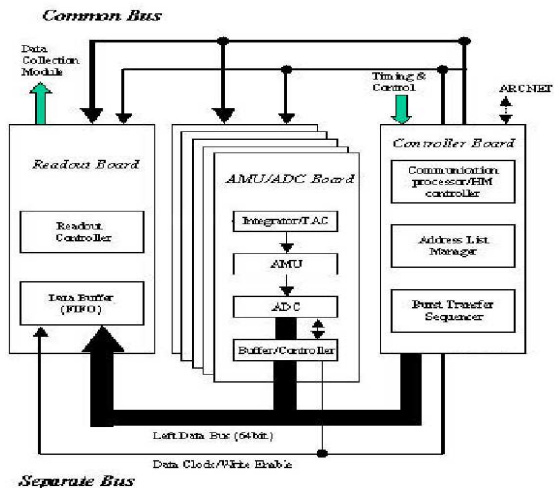


Figure 76: Block diagram of Aerogel FEE

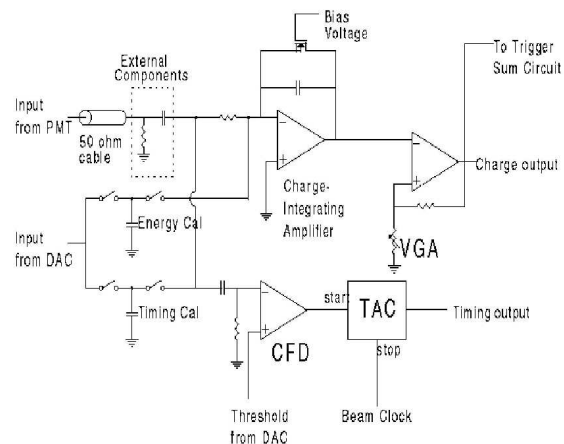


Figure 77: Block diagram of a channel of chip on AMU/ADC

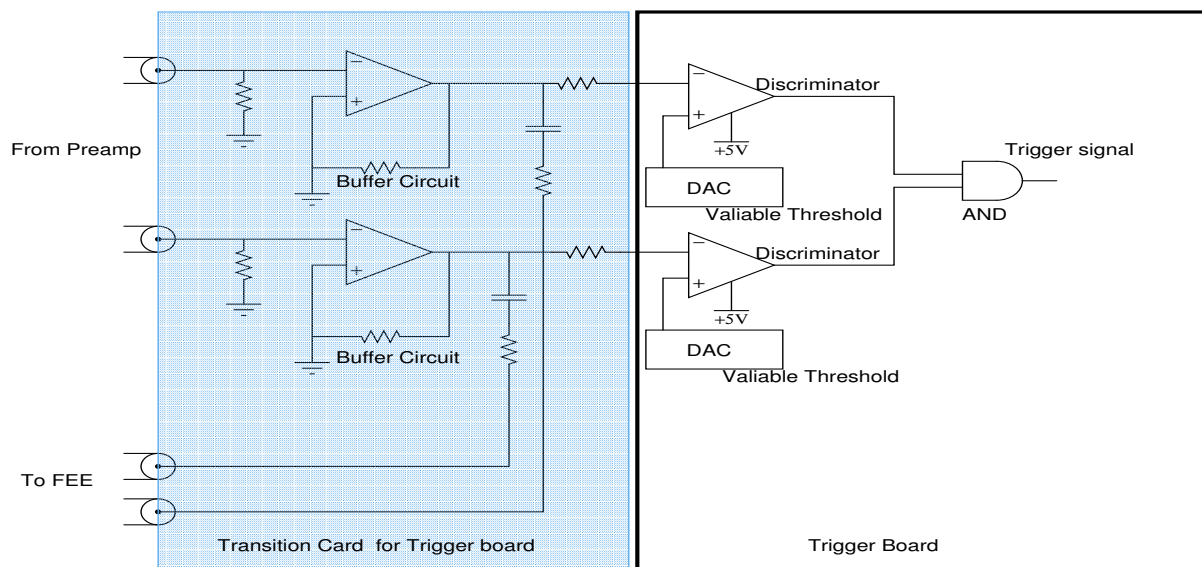


Figure 78: Trigger Circuit design for Aerogel Counter



## 4 Simulation

### 4.1 Expected PID capability

Expected particle identification capability was studied by assuming the shape of the transverse momentum distributions and the relative yield among  $\pi$ ,  $K$  and  $p + pbar$  are given by the Pythia (200GeV p+p) simulation package. The efficiency and the purity of the selected particle will be given at the end of section. Since the ratios  $K/\pi$  and  $p + pbar/\pi$  in 200GeV Au+Au collisions are expected to be larger than in the Pythia simulation and our aim is to have good sample of high  $p_T$   $K$  and  $p + pbar$ , this Pythia assumption for the efficiency and the purity will correspond to an pessimistic case. Fig. 79 (left) shows Pythia p+p 200GeV  $p_T$  distributions for different particles. The power law function is used to describe the shape of the distribution and is also used to get the relative yields among different particles in the following simulation. The time of flight of with TOF wall or electro-magnetic calorimeter (EMcal) will be used for the low momentum particle identification up to 2-4GeV/c depending on their timing resolutions and the ring imaging Cherenkov detector (RICH) for the high momentum  $\pi$  identification. Then we add aerogel Cherenkov counter (ACC) information to extend or cover the missing region of the  $p_T$  acceptance of particle identification.

The methods and the parameters used in the following simulation is described here. Using the timing resolution in the TOF wall at 5m from the collision point and the momentum resolution in the drift chamber (Dch), the mass square is used for the particle separation, where the timing resolution is assumed to be 110ps for the TOF and 360ps for the EMcal. The Cherenkov photons in RICH and ACC are given by the Poisson statistics. The used index of refraction in the simulation is 1.00044 ( $\text{CO}_2$ ) or 1.00071 ( $\text{C}_2\text{H}_6$ ) for the radiator gas in the RICH and 1.011 (aerogel) for the ACC. The average number of photon electrons is 12 p.e. for the ACC and is 10ps for the RICH( $\text{CO}_2$ ) for the particle with  $\beta = 1$ . About 8% of random back grounds are added and they are assumed to be electrons ( $\beta = 1$ ). This accidental background particle hits is the large fraction of the occupancy about 8%, which is estimated in the separate simulation with the PHENIX GEANT code (PISA).

Fig. 79 (right) show the momentum slice of the number of photo-electron distribution in the RICH and ACC for 2 different momentum slices and for different particles, see details in the caption. The index of refraction is 1.00044 in RICH and is 1.011 in ACC. Above 1GeV/c and below 3GeV/c  $\pi$  is identified in ACC, but for the  $K/p$  separation can only be done by the time of flight. Above 3.5GeV/c  $K$  will also fire ACC, so just by vetoing ACC hits,  $p$  can be identified up to the  $p$  threshold at 6.5GeV/c in ACC. Between 6 and 7 GeV/c,  $\pi$  in the RICH and  $\pi+K$  in the ACC are fired, so that 3 particle species can be identified unambiguously by 2 Cherenkov detectors alone as shown in the most-right two panels in Fig. 79. With lowering the  $\pi$  threshold in the RICH, (by changing the gas from  $\text{CO}_2$  to  $\text{C}_2\text{H}_6$ , or by mixing Freon gas) in order to have matching with the  $K$  threshold in ACC, this 6GeV/c lower limit of high momentum full particle identification region can be lowered down to about 4GeV/c. However, since the higher limit of the high

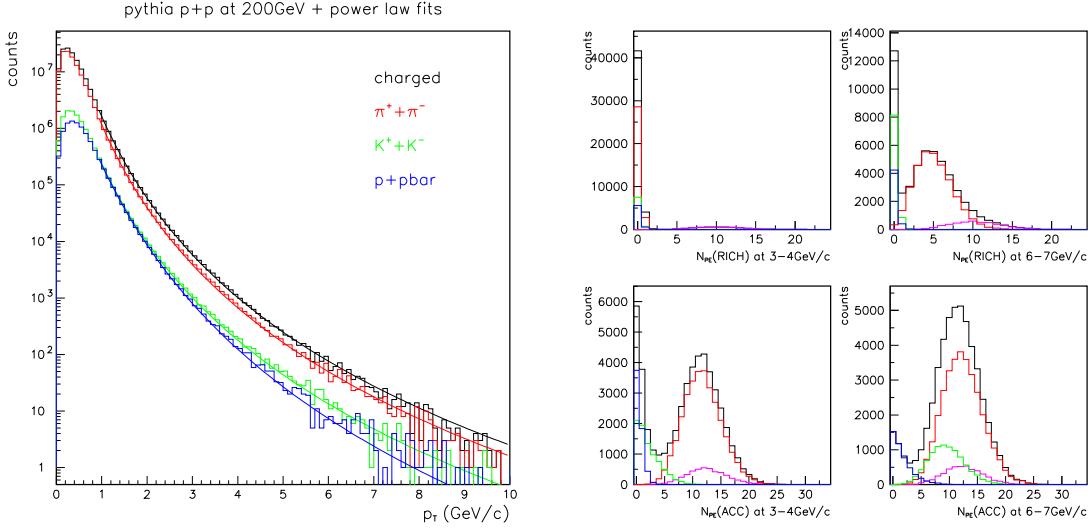


Figure 79: left: Pythia p+p 200GeV  $p_T$  distributions for charged particle,  $\pi$ ,  $K$  and  $p + pbar$ , solid lines show fitted functions with power law. right: The number of photo-electron distribution in the RICH (top) and in the ACC (bottom) for 3-4GeV/c in the left and 6-7GeV/c in the right panel. Different particles are shown in the different colors,  $\pi$ : red,  $K$ : green,  $p + pbar$ : blue,  $e$ : pink and total is in black,  $e$  (electrons) are added as backgrounds. The index of refraction is 1.00044 for the RICH and 1.011 for the ACC.

momentum particle identification region is unchanged by modifying the RICH gas, this will be an future option, if one would like to narrow down the gap between the low and high momentum particle identification regions.

The left panel in Fig. 80 shows the mass square distribution as a function of momentum, where top is for the TOF timing resolution (110ps) and the bottom is for the EMcal resolution (360ps). The middle panel in Fig. 80 shows the number of photo-electron measured in RICH, where index of refraction of the radiator gas is 1.00071 ( $C_2H_6$ ) for the top and and 1.00044 ( $CO_2$ ) for the bottom. The light panel in Fig. 80 shows the number of photo-electron measured in ACC, where the index of refraction of the aerogel radiator is 1.011. Since the new TOF wall behind the ACC is still an option and the radiator gas in the RICH is currently  $CO_2$ , the bottom 3 sets of figures will be the realistic option for run4-AuAu running. If we use the EMcal for the time of flight measurement, an upper limit of the low momentum PID region will be lower by about 1-1.5GeV/c, compared to the TOF. If we use the current  $CO_2$  gas, an lower limit of the high momentum PID region will be higher by about 1-1.5GeV/c, compared with the originally planned  $C_2H_6$  gas. So both effects would increase the inefficient PID gaps between low and high momentum region especially for the  $K$  identification, so this (top 3 sets) will be an option the future improvement.

The particle identification efficiency and the purity is calculated based on the simula-

tion described above. The definition of the efficiency is  $N_{\text{Correctly Reconstructed}} / N_{\text{True}}$ , and the definition of purity is  $N_{\text{Correctly Reconstructed}} / N_{\text{Reconstructed}}$ . Those two values are plotted as a function of momentum and with the different options for the particle identification selection as shown in the Fig. 81 for  $\pi$ ,  $K$  and  $p + pbar$ , respectively. They are calculated with TOF wall timing resolution and  $\text{CO}_2$  index of refraction, so the higher edge of the low momentum particle identification region will be lower, when EMcal timing resolution is used, however the high momentum particle identification regions, where we are most interested in for this coming run4, are unaffected by this.

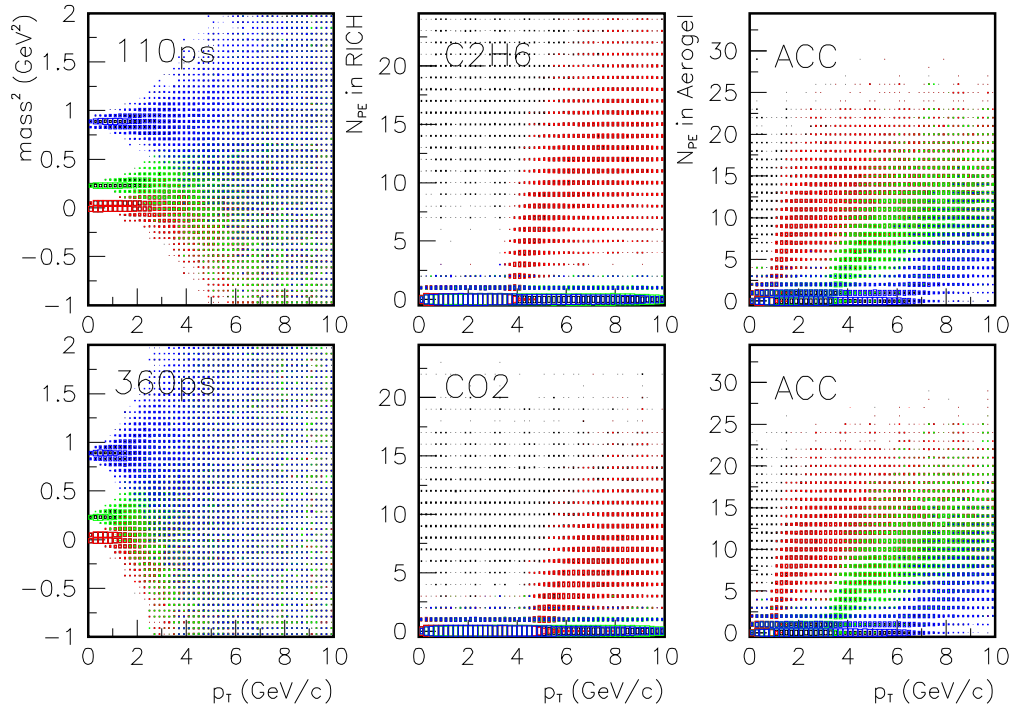


Figure 80: left: the mass square measure with the time of flight (TOF), center: the number of photo-electrons measured in the ring imaging Cherenkov detector (RICH) and right: the number of photo-electrons measured measured in the aerogel Cherenkov Counter (ACC) are shown as a function of momentum. Different particles are shown in the different colors,  $\pi$ : red,  $K$ : green and  $p + pbar$ : blue, where some electrons are added as background. The bottom figures show the same definition as in top figures, the difference is the worse timing resolution for the time of flight measurement (top: 110ps, bottom:360ps) which corresponds to the TOF / EMcal and the lower index of refraction in the RICH (top:1.00071, bottom:1.00044) which corresponds to the current C<sub>2</sub>H<sub>6</sub> / CO<sub>2</sub> gas. The bottom-right panel is unchanged compared to the top-right.

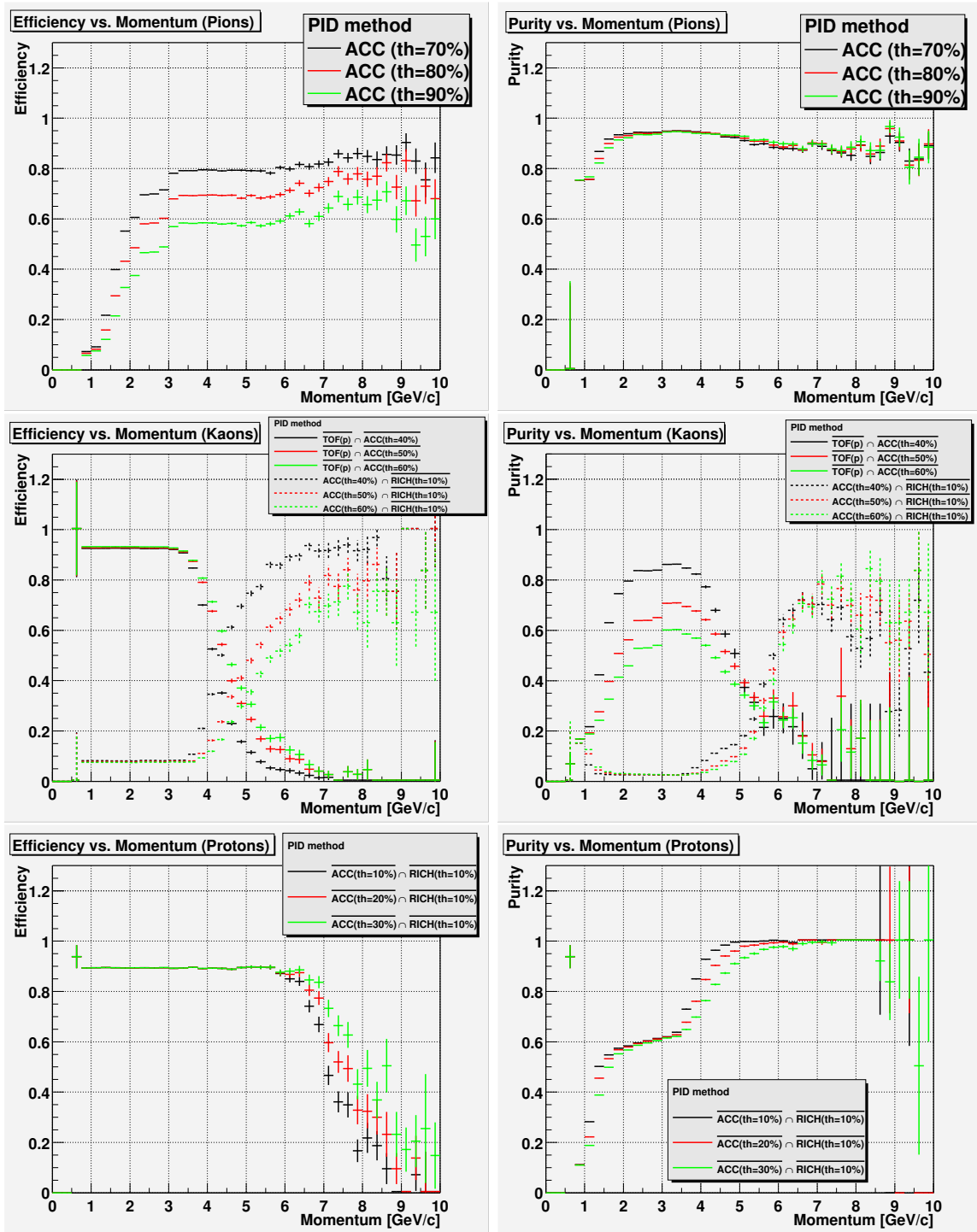


Figure 81: pion efficiency (top-left), purity (top-right), kaon efficiency (middle-left), purity (middle-right), proton efficiency (bottom-left) and purity (bottom-right)

## 4.2 PISA

Installation of the PHENIX Aerogel Cherenkov Counter (ACC) system into PISA is very important to evaluate the performance of the ACC system. Most of the materials which construct the ACC has installed into PISA, which is located in W1 sector between PC2 and PC3 (refer to Figure 83). What was installed into PISA is the Aluminum Box, Aerogel, Mylar sheet, Goretex sheet, G10 plate, Mumetal shield, PMT glass and PMT base board (see Figure 82).

As shown Figure 83, there are 10 counters in the direction of  $\phi$  and 16 counters in the direction of Z. So, the ACC system consists of a total of 160 counters. The ACC system is located about 456cm away from the vertex point, and they cover 391.64cm in the direction of Z and 118.5cm in the direction of  $\phi$ . Figure 83 shows the PHENIX detector in PISA, which has the ACC system.

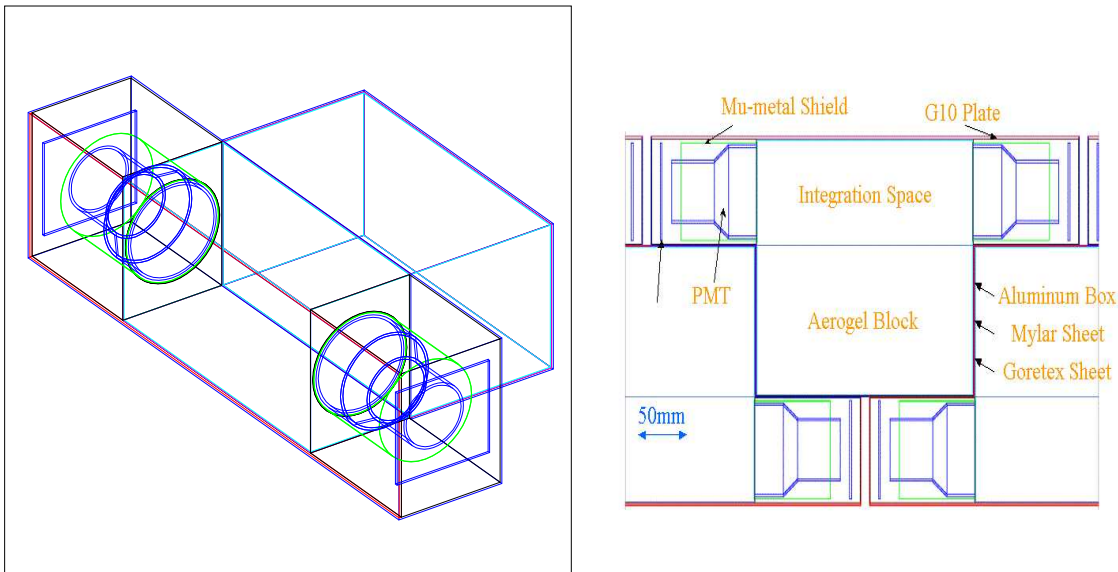


Figure 82: single counter configuration (left side) and a horizontal section of ACC (right side)

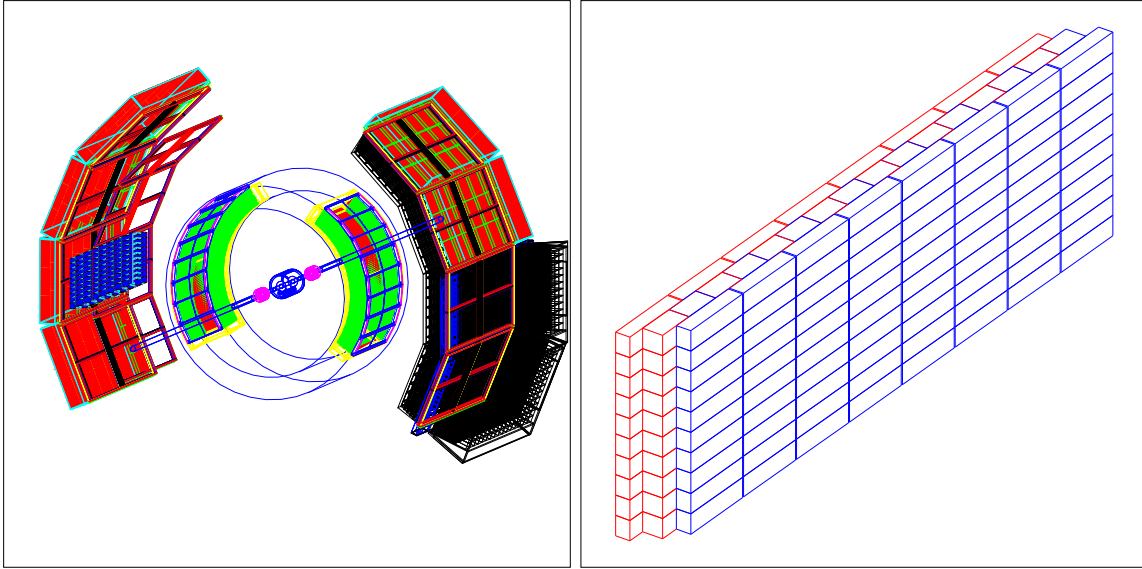


Figure 83: the PHENIX detector which has the ACC system in W1 sector between PC2 and PC3 (left side) and situation of the stacked ACC (right side)

#### 4.2.1 Overall Radiation Length

In order to reduce the influence to the other subsystems, it is necessary to shorten the radiation length of the ACC as much as possible.

The ACC was designed so that they might not be background sauce. In the following table, the radiation length is listed for principal materials which construct the ACC system, which is calculated in GEANT3(PISA).

<i>Material</i>	<i>Density (g/cm<sup>3</sup>)</i>	<i>thickness (mm)</i>	<i>Radiation Length (cm)</i>	<i>Radiation Length (%)</i>
<b>Aerogel</b>	0.05	120.0	539.62	2.24
<b>Aluminum</b>	2.70	0.80	8.9	0.89
<b>Goretex</b>	2.20	0.50	15.79	0.32
<b>G10</b>	1.70	2.0	16.39	1.22
<b>Mylar</b>	1.39	0.10	31.09	0.03
<b>Mu-metal</b>	8.58	0.50	1.50	3.33
<b>PMT Glass</b>	2.23	2.0	12.41	1.61
<b>PMT base</b>	1.70	2.0	16.39	1.22

**Table1** : the property of the principal materials of the ACC in PISA

The overall radiation length of the ACC system was calculated in PISA by using single

track which was generated at random toward the ACC system. Figure 84 shows the overall radiation length of the ACC system for track. When Figure 84 is seen, the overall radiation length of the ACC system is about 19.2%.

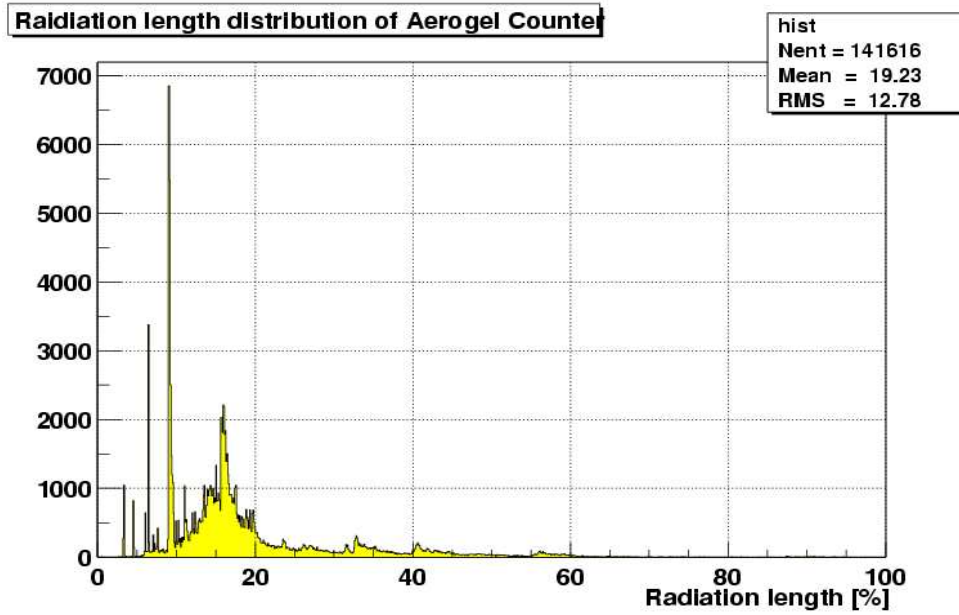


Figure 84: the overall radiation length of the ACC system



### 4.2.2 Effect on EM-Cal

There is a reference around the BaBar CsJ electromagnetic calorimeter which has a similar amount of material in front of the crystals (20% Lrad) and declared (measured)  $\pi^0$  width of 7.7 MeV (6%) for  $\pi^0$  momenta above 500 MeV/c what is well below our measured  $\pi^0$  width which is of the order of 10% (see for example D.Boutigny, 3rd International Conference on B physics and CP violation, Taipei, 1999).

A similar conclusions were reached as an outcome of the Monte-Carlo studies and test beam efforts made during LHCb calorimeter studies (LHCb 2001-065 EDR):

In contrast to HERA-B, a preshower detector is placed in front of the LHCb ECAL, and the overall performance of the system could be affected by dead material in between the preshower and the first scintillator of the shashlik stack. The effect of dead material in front of ECAL was studied with Monte Carlo. If no correction is applied, then the energy loss in a 5 mm thick iron plate (0.3 Lrad) in front of the shashlik stack increases the relative error on the energy measured in ECAL by less than 1 % for electrons of more than 10 GeV. However, if this material is taken into account when calibrating the overall system, no sizeable degradation of the energy resolution is observed. This is confirmed by test-beam data with 20 GeV electrons where no degradation of the ECAL resolution was observed due to the 12 mm lead absorber of the preshower detector.

The presence of a 20% Lrad amount of material in front of the calorimeter may result in the need for additional correction efforts in the analysis of the calorimeter data but it will definitely be helped by the fact that all showers which could be affected by aerogel detector are easy to identify by the presence of a matching signal in aerogel detector (electrons in the shower).

Aerogel detector combined with the calorimeters will certainly serve to improve electron identification in the low Pt limit when calorimeter resolution becomes too low for effective e/p matching.

### 4.3 Level-2 Trigger

For the measurement of identified high  $p_T$  hadrons ( $\pi/K/p$ ), online Level-2 (LVL2) trigger to tag high  $p_T$  charged tracks is very useful. Efficiency and rejection power of the trigger should be studied for online tracking, such as Pad Chambers (PC1/2/3).

We have studied trigger rejection by using real RUN2 Au+Au data. In this section, we discuss possible trigger design and show the result of trigger rejection by offline analysis.

**Trigger Design** A signal for a high  $p_T$  charged track in the PHENIX apparatus is an almost straight track from the vertex in the outer detectors. Therefore the Aerogel LVL2 trigger uses outer detectors in the central arms (PC1/2/3 in the West arm).

First plan for Run4 Aerogel LVL2 trigger is as following;

1. Select PC3 hit in Aerogel acceptance (W1 sector).
2. Select tracks combined PC1 and PC3 hit with  $|\theta_3 - \theta_1| < 0.006$ .
3. Select the nearest hit on PC2 plane with  $\Delta y$  and  $\Delta z$  matching cut. ( $1 \sigma$  is about 0.7 cm both y and z)
4. If a PC2 hit is found, the PC1/2/3 cluster combination is declared to be a candidate and is recorded.
5. Cut on momentum (two point tracking with PC1/3 has about 5 % momentum resolution).

**Offline Study of Rejection** In order to develop the cuts described previously, the trigger rejection was studied using RUN2 minimum-bias Au+Au events. Rejection factors are summarized in Table 10.

momentum threshold	PC1/3	PC1/2/3	E/p>0.1	E/p>0.2
3.0 GeV/c	3.3	16.7	65.7	176.0
4.0 GeV/c	3.8	22.4	143.5	544.9
5.0 GeV/c	4.3	27.6	272.4	1600.6
6.0 GeV/c	4.7	32.1	419.8	3201.1

Table 10: Summary of rejection factor.

where PC1/3 is two point tracking by using PC1 and PC3, PC1/2/3 includes additional matching cut at PC2 and E/p>0.1(0.2) includes additional E/p cut in PC1/2/3 tracks.

Figure 85 shows comparison of DCH tracks and two point tracking by PC1/3 in aerogel acceptance.

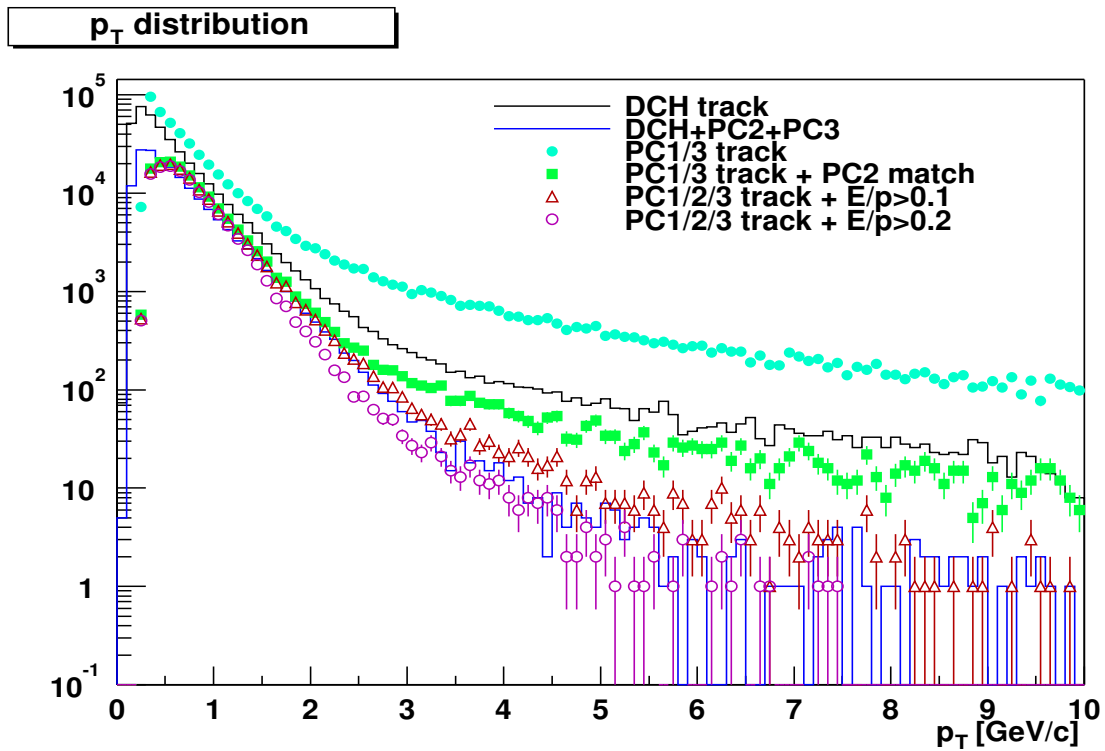


Figure 85: Comparison of  $p_T$  distribution of DCH tracks and two point tracking by PC1/3. All  $p_T$  distribution is in aerogel acceptance. Black line is the distribution of DCH tracks and blue line includes additional matching cut at PC2 and PC3. Solid circle line (top, light-blue) shows the distribution of PC1/3 tracks and Solid square line (green) includes additional matching cut at PC2. Open triangle line (red) and open circle line (purple) shows the distribution PC1/2/3 tracks with additional  $E/p > 0.1$  and  $E/p > 0.2$  cut, respectively.

## 5 Appendix

### 5.1 Appendix A: Heating Test

In order to study the heat produces by the PMT base, measurements and simple calculation were done as follows. The calculations are consistent with the measurement. Even without gas flow, the temperaure rise of the unit due to heat dissipation from the PMT bases is only 3.4K.

Therefore, we do not need gas flow for cooling.

#### 1. Heating Test

A single counter with two PMTs installed was encapsulated into thermal insulation enclosure made of thick layers of polyurethane. Only the surface of the lid was left in direct contact with ambient air. This is the environment expected under normal operating conditions.

Both PMT bases were supplied with -1.5kV HV, and left energized for approximately 6 hours. Power dissipated by individual PMT bases was in the range of 0.68 W, and the total power dissipated within the box was  $\sim 1.4$  W.

Figure 86 shows the initial rather fast rise in the detector temperature which then saturates at a value of 3.5K above the ambient temperature. (The ambient one is constantly at 24.8 deg C.)

#### 2. Heat Calculation

##### (a) Setup and Preconditions

Heating source is the PMT base, containing resistance dividers (680k-ohm each):

$$220\mu A \times 1500V = 0.330W$$

Because Aerogel is thermal insulative material ( $\sim 0.02$  W/m/K), we can ignore the heat transmission through the bulk of aerogel tiles. Heat can be transmitted through the surface of the lid. The lid consists of 0.8mm-Al plate and 2mm-G10 board. Inside the box, nitrogen gas is filled and circulated. Moreover, the temperature of the gas is the same as outside one.

##### (b) Thermal constants

The thermal constants are tabulated in Table 2b.

##### (c) Volume, Surface area

The total volume of each cell is 7.91 L. Subtracted the Volume of PTMs ( $2 \times 0.50L$ ) and Aeogel tiles ( $22 \times 0.14L$ ), Filling volume of  $N_2$  is 4.33 L. On the other hand, the surface area of the lid is  $5.28 \times 10^{-2}mm^3$ .

Specific heat at constant pressure ( $N_2$ )	1.034 J/g/K
Thermal conductivity (G-10)	0.2 W/m/K
Thermal conductivity (Al)	240 W/m/K
Heat transfer coefficient (Air) (boundary condition)	15 W/m <sup>2</sup> /K

Table 11: Thermal constants

(d)  $N_2$  gas for cooling

The number density of  $N_2$  gas (1atm, 16 degC) is 24.0 L/mol, hence, the filling gas is  $4.33/24.0 = 0.18mol$ , 5.04g in mass. Heat capacity of the cooling gas is  $5.04 \times 1.034 = 5.21J/K$ .

(e) Thermal conductivity of the lid

Al	$(240 \text{ W/m/K}) / 0.8 \text{ mm} = 300000 \text{ W/m}^2/\text{K}$
G10	$(0.2 \text{ W/m/K}) / 2.0 \text{ mm} = 100 \text{ W/m}^2/\text{K}$
Air ( $N_2$ )	15 W/m <sup>2</sup> /K

Table 12: Thermal conductivity of the parts

The thermal conductivity of the parts is listed in Table 2e. The total thermal conductivity of the lid is estimated with the same law of series connection of resistors:  $(15^{-1} + 300000^{-1} + 100^{-1} + 15^{-1})^{-1} = 7.0W/m^2/K$   $7.0W/m^2/K \times 5.28 \times 10^{-2}m^2 = 0.37W/K$

(f) Equilibrium equation (constant temperature)

$$2 \times 0.330W - 0.37W/K \times dT - (F/4.33L) \times 5.21J/K \times dT = 0$$

where dT is temperature rise (K), F is flow of  $N_2$  (L/sec).

$$\text{then, } 2 \times 0.330 - (0.37 + 1.20 \times F) \times dT = 0$$

$$dT = 0.660/(0.37 + 1.20 \times F)$$

if F=0, the rise is 1.8K. if F=100 cc/sec, then 1.3K.

(In case of the measurement(330k-ohm), 3.5K rise at F=0.)

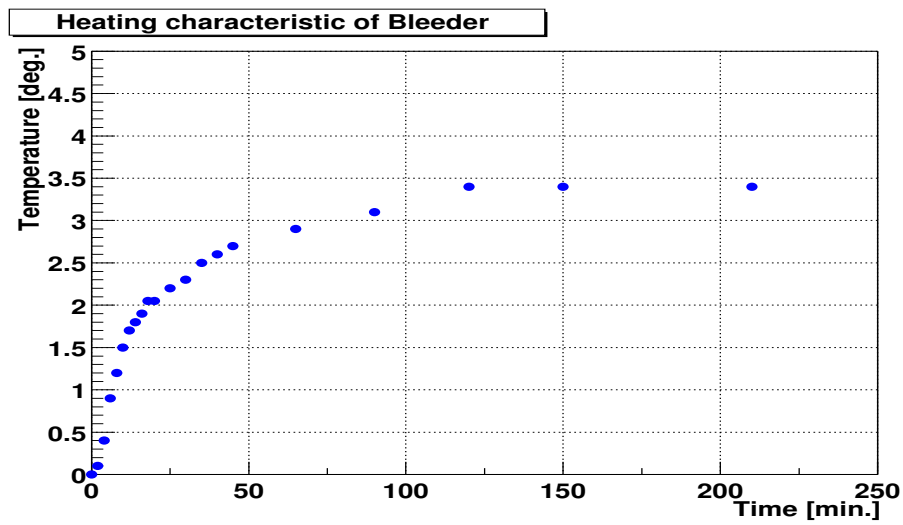


Figure 86: Heating characteristic of PMT base

## 5.2 Appendix B: Connector List

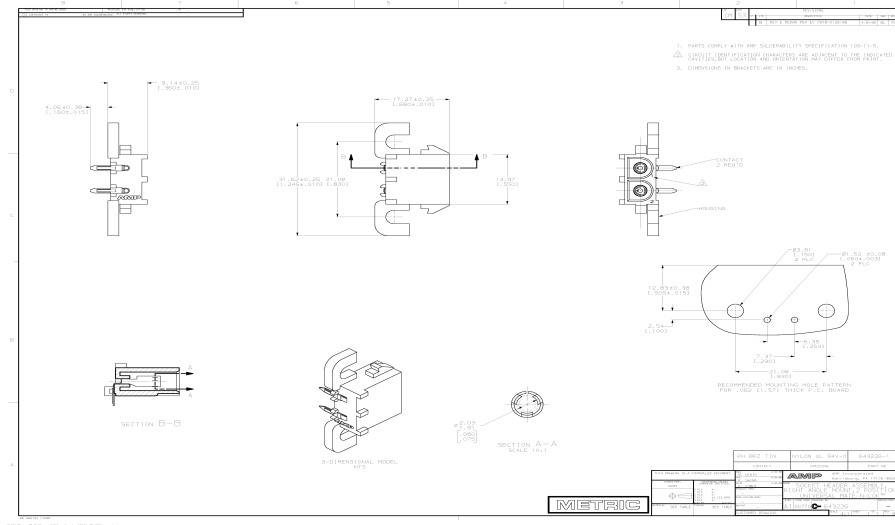


Figure 87: connector # 643226-1





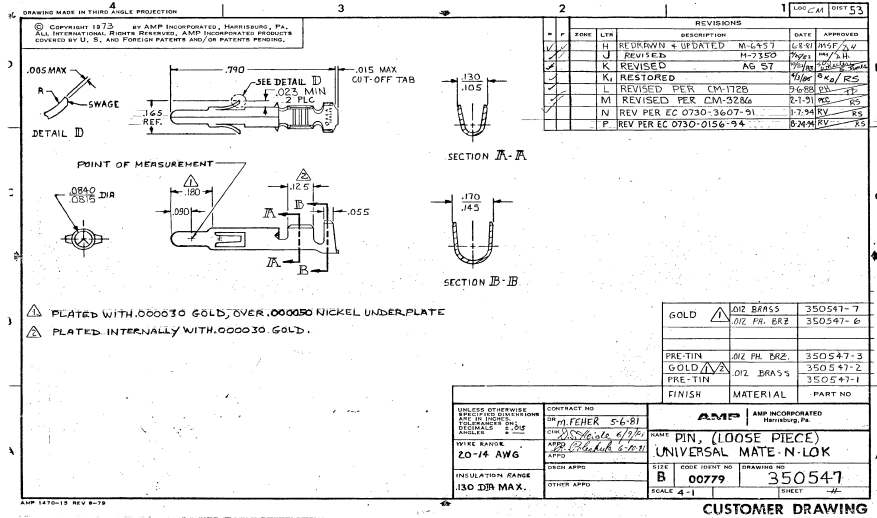


Figure 90: connector # 350547-1

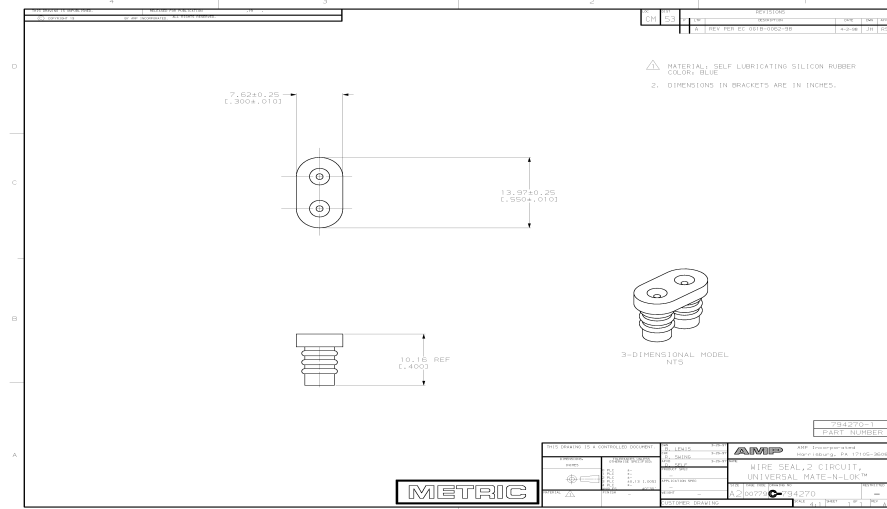


Figure 91: connector # 794270-1



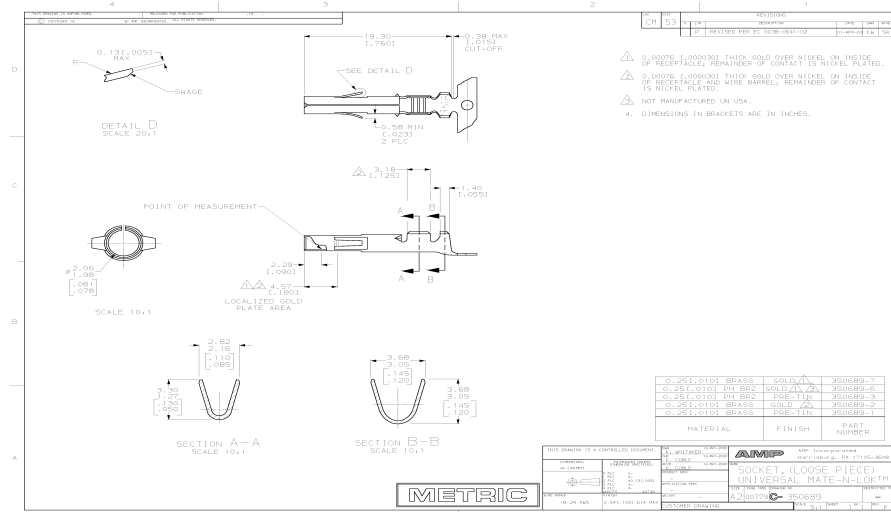


Figure 94: connector # 350689-1

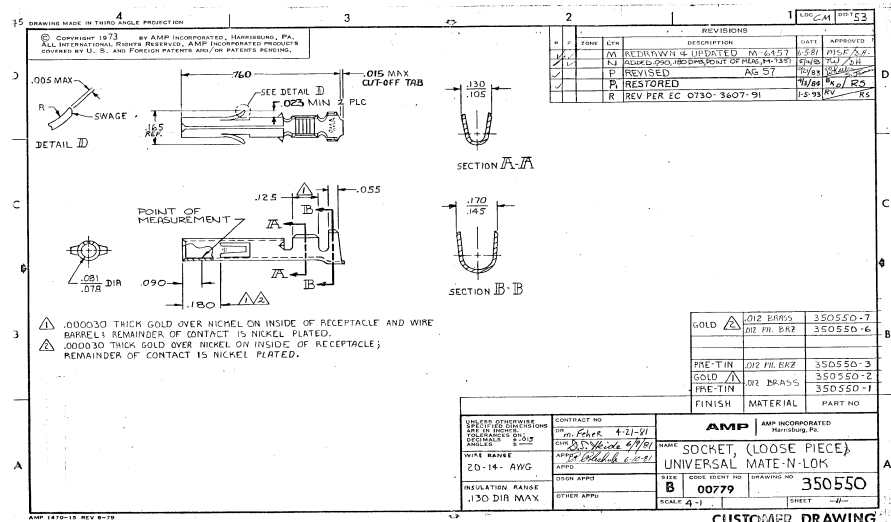


Figure 95: connector # 350550-1

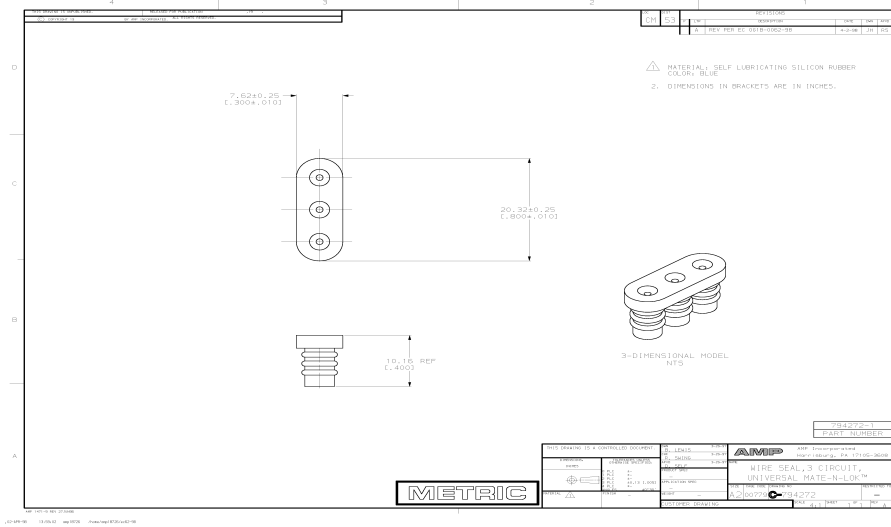


Figure 96: connector # 794272-1

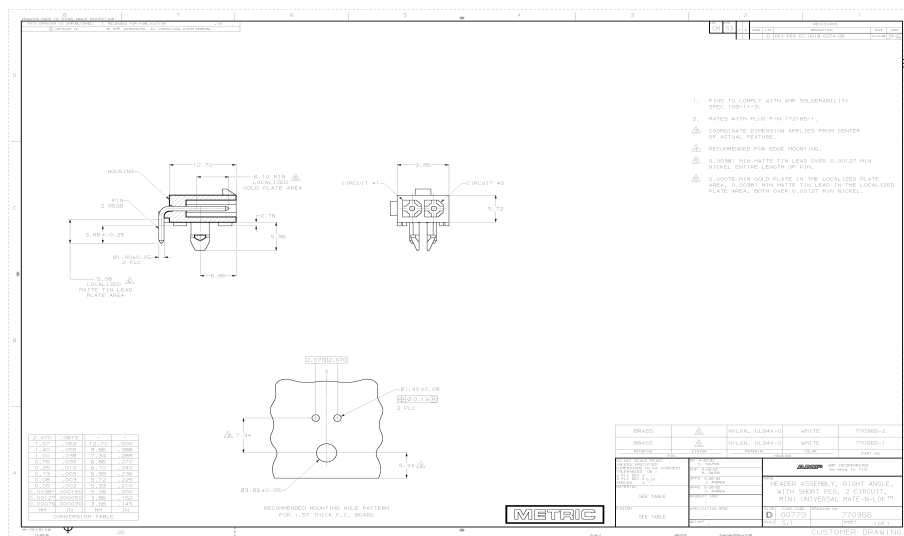


Figure 97: connector # 770966-1

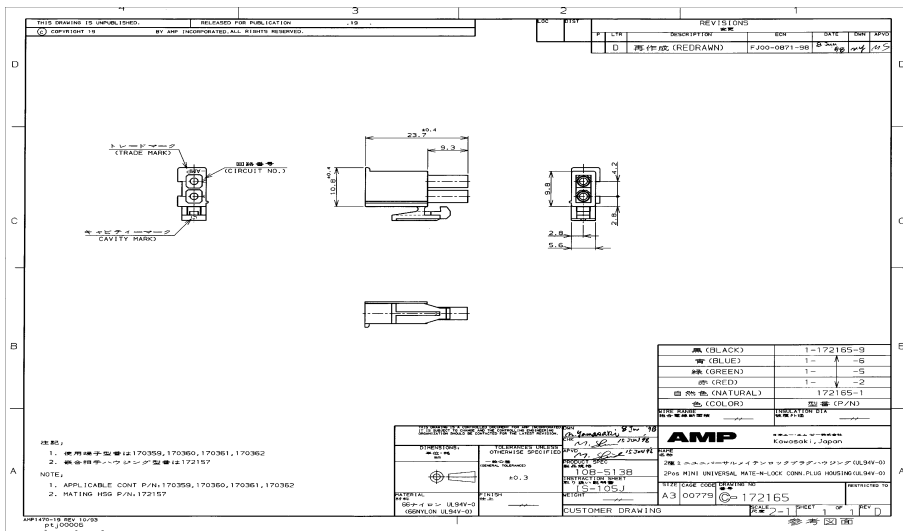


Figure 98: connector # 172165-1

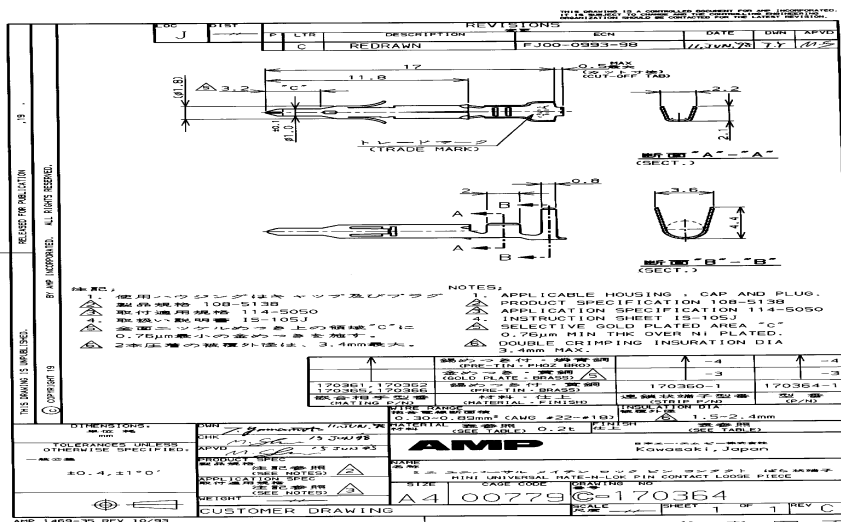


Figure 99: connector # 170364-1

### 5.3 Appendix C: Parts List

# Parts List of Aerogel detector

last updated on Wednesday, 23-Jul-2003 12:37 EDT by [M. Konno](#)

- [1. Aerogel](#)
- [2. PMT](#)
- [3. Aluminum Box](#)
- [4. Inner Box](#)
- [5. Connectors](#)
- [6. Cables](#)
- [7. LED](#)
- [8. PreAMP](#)
- [9. Transition Card](#)
- [10. FEE](#)
- [11. Trigger module](#)
- [12. Power supply](#)
- [13. Gas system](#)
- [14. Supporting frame](#)

## 1. Aerogel

Serial No.	Part	Type, P/N	Maker	Material	Quantity for Run4	Unit price	Present status	Shipping schedule	Person in charge	Comments
1-1	Aerogel	SP-12M	Matsushita Electric Works, Ltd.	Silica aerogel	3520 tiles (490 liter)	-	in Tsukuba 3000 tiles (418 liter)	-	M. Konno,	n=1.0114 +/- 0.0008 Size:112.5(+/-1.0)x112.5(+/-1.0)x11.0 (+/-0.5) Lot No: 320304, 330306 Load:22 tiles/box (3.06L), Note:Very fragile

## 2. PMT (Photomultiplier tube)

Serial No.	Part	Type, P/N	Maker	Material	Quantity for Run4	Unit price	Present status	Shipping schedule	Person in charge	Comments
2-1	PMT	<a href="#">R6233-01HA</a>	Hamamatsu Photonics	-	320	-	in Tsukuba, 320 PMTs	-	M. Konno	Size:76/52(D)x(87+13), <a href="#">Basic Parameters</a> <a href="#">Serial Number</a> <a href="#">Sk, Sp, ldb, Skb</a>
2-2	Light shielding paint	Two-liquid Silicone	Hamamatsu Photonics	-	-	-	to Tsukuba, Jul/24	-	M. Inaba	Back of PMT
2-3	Bleeder	Original (ver.3)	-	-	320	-	-	-	M. Inaba	Size:75x80x14(1.6) Divider resistance:680k-ohm <a href="#">Circuit diagram</a> <a href="#">Layout pattern</a> <a href="#">Parts arrangement</a> <a href="#">Parts specification</a>
2-4	Magnetic shield	Original	CI Industry Co.Ltd	Permalloy	320	-	to Tsukuba, Aug/8;Half, Aug/15;All	-	M. Konno	<a href="#">Cylinder(0.5t)</a> (length;80,diameter;80), <a href="#">Test results</a>
2-5	PMT Holder	Original	CI Industry Co.Ltd	MC-Nylon (MC901)	320 x 3	-	to Tsukuba, Aug/1st-week	-	M. Konno	<a href="#">A, B1, B2</a>
2-6	Band	-	CI Industry Co.Ltd	Stainless steel	320	-	to Tsukuba,	-	M. Konno	For Holder B1,B2, <a href="#">Drawing</a>

2-7	Packing	-	-	MC nylon	320	-	-	-	-	M. Konno	PMT - Magnetic shield
2-8	Screw	-	-	Plastic	320 x 2	-	-	-	-	M. Konno	For Shield, M3;11(0.5-12.5)
2-9	Screw	-	-	Plastic	320 x 2	-	-	-	-	M. Konno	For Holder A, M4;16<
2-10	Screw	-	-	Plastic	320 x 2	-	-	-	-	M. Konno	For Holder B1, M4;6.5(3.1-7.3)
2-11	Screw	-	-	Plastic	320 x 2	-	-	-	-	M. Konno	For Holder B2, M4;10.0(3.1-11.0)
2-12	Screw	-	-	Plastic	320 x 4	-	-	-	-	M. Konno	For Band, M4;18(13-23)

### 3. Aluminum Box

Serial No.	Part	Type, P/N	Maker	Material	Quantity for Run4	Unit price	Present status	Shipping schedule	Person in charge	Comments
3-1	Box	Original	JINR workshop, Dubna	Aluminum (0.8t)	160	-	-	Aug/1st-week; 90boxes Aug/last-week; 70boxes	L. Zolin	ReV.C( <a href="#">dwg</a> , <a href="#">pdf</a> )
3-2	Lid	Original	JINR workshop, Dubna	Aluminum (0.8t)	160	-	-	Aug/1st-week; 90boxes Aug/last-week; 70boxes	L. Zolin	ReV.D( <a href="#">dwg</a> , <a href="#">pdf</a> ), ReV.C( <a href="#">dwg</a> , <a href="#">pdf</a> )
3-3	Screw	-	-	-	160 x 4	-	-	-	L. Zolin	To fix the lid
3-4	Glue	PermaPoxy No.84112	<a href="#">Permatex</a>	Epoxy glue	-	-	-	-	L. Zolin	To glue the plates multi-metal epoxy,Black
3-5	HV safety cover	-	-	-	320	-	-	-	-	-
3-6	Spacer	washer or shim	-	plastic	-	-	-	-	-	for connectors
3-7	PC board	-	CI Industry Co.Ltd	G10 (2.0t)	160	-	to Tsukuba, in July	-	M. Konno	Drawings( <a href="#">Inside</a> , <a href="#">Outside</a> )
3-8	Black Paper	-	-	-	160	-	to Tsukuba, July 29	-	M. Konno	Lid - SupportBoard for light tightness 111 x 445

### 4. Inner Box

Serial No.	Part	Type, P/N	Maker	Material	Quantity for Run4	Unit price	Present status	Shipping schedule	Person in charge	Comments
4-1	Reflector (Goretex)	DRP reflector	Japan Goretex Inc.	PTFE	160	-	in Tsukuba, 200 sheets	-	M. Konno	with cutting, Ref.( <a href="#">A</a> , <a href="#">B</a> ), <a href="#">Meas.</a>
4-2	Support film	Mylar (0.1t)	-	Polyester	160	-	to Tsukuba, in July	-	M. Konno	with cutting, <a href="#">Test results</a>
4-3	Insulator	Mylar (0.1t)	-	Polyester	320	-	-	-	M. Konno	Back of bleeder
4-4	Double-sided tape	-	-	-	-	-	in Tsukuba	-	M. Konno	Reflector - Support film
4-5	Stapler	-	-	-	-	-	in Tsukuba	-	M. Konno	Reflector - Support film



## 5. Connectors

Serial No.	Part	Type, P/N	Maker	Material	Quantity for Run4	Unit price	Present status	Shipping schedule	Person in charge	Comments
5-1	HV connector (3 pins)	Plug Housing <a href="#">350766-1</a>	AMP, Tyco Elec Corp.	-	160 x2	-	Ordered in US	-	M. Inaba	White
		Pin Header <a href="#">1-350943-0</a>		-	160 x2	-				White, Right-angle
		Socket Contact <a href="#">350689-3</a>		-	160 x2	-				24-18AWG, for Core
		Socket Contact <a href="#">350550-3</a>		-	160 x2	-				20-14AWG, for GND
		Seal Protector <a href="#">794272-1</a>		-	160 x2	-				for 3 pins
5-2	Signal connector (2 pins)	Plug Housing <a href="#">350777-1</a> , or <a href="#">1-480698-9</a>	AMP, Tyco Elec Corp.	-	160 x2	-	Ordered in US	-	M. Inaba	White -> Order as Black color, Black
		Socket Header <a href="#">643226-1</a>		-	160 x2	-				White, Right-angle -> Order as Black color
		Pin Contact <a href="#">350690-3</a>		-	160 x2	-				24-18AWG, for Core
		Pin Contact <a href="#">350550-6</a>		-	160 x2	-				20-14AWG, for GND
		Seal Protector <a href="#">794270-1</a>		-	160 x2	-				for 2 pins
5-3	LED connector (2 pins)	Plug Housing <a href="#">172165-1</a>	AMP, Tyco Elec Corp.	-	160 x1	-	Ordered in US	-	M. Inaba	Natural
		Pin Header <a href="#">770966-2</a>		-	160 x1	-				White, Right-angle ->Order as Natural color
		Socket Contact <a href="#">770986-3</a>		-	160 x2	-				22-18AWG, in common
		Single Wire Seal <a href="#">794758-1</a>		-	160 x2	-				-
5-4	Hand tool	Insertion tool 455830-1	AMP, Tyco Elec Corp.	-	2	-	Ordered in US	-	M. Inaba	for 350689-3, 350690-3
		Insertion tool 91002-1		-	2	-				for 350550-3, 350547-3
		Extraction tool 318851-1		-	2	-				for 350689-3, 350550-3, 350690-3, 350547-3
		Crimper 90300-2		-	2	-				for 350689-3, 350690-3
		Crimper 90296-2		-	2	-				for 350550-3, 350547-3
		Crimper 90711-2		-	2	-				for 170364-1

5-5	Signal connector (PreAmp-side)	Connector HIF3BA-16D	HIROSE	-	40	-	Ordered, 50 sets	-	M. Inaba	PMT - PreAMP, 8ch per connector
		Contact HIF3-2226SC		-	640	-	Ordered, 800 pins			
5-6	Gas (N2) connector	-	-	-	160 x2	-	-	-	E. Kistenev	On the lid

## 6. Cables

Serial No.	Part	Type, P/N	Maker	Material	Quantity for Run4	Unit price	Present status	Shipping schedule	Person in charge	Comments
6-1	Short cable (HV)	-	-	-	160 x2	-	-	-	M. Inaba	Bleeder - Connector (Inside box)
6-2	Short cable (Signal)	RG174/U	FUJIKURA	-	160 x2	-	-	-	M. Inaba	Bleeder - Connector (Inside box)
6-3	HV cable	RG-59/U	-	-	320	-	-	-	M. Inaba	The same as RICH
6-4	LV cable	-	-	-	40	-	-	-	-	Same as RICH Preamp
6-5	Signal cable 1	RG174/U	FUJIKURA	-	320	-	in Tsukuba, 1200m	-	M. Inaba	PMT - PreAMP, Now estimating each length Assembly; 2weeks after order
6-6	Signal cable 2	UL8233	HITACHI	-	40	-	-	-	M. Inaba	PreAMP - FEE, Multi coaxial cable, 8ch per cable
6-7	LED cable	UTP cable	-	-	160	-	-	-	M. Inaba	Category-5, 24AWG in common

## 7. LED

Serial No.	Part	Type, P/N	Maker	Material	Quantity for Run4	Unit price	Present status	Shipping schedule	Person in charge	Comments
7-1	LED	-	-	-	160x(2or1)	-	Now testing	-	M. Inaba	-
7-2	LED driver	PHENIX TTL Driver	PHENIX original	-	2	-	in Tsukuba (1)	-	S. Boose	8 channels per board, 10 LEDs per channel <a href="#">Circuit</a>
7-3	Divider	-	PHENIX original	-	16	-	-	-	-	-

## 8. PreAMP

Serial No.	Part	Type, P/N	Maker	Material	Quantity for Run4	Unit price	Present status	Shipping schedule	Person in charge	Comments
8-1	PreAMP	Original	Kindai Electronics Co.Ltd	-	40	-	in July	-	N. Kurihara	Gain: 4.2, Voltage sensitive, Non-reverse, 8ch per board, <a href="#">Circuit</a> , <a href="#">Photo</a>
8-2	PreAMP Box	Original	-	-	40	-	-	-	N. Kurihara	-
8-3	Op-amp	<a href="#">AD8009</a>	Analog Devices, Inc.	-	320	-	-	-	N. Kurihara	Band width 1GHz, Slew Rate 5500V/us
8-4	Regulator (+5V)	MICREL	MIC2954-02BT	-	40	-	-	-	N. Kurihara	Power regulator

8-5	Regulator (-5V)	TOSHIBA	TA79005S	-	40	-	-	-	N. Kurihara	Power regulator
8-6	Input connector	3M	3408-5602	-	40	-	-	-	N. Kurihara	-
8-7	Output connector	KEL	8831E-020-170L	-	40	-	-	-	N. Kurihara	-
8-8	Power connector	JAE	IL-3P	-	40	-	-	-	N. Kurihara	-

### 9. Transition Card

Serial No.	Part	Type, P/N	Maker	Material	Quantity for Run4	Unit price	Present status	Shipping schedule	Person in charge	Comments
9-1	Transition Card	Original	Kindai Electronics Co.Ltd.	-	-	10	in July	-	N. Kurihara	-
9-2	Input connector	8831E-020-170L	KEL	-	-	80	-	-	N. Kurihara	-
9-3	Output connector	352069-1	AMP, Tyco Elec Corp	-	-	20	-	-	N. Kurihara	-
9-4	Output connector	338110-2	AMP, Tyco Elec Corp.	-	-	20	-	-	N. Kurihara	Back shield for 352069-1

### 10. FEE (Front-End Electronics)

Serial No.	Part	Type, P/N	Maker	Material	Quantity for Run4	Unit price	Present status	Shipping schedule	Person in charge	Comments
10-1	Controller Board	The same as RICH FEE	Kindai Electronics Co.Ltd.	-	-	2	in July	-	N. Kurihara	-
10-2	AMU/ADC Board	The same as RICH FEE	Kindai Electronics Co.Ltd.	-	-	10	in July	-	N. Kurihara	Dynamic range: 0-160 pe
10-3	Readout Board	The same as RICH FEE	Kindai Electronics Co.Ltd.	-	-	2	in July	-	N. Kurihara	-
10-4	Back Plane	The same as RICH FEE	-	-	-	2	in July	-	N. Kurihara	-
10-5	Crate	The same as RICH FEE	-	-	-	2	in July	-	N. Kurihara	-

### 11. Trigger module

Serial No.	Part	Type, P/N	Maker	Material	Quantity for Run4	Unit price	Present status	Shipping schedule	Person in charge	Comments
11-1	Trigger module	Aerogel LVL-1 trigger	-	-	Not installed in Run4	-	-	-	N. Kurihara	LVL-2 trigger to be used for Run4 Au-Au

### 12. Power supply

Serial No.	Part	Type, P/N	Maker	Material	Quantity for Run4	Unit price	Present status	Shippig schedule	Person in charge	Comments
12-1	HV module	-	-	-	14 modules (160+8 ch)	-	-	-	-	12 channels/module
12-2	LVL for preamp	-	-	-	-	-	-	-	-	-
12-3	LVL for LED driver	-	-	-	-	-	-	-	-	-
12-4	LVHP for FEE	Same as RICH	-	-	-	-	-	-	-	-

### 13. Gas system

Serial No.	Part	Type, P/N	Maker	Material	Quantity for Run4	Unit price	Present status	Sipping schedule	Person in charge	Comments
13-1	Gas system	-	-	Nitrogen gas	-	-	-	-	-	Advice from Rob Pisani

#### 14. Supporting frame

Serial No.	Part	Type, P/N	Maker	Material	Quantity for Run4	Unit price	Present status	Sipping schedule	Person in charge	Comments
14-1	Supporting frame	-	-	-	-	-	-	-	P.Kroon	Drawings(A, B) - Not Latest

[back to TOF page](#)